UNIVERSITÉ DU QUÈBEC À MONTRÉAL

ÉVALUATION DU BILAN DE LA RADIATION À LA SURFACE SUR L'AMÉRIQUE DU NORD POUR QUELQUES MODÈLES RÉGIONAUX CLIMATIQUES ET LES DONNÉES DE RÉ-ANALYSES

MÉMOIRE

PRÉSENTÉ

COMME EXIGENCE PARTIELLE

DE LA MAÎTRISE DE SCIENCES D'ATMOSPHÈRE

PAR

MARKO MARKOVIC

NOVEMBRE 2007

UNIVERSITY OF QUEBEC AT MONTREAL

AN EVALUATION OF THE SURFACE RADIATION BUDGET OVER NORTH AMERICA FOR A SUITE OF REGIONAL CLIMATE MODELS AND REANALYSIS DATA

THESIS

PRESENTED

IN PARTIAL FULLFILTMENT OF THE REQUIREMENTS FOR THE

MASTER'S DEGREE IN ATMOSPHERIC SCIENCES

BY

MARKO MARKOVIC

NOVEMBER 2007

CONTENTS

LIST OF FIGURES

LIST OF TABLES

LIST OF ACRONYMS

ARM	Atmospheric Radiation Measurement Program
BSRN	Baseline Surface Radiation Network
CERES	Clouds and the Earth's Radiant energy System
CF	Cloud Free
CKD	Correlated-k Distribution
CO	Colorado
CRCM	Canadian Regional Climate Model
CRF	Cloud Radiative Forcing
DJF	December-January-February
DLR	Downwelling Longwave Radiation
DLR CRF	Downwelling Longwave Cloud Radiative Forcing
ECMWF	European Centre for Medium-Range Weather Forecast
ECMWF-IFS	ECMWF-Integrated-Forecast System
ERA40	European Reanalysis, covering 40 years
ERA15	European Reanalysis, covering 15 years
ERBE	Earth Radiation Budget Experiment
FM	February-March
GEM-LAM	Global Environmental Multiscale-Limited Area Model
GCM	Global Climate Model
IL	Illinois

ISCCP	International Satellite Cloud Climatology Project
ISR	Incoming Shortwave Radiation
ISR CRF	Incoming Shortwave Cloud Radiative Forcing
IR	Infrared
IWP	Ice Water Path
JJA	June-July-August
LST	Local Standard Time
LW	Longwave
LWP	Liquid Water Path
MS	Mississippi
MT	Montana
NARR	North American Regional Reanalysis
NASA	National Aeronautics and Space Administration
NCEP	National Centre for Environmental Prediction
Net CRF	Net Cloud Radiative Forcing
NV	Nevada
PA	Pennsylvania
PDF	Probability Density Function
RCA3	Rossby Centre Atmospheric Model
RCM	Regional Climate Model
RGB	Red-Green-Blue
SRB	Surface Radiative Budget
SURFRAD	Surface Radiation

SW	Shortwave
SZA	Solar Zenith Angle
TOA	Top of the Atmosphere
UTC	Coordinated Universal Time

LIST OF SYMBOLS

ε	Emissivity of the body
ε_a	Atmospheric emissivity
ε_g	Ground emissivity
T	Temperature of the body
σ	Stefan-Boltzman constant
$\lambda_{\max}$	Maximal wavelength
A	Constant
a	Ground albedo
T_s	Surface temperature
$LW\|_{all}$	Longwave radiation in all-sky condition
$LW\|_{clr}$	Longwave radiation in clear-sky condition
$SW\|_{clr}$	Shortwave radiation in clear-sky condition
$SW\|_{all}$	Shortwave radiation in all-sky condition
$CRF\|_{sw}$	Shortwave cloud radiative forcing
$CRF\|_{lw}$	Longwave cloud radiative forcing
$CRF\|_{net}$	Net cloud radiative forcing
T_{CLD}	Cloud temperature
T_{SFC}	Surface temperature
$SW\downarrow$	Total incoming solar radiation

$LW\downarrow$	Longwave radiation emitted downwards from the atmosphere
$SH\uparrow$	Sensible heat flux
$LH\uparrow$	Latent heat flux

RÉSUMÉ

Le rayonnement solaire incident (ISR) (direct et diffus) et le rayonnement atmosphérique de longue longueur d'onde (DLR) sont les paramètres qui déterminent le bilan de la radiation à la surface (SRB) et jouent un rôle très important dans l'échange d'énergie entre la Terre et l'atmosphère. La représentation exacte de ces composantes dans les modèles climatiques est donc cruciale. Dans ce travail, nous évaluons les composantes de l'ISR, du DLR et de la couverture nuageuse des trois modèles suivants : 1. le Modèle Régional Canadien du Climat (MRCC), 2. la version régionale du Modèle Global Environnemental à Multi-échelle (GEM-LAM) et 3. le modèle atmosphérique du centre Rossby (RCA3) sur un domaine couvrant l'Amérique du Nord. Premièrement, les trois modèles sont comparés avec les observations de surface fournies par le réseau SURFRAD afin d'identifier les conditions dans lesquelles ils ne performent pas correctement. Puisque ces observations ne fournissent pas une couverture spatiale adéquate, trois bases de données différentes sont comparées à trois bases de données disponibles sur l'ensemble du territoire. Les substituts aux observations que nous évaluons sont: les ré-analyses ERA40 de ECMWF couvrant 40 années, les ré-analyses régionales d'Amérique de Nord (NARR) et les composantes du SRB provenant du Projet International de Climatologie Satellitaire des Nuages (ISCCP). La base de donnée la plus représentative est utilisée comme substitut aux observations afin de la comparer avec le SRB simulé par les modèles sur tout le domaine d'Amérique du Nord.

Les comparaisons entre les modèles et les observations montrent que les biais les plus importants sont présents pour des conditions atmosphériques froides et sèches ce qui nous indique soit une mauvaise représentation de l'émission de la vapeur d'eau pour des conditions atmosphériques sèches, soit un biais négatif dû aux omissions des contributions des gaz traceurs dans le DLR pour les conditions de ciel clair. Les biais du ISR constatés dans cette étude viennent surtout de la mauvaise représentation des nuages dans les modèles qui ne sont pas assez opaques pour le rayonnement solaire incident.

La comparaison avec six sites d'observations différents a confirmé qu'ERA40 est le meilleur substitut aux observations pour les composantes ISR et DLR sur l'Amérique du Nord. La comparaison des modèles avec ERA40 sur toute l'Amérique du Nord apporte des conclusions similaires à celles obtenues lors de la comparaison des modèles directement avec les sites d'observations. Ces résultats confirment que les biais trouvés dans cette étude proviennent de l'imperfections des modèles ce qui influence les composantes du SRB pour les différents régimes climatiques d'Amérique du Nord.

Mots clés: rayonnement, modèles régionaux du climat, ré-analyses, forçage radiatif des nuages.

ABSTRACT

Incoming solar radiation (ISR) (direct+diffuse) and downwelling longwave radiation (DLR) are parameters that determine the total surface radiative budget (SRB) and play important role in energy exchange between the Earth and Atmosphere. Therefore, an accurate representation of these components is crucial for climate modeling. In this work, we evaluate ISR, DLR and cloud cover from: 1. the Canadian Regional Climate Model (CRCM), 2. the Climate version of Global Environmental Multiscale Model (GEM-LAM) and 3. the Rossby Centre Atmospheric Model (RCA3), over the entire North America. These models are first evaluated against surface observations, provided by the SURFRAD network, trying to identify regimes where respective models operate poorly. As surface observations doesn't offer adequate spatial coverage, three different gridded data sets are assessed against surface observations and the most accurate one used as an observational surrogate for comparison of the model simulated SRBs over the entire North America. As observational surrogates, we evaluate: the ECMWF 40 year reanalysis (ERA40), the North American Regional Reanalysis (NARR) and a satellite derived SRB from the International Satellite Cloud Climatology Project (ISCCP).

Comparison between models and observations showed that the biggest DLR biases are found in cold and dry conditions suggesting either a poor representation of water vapor emission in dry atmospheric conditions and a negative bias arising from the omission of trace gas contributions to the clear-sky DLR. ISR is simulated quite accurately, but errors in the cloud cover representation, especially for the summer season, influence summer ISR all-sky biases. Normalised frequency distribution comparison revealed that DLR all-sky biases, for all models, come either from clear-sky DLR or erroneous cloud emissivity. ISR frequency distributions showed that ISR all-sky biases come mainly from erroneous cloud cover.

ERA40 showed to be the most representative gridded data set and comparison across the 6 separate observational sites confirmed ERA40 to be an accurate surrogate observational data set both for ISR and DLR across North America. Nighttime DLR representation was shown to be the potential cause of a small negative bias in winter season DLR in ERA40. Lack of nighttime cloud observations prevented a determination of this error cause for clear or cloudy-sky conditions.

Comparison of models against ERA40 over the entire domain of North America confirmed similar conclusions as in model-observation comparisons, indicating that errors found in this study are genuine model shortcomings influencing the simulated SRB across various climate regimes of North America.

Key words: radiation, regional climate models, reanalysis, cloud radiative forcing.

INTRODUCTION

The overwhelming majority of the energy available to the Earth comes from the Sun, almost 99.9%, the remaining 0.1% coming from Earth's geothermal and tidal energy. With a surface temperature of around 6000 K, the spectra of solar radiation ranges from 0.1μm to 7μm. With a mean Earth-Sun distance of 1.5×10^{11} meters, the solar radiation reaching the top of the Earth's atmosphere is around 1367 Wm^{-2}. This is referred to as the solar constant, though its value can change slightly depending on the eccentricity of the Earth's solar orbit, Sunspots cycle, period of the year, latitude, etc. How the incoming $1367 Wm^{-2}$ influences the Earth's climate depends on a number of factors such as: cloudiness (e.g. types of clouds, water content, quantity) aerosol concentration, presence of water vapor and the other radiatively active gases in the atmosphere, and the state of the Earth's surface (e.g. albedo).

The mean annual global energy balance that reaches the Earth's atmosphere is presented in figure I1 (Kiehl and Trenberth, 1997). The radiation spectra is divided into short wave radiation (incoming from Sun) and long wave radiation (outgoing from the Earth's surface and emitted from the atmosphere). All bodies with a temperature greater than 0 K emit energy over a different range of wavelengths. This energy can be derived from the Stefan-Boltzman law as $\varepsilon \sigma T^4$ where ε is emissivity of the body, σ is Stefan-Boltzman constant and T the temperature of the body. The wavelength of maximum energy given by the Stefan-Boltzman law can be calculated using Wiens displacement law (Peixoto and Oort, 1992):

$$\lambda_{max} = \frac{A}{T} \tag{1.1}$$

where λ_{max} is wavelength and $A = 2898 \mu m K$ is constant. As a result of the large temperature difference between the Sun and Earth the maximum wavelength of

radiation emitted by each body is distinctly different. This allows solar and terrestrial radiation to be treated independently in most climate models.

Averaging the solar constant, annually and globally, leads to ~342 Wm^{-2} radiant energy entering the Earth-Atmosphere system at the top of the Atmosphere (TOA). From this total amount of radiation ~77 Wm^{-2} is reflected back to space by clouds and aerosols in the clear-sky atmosphere, ~30 Wm^{-2} reflected from the surface (albedo) and ~67 Wm^{-2} absorbed in the atmosphere. As we see on Figure I1, ~168 Wm^{-2} of solar radiation incident at the TOA reaches the Earth's surface.

Solar radiation reaching the Earths surface warms the surface, which than emits ~390 Wm^{-2} (calculated from $\varepsilon\sigma T^4$) of radiation. This occurs at longer wavelengths because the Earth is so much cooler than the sun (Wiens law). Also because of temperature and humidity gradients between the surface and overlying atmosphere, there is sensible and latent transfer of energy 102 Wm^{-2} (24 Wm^{-2} from sensible and 78 Wm^{-2} from latent heat) from the surface into the atmosphere. Of the surface emitted 390 Wm^{-2}, 40 Wm^{-2} goes through to space (through the atmospheric window), the remaining 350 Wm^{-2} is absorbed in the atmosphere, along with the 67 Wm^{-2} of solar absorbed leading to 519 Wm^{-2} entering the atmosphere.

Because the clear-sky atmosphere is opaque to longwave (LW) radiation, a significant fraction of the surface upwelling terrestrial radiation is absorbed in the atmosphere and subsequently re-emitted up and down at the local atmospheric temperature. The balance at the surface gives the net LW that actually cools the surface. The radiation emitted upward to space, by the atmosphere, is 165 Wm^{-2}, which combined with the direct loss of LW radiation to space from the surface leads to a TOA emission of LW radiation of ~235 Wm^{-2}. This emission balances the net incoming solar radiation at TOA, leading to a balance in net radiation at the TOA. The role of the atmosphere can be seen as absorbing 67 Wm^{-2} of solar radiation and

$350\,Wm^{-2}$ of surface emitted terrestrial radiation with a significant fraction of this absorbed radiation being emitted back to the surface. It is calculated that mean temperature of the earth's surface without an absorbing atmosphere would be 255 K (Wallace and Hobbs, 1977). As the mean annual surface temperature is 285 K, the existence of an absorbing atmosphere increases the global mean surface temperature by $\sim 33^{\circ}C$. It should be highlighted that all the numbers representing energy budget of the atmosphere and surface (Figure I1) are approximate.

From a global mean perspective, when averaged over a sufficient time period the Earth-Atmosphere system is in radiative balance (the amount of energy which enters is equal to the energy leaving the system). If this was not the case, the Earth would warm or cool and the balance would naturally be reestablished by a changed long-wave outgoing flux which is equal to the $\varepsilon\sigma T^4$. On a more local level, this balance is not so steady, the equatorial region receives more radiation than it emits while the situation in polar regions is the reverse. Atmospheric circulations (Hadley, Ferrel and Polar cells, Figure I2) and ocean currents redistribute this imbalance maintaining relatively constant thermal conditions on Earth. The primary cause of atmospheric and oceanic circulations is the latitudinal gradient of radiant energy at the TOA. The resulting circulations produce a latitudinal thermal gradient smaller than would result solely from radiative considerations.

Increased concentrations of CO_2 and other green house gases (water vapor, $CH_4, N_2O, HFCs$) increases the emissivity of the atmosphere with respect to longwave radiation. As a result, more outgoing longwave radiation is absorbed in the atmosphere. This excess is emitted upwards and downwards reducing the net IR (Infrared) radiation cooling at the surface and leading to a surface warming. The increasing absorption of surface IR radiation leads to a reduction in IR radiation at the TOA and radiative imbalance at TOA. Balance is restored as a result of the surface warming due to the increased downward emission. This warming leads to an increase

in the surface emission of terrestrial radiation and therefore a re-established TOA balance at a slightly warmer surface temperature. A doubling of CO_2 in the atmosphere is thought to lead to a $\sim 4\,Wm^{-2}$ increase in downwelling IR radiation, with feedbacks potentially amplifying this. Clearly an accurate simulation of the surface SRB in climate models is crucial for an accurate estimate of future temperatures in response to increasing levels of CO_2.

Equation 1.2 describes the surface energy balance at the Earth-Atmosphere surface.

$$SW\downarrow -(1-a)SW\downarrow +\varepsilon_a LW\downarrow -\varepsilon_g \sigma T_s^4 = SH\uparrow +LH\uparrow \qquad (1.2)$$

$SW\downarrow$ represents the total incoming solar radiation (direct plus diffuse) while $(1-a)SW\downarrow$ is solar radiation absorbed at the ground, a is ground albedo. $\varepsilon_a LW\downarrow$ stands for long wave atmospheric radiation emitted from the atmosphere downward to the surface of which ε_g is absorbed at the ground while ε_a and ε_g are atmospheric and ground emissivity respectively. $\varepsilon_g \sigma T_s^4$ stands for long wave radiation emitted from the Earth's surface where T_s is surface temperature. $SH\uparrow$ and $LH\uparrow$ describe the turbulent fluxes of sensible and latent heat at the surface. The latent and sensible heat play an important role redistributing energy within the atmosphere by conduction and convection. Equation 1.2 contains all the components of the surface energy budget. Compared to the heat terms on the right hand side of equation 1.2, the parameters of the surface radiation budget (left hand side of equation 1.2) are bigger and therefore of greater importance to the total energy budget emphasizing the importance of their assessment in this work.

Clouds have a major impact on the Earth-Atmosphere radiation balance though their role is complex. In different circumstances they can influence the surface and TOA radiation fluxes in very different ways. During the day, clouds generally

cool the surface through reflection of incoming solar radiation, by night they generally warm the system through reducing the loss of long wave radiation from the Earth's surface. This warming effect of clouds is due to absorption (by droplets and water vapor) and isotropic emission of LW radiation.

The impact of clouds on surface radiative budget (SRB) can be quantified by use of a cloud-radiative forcing (CRF), which can be formulated either for the TOA (Ramanathan et at., 1989) or surface (Cess et al., 1995). One definition of surface CRF is the difference between incoming radiation for all-sky and cloud-free conditions. All-sky refers to the surface radiation simulated when both fractional cloudiness and clear-sky radiation is included. Incoming shortwave CRF (ISR CRF) is represented by equation 1.3 where $SW|_{all}$ and $SW|_{clr}$ are incoming SW radiation for all-sky and clear-sky conditions respectively. Downward longwave CRF (DLR CRF) is given by equation 1.4 where $LW|_{all}$ and $LW|_{clr}$ represent LW radiation in all-sky and cloud-free conditions. Net CRF represents the addition of ISR CRF and DLR CRF and is represented by equation 1.5. If the Net CRF is greater than zero (more energy arriving at the surface in all-sky conditions than clear-sky), clouds will heat the surface. If the Net CRF is less than zero clouds act to cool the surface, likewise for the solar and longwave components of the CRF.

$$CFR|_{sw} = SW|_{all} - SW|_{clr} \tag{1.3}$$

$$CRF|_{lw} = LW|_{all} - LW|_{clr} \tag{1.4}$$

$$CRF|_{nett} = CRF|_{sw} + CRF|_{lw} \tag{1.5}$$

The Earth Radiation Budget Experiment (ERBE) (Barkstrom, 1984) monitors cloud fraction and various radiation components at the TOA and helps in understanding the role of clouds in the Earth-Atmosphere radiation budget. As an

example Figures I3, I4 and I5 illustrate the annual mean TOA ISR CRF, TOA DLR CRF and TOA Net CRF respectively for the years 1985-1986. Over most of the tropical regions the main impact of clouds is to cool the Earth-Atmosphere system. In these regions, TOA ISR CRF (Figure I3) is much larger than the DLR CRF (Figure I4), which results in a negative TOA Net CRF (Figure I5). However in the tropical western Pacific, due to presence of very high optically thick clouds, forced by convection, the indicated ISR CRF and DLR CRF terms are large but opposite signed causing near cancellation. Emphasizing the effect of clouds on total energy budget, we compare mean TOA ISR CRF in mid-latitudes (~50 Wm^{-2} loss due to clouds blocking the SW radiation, see Figure I3) with a ~4 Wm^{-2} energy gain due to doubling CO_2 concentration since the pre-industrial period. It is apparent that the energy loss coming from cloud cover reflecting solar radiation or energy gain due to re-emmiting of LW radiation is very important (e.g. surface temperature, sea-ice cover), suggesting the accurate representation of clouds and the response of clouds in a changing climate, in climate models is essential for an accurate estimate of future climate conditions.

The type of cloud and its altitude are the main determinants as to whether a cloud warms or cools the surface. Optically thin clouds (e.g. liquid water path < 40 gm^{-2}) warm the system because their emissivity is generally greater than their albedo (DLR CRF > ISR CRF). As DLR CRF also depends on $T_{CLD} - T_{SFC}$, where T_{CLD} and T_{SFC} are cloud and surface temperature higher clouds have a larger DLR CRF effect (Stephens and Webster, 1980). On the contrary, optically thick clouds cool the surface (ISR CRF > DLR CRF). Regardless of the altitude clouds always warm the surface at night indicating the importance of an accurate simulation of the diurnal cycle of cloud-radiation interaction in climate models (Slingo, 1990). Clouds-radiation interaction is different with respect to season. During the winter clouds generally increase the near surface temperature (DLR CRF > ISR CRF), while in summer they reflect large amounts of solar radiation, leading to a decrease of the

surface temperature. The albedo of clouds depends mainly on the integrated water path within a given cloud, although the phase of the water (liquid or solid) influences the median cloud effective radius and therefore the cloud albedo and to a lesser extent cloud emissivity. Cloud Albedo can vary from 20% for cirrus clouds to 70% for nimbostratus.

Aerosols also play a significant role in the Earth-Atmosphere radiation budget. A definition of aerosols would be suspensions of liquid or solid particles in the air, excluding cloud droplets and precipitation (Peixoto and Oort, 1992). Most aerosols originate from: volcanoes, desert dust, sea salt and human activities. The mean radius of aerosols can range from 0.001- 0.1 μm (Aitken aerosols), to 0.1-1 μm (large aerosols) and up to 10 μm (giant aerosols). They influence climate in two ways. First, they can directly absorb and scatter incoming solar radiation in both cloud-free and cloudy conditions, thus cooling the Earth-Atmosphere system by reducing the amount of absorbed shortwave radiation, second they can serve as cloud condensation nuclei in the process of cloud formation. As a result of increased cloud condensation nuclei two indirect aerosol effects can potentially occur. The first indirect effect (also known as the Twomey effect, Twomey, 1974): an increased number of aerosol particles leads to a given amount of cloud water being distributed over a larger number of smaller droplets, this reduces the median effective radius and significantly increases cloud albedo. The second indirect effect (Albrecht, 1989) arises from the increased number of smaller droplets potentially delaying precipitation onset and cloud water removal hence clouds potentially have a larger lifetime in an aerosol loaded atmosphere.

Occasional, large volcanic eruptions can inject a high concentration of aerosols into the stratosphere and thus have a big impact on the Earth-Atmosphere radiation budget. It is calculated that the eruption of Mount Pinatubo in 1991, lowered the amount of solar radiation absorbed by Earth-Atmosphere system by 1.5

Wm^{-2} resulting in a surface temperature cooling of $\sim 0.5^{\circ}C$ over the following two years. Tropospheric aerosols act as cloud condensation nuclei and can be washed out of the atmosphere by rain. Stratospheric aerosols have a long residence time due to the high static stability and the low humidity in the stratosphere and subsequent absence of cloud and rain-out processes. Stratospheric aerosols impact the system by scattering and absorbing incoming solar radiation. With the boost of industrialization, atmospheric aerosol concentrations have increased worldwide. Although with concerns regarding acid rain, sulphur emissions into the atmosphere have been decreasing since the late 1980's.

With respect to modeling the Earth-atmosphere radiation budget, the correct representation of clouds and aerosols and their radiative impact is essential. The impact of clouds on the surface radiation budget is crucial to simulate for an accurate SRB. The SRB is a crucial term to represent correctly if climate models are to accurately simulate surface temperatures, soil moisture, snow cover and sea ice amounts, all of which are strongly influenced by variability in SRB.

In this thesis we evaluate the simulation of the surface radiation budget in three different Regional Climate Models (RCM). High quality surface observations from a number of sites over North America are used to evaluate the RCMs SRB. The study aims to characterize the quality of both the simulated shortwave and longwave radiation in the analyzed models, and to determine the relative accuracy of both cloudy and clear-sky radiation budgets, as a function of both the seasonal and diurnal cycle. We aim to identify key errors in the components controlling the simulated SRB in the respective models, from this we will identify key areas requiring improvement in order to accurately simulate the SRB in a physical consistent manner in the respective RCMs.

The parameters of the surface radiation budget that will be evaluated are: the incoming solar radiation (direct plus diffuse) (ISR) and the downwelling long wave

radiation (DLR). These parameters are the main terms in the surface energy balance controlling the evolution of surface temperature and moisture. It is important that these parameters are well represented in climate models, otherwise severe errors in surface temperature, moisture, and snow cover or ice cover can occur. As an example, systematic errors of SW radiation in spring could lead to erroneous melting of ice, which can reduce the ground albedo and lead to further melting through a positive feedback. Errors in LW downward radiation can also impact on sea-ice and snow cover and depth. Reduced LW radiation implies a deficit of energy reaching the Earth's surface and an increased ice extent/thickness. Downwelling longwave radiation is key indicator of the anthropogenic greenhouse effect. Increasing CO_2 concentrations in the atmosphere directly increases the downwelling longwave radiation from the atmosphere to the surface. Feedbacks involving water vapor amplify an initial DLR increase due to increasing CO_2. Measurements of DLR can be used to track the global greenhouse effect in terms of changes in observed surface DLR (Wild and Ohmura, 2004). The surface radiation budget is also an important control on the hydrological cycle, in particular influencing surface evaporation rate.

There are two methods to monitor the surface radiation budget. First, from satellites, top of atmosphere radiation values can be accurately measured. Inclusion of observed cloud data and the use of detailed radiative transfer schemes allow the surface radiation budget to be derived from satellite TOA values. This method suffers from potential inaccuracies (e.g. cloud amount, specifications of cloud optical properties and water vapor amounts have to be assumed). Second, to measure directly at the surface, downwelling atmospheric radiation with a pyrgeometer and total solar radiation with broadband pyranometer. Direct surface measurements are the most accurate observation of the SRB, but while offering high temporal resolution, observations are taken at only a few sparsely distributed sites. Satellite derived SRBs are less accurate but offer good spatial coverage.

In this thesis, surface observations at a number of sites across North America are used to evaluate the RCM SRB. We further use these point observations to evaluate satellite derived surface radiation and the SRB from the NCEP North American Regional Reanalysis and for the ECMWF ERA40 global analysis. This evaluation is done to determine which of these geographically complete, gridded datasets is most appropriate for evaluation of the RCM simulated SRB across the entire North America. The reanalysis products are derived from analysed variables (e.g. pressure, temperature, humidity, wind, etc.) in the atmosphere from satellites, radiosondes and from surface measurements. Cloud data is not assimilated. From this analysis state, a short range forecast is made (e.g. 24h) and the surface radiation and cloud forecast fields are saved in the analysis. A second assimilation-analysis uses the 6 hour cloud forecast from an earlier short range forecast as the initial cloud amount and a second short range forecast is made. This procedure is repeated continuously with a frozen model-assimilation system to give 6 hourly estimates of the 3D state of the atmosphere, including surface radiation and forecast cloud fields. It is therefore important to remember that analysed surface radiation and cloud amounts are a result of continuous short range forecasts from an accurate analysed atmospheric state (i.e. they are not direct observations). The two sets of reanalysis that we test are: ERA40 (Uppala et al. 2005) from the European Centre for Medium Range Weather Forecasts (ECMWF) and NARR (Mesinger et al. 2004), the North American Regional Reanalysis from the National Centre for Environmental Prediction (NCEP). As with reanalysis, satellite-based measurements can provide estimates of surface radiation over the entire North America. The results of the International Satellite Cloud Climatology Project (ISCCP) (Zhang et al. 2004) coordinated by NASA, will also be compared to surface observations. The data set (ERA40, NCEP or ISCCP) that shows the best agreement with surface SRB observations at discrete locations across North America will be used to evaluate the RCM SRBs across the entire North American continent.

The RCM's we will evaluate in this study are: The Canadian Regional Climate Model (CRCM) (Caya and Laprise, 1999), GEM-LAM, the regional version of the Global Environmental Model (Côté et al, 1997) developed in Canada and third, RCA3, the regional model from Rossby Centre in Sweden (Jones et al. 2004). All models will be evaluated over North America. It is planned to use three RCMs in regional climate change studies over Canada in the near future, hence an evaluation of the SRB is highly relevant. The resolution used by the models in this study is $\sim 0.5^{\circ}$ and boundary conditions used are NCEP analysis for CRCM and ERA40 for GEM-LAM and RCA3. It is noteworthy that we compared results of GEM-LAM simulations forced by both NCEP and ERA40 boundary conditions finding only small changes in the simulated SRB.

Moreover, all three models use different radiation and cloud schemes, characterizing systematic errors in the SRB as a function of climatic conditions will aid in model improvement.

The RCMs will be directly compared with available ground-based measurement over different conditions. Following an initial analysis we will determine the quality of the simulated radiation budget in the respective models and target the areas and climatic conditions where the models give the worst results. By evaluating the surface radiation budget in a variety of climate conditions, for cloudy and clear conditions separately and as function of season and time of day, we aim to isolate conditions and situations where the respective cloud and radiation schemes operate poorly and identify aspects of the parametrization schemes that are causing these simulation errors.

The surface ground measurements are taken from the Surface Radiation Network (SURFRAD) coordinated by NASA. There are six observational sites representing a cross-section of various climate types over North America. Figure 1.1

(modified from www.srrb.noaa.gov/surfrad/sitepage.html, Accessed March 28, 2007) shows the location of the SURFRAD sites used in this work.

Initially we compare the long-term mean annual cycles of ISR and DLR from the three RCM's against surface observations. If there are systematic biases in a given season, the erroneous season can be further analysed in the form of the long-term mean diurnal cycle. This can give a better view in which period of the day SRB problems occur (morning, noon, evening) allowing a better identification of the physical process that are poorly simulated. In climate models, simulation of the SRB depends on numerous factors, such as the parametrization of convection, turbulence, cloud and radiation schemes and it is not easy to determine which of these contribute to the simulation errors. The radiation will be compared in cloud-free, overcast and all-sky conditions. Cloud-free and overcast conditions are analysis of observations and RCMs when and where they each have clear (clouds <10%) or totally cloudy (clouds >90%) so that separate radiation physics can be evaluated. As an example if there are biases in the all-sky and no biases in cloud-free conditions this would suggest either the basic simulation of cloud amount is wrong or the cloudy-sky radiation physics are simulated incorrectly. A separate evaluation of surface radiation just for cloudy-sky and for simulated cloud amounts will help to isolate the problem further. If biases are present in clear-sky conditions this will indicate an error in the clear-sky radiation calculation. Unfortunately at the SURFRAD Network measurement sites there is no information about cloud type, altitude or liquid water concentration so we are forced to derive conclusions based on cloud fraction alone.

The geographic domain used by the 3 RCMs are very similar but due to different projections it was necessary to interpolate the 3 model data sets to a common grid. Once the most accurate surrogate observation data set has been identified using surface observations as guidance, we will evaluate the seasonal mean

surface radiation budget for the 3 RCMs against the best surrogate across the entire North American continent.

This work will be presented in the form of scientific articles, in English.

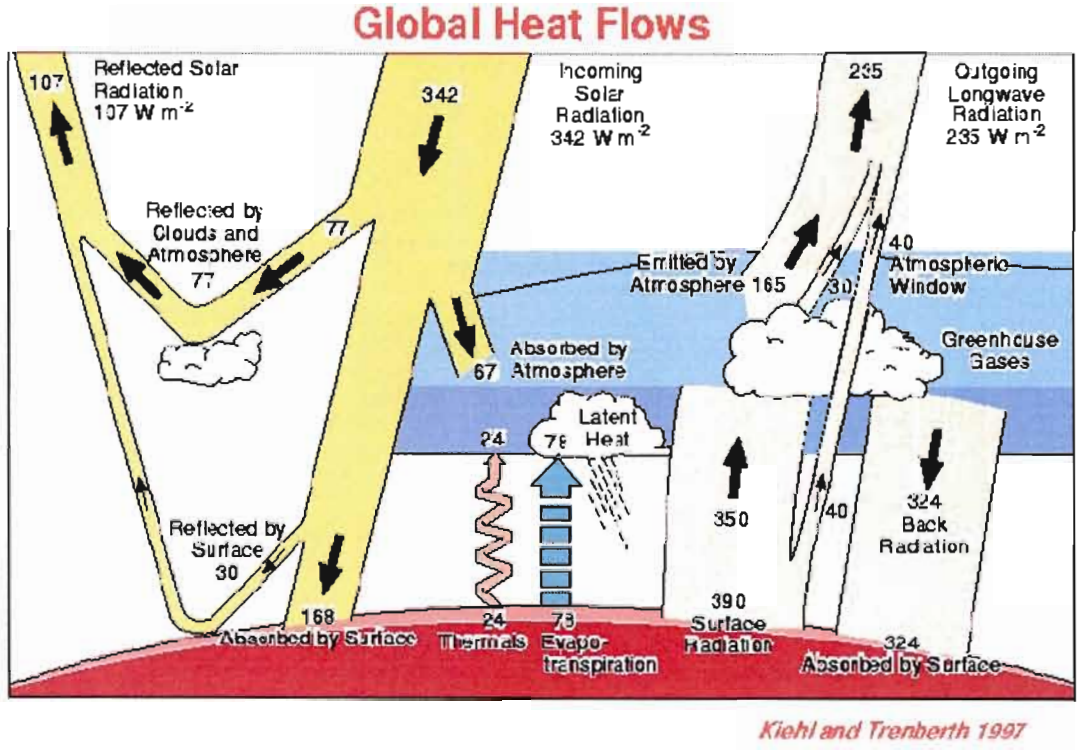

Figure I1: Radiation balance Earth-Atmosphere.

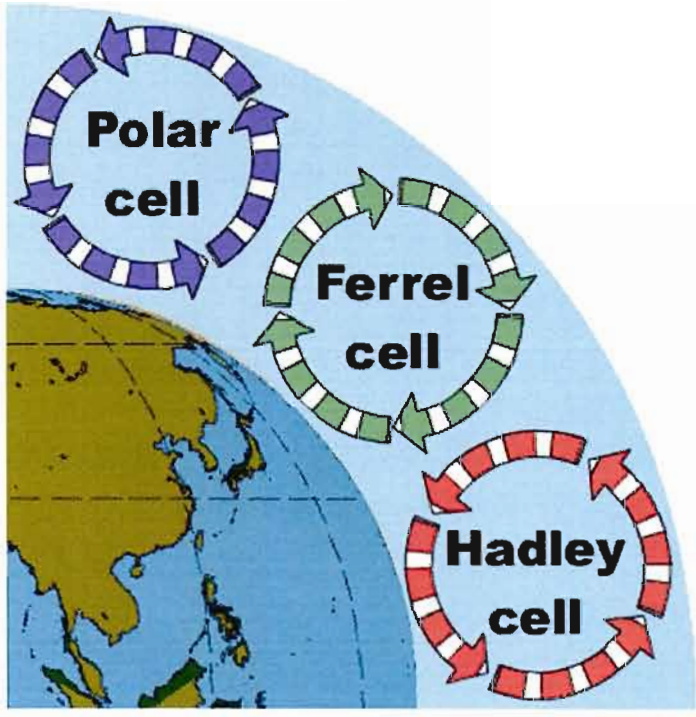

http://sparce.evac.ou.edu/q_and_a/air_circulation.htm

Figure I2: Equator to pole air circulation.

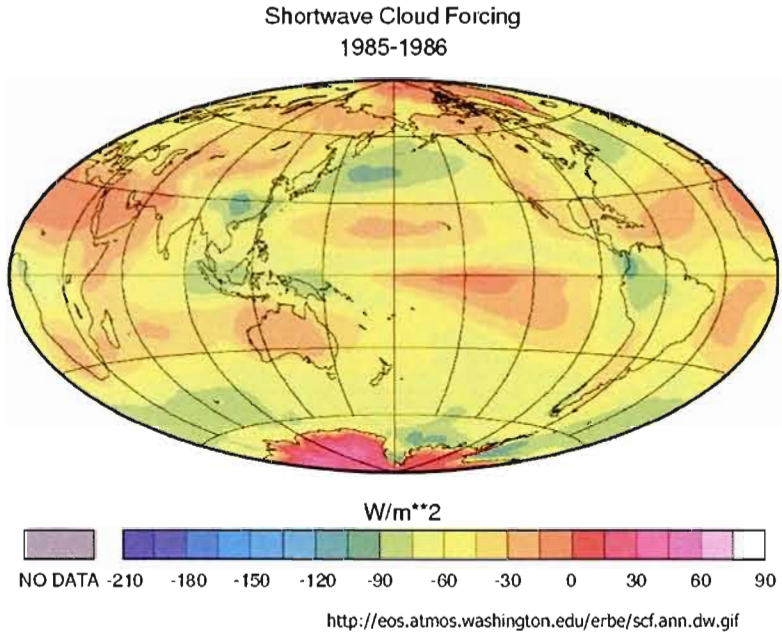

Figure I3: Annual ISR CRF.

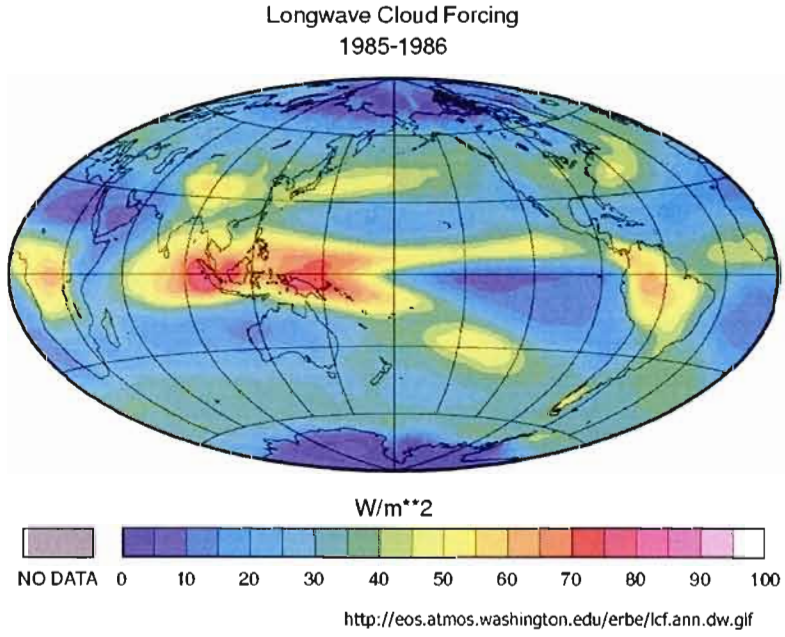

Figure I4: Annual DLR CRF.

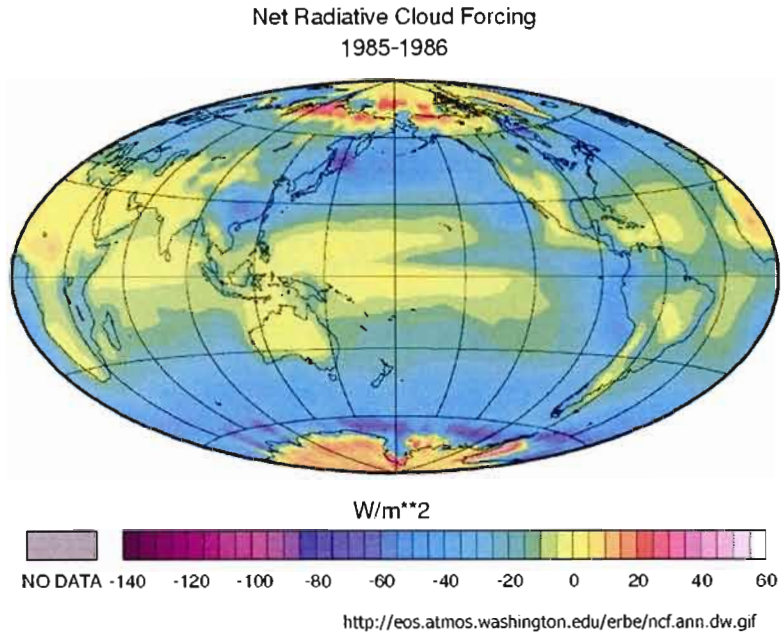

Figure I5: Annual Net CRF.

1. AN EVALUATION OF THE SURFACE RADIATIVE BUDGET OVER NORTH AMERICA FOR A SUITE OF REGIONAL CLIMATE MODELS AND REANALYSIS DATA, PART: 1 COMPARISON TO SURFACE STATION OBSERVATIONS

This chapter will be present as first of two-part Article in a suitable format. The article will be submitted to the evaluation committee in the following months. List of figures from this chapter can be found in the opening part, while references are given at the end of this thesis.

An Evaluation of the Surface Radiation Budget Over North America for a Suite of Regional Climate Models and Reanalysis Data, Part 1: Comparison to Surface Stations Observations

Marko Markovic
Department of Earth and Atmospheric Sciences. University of Quebec at Montreal.
Ouranos, 550 Sherbrooke West, 19th floor, West Tower, Montreal, Quebec H3A 1B9, Canada

Colin Jones
Department of Earth and Atmospheric Sciences. University of Quebec at Montreal

Paul A. Vaillancourt
Recherche en Prévision Numérique, Meteorological Research Division,
2121 Route Transcanadienne Dorval, Quebec, H9P 1J3, Canada

Dominique Paquin
Consortium Ouranos
550 Sherbrooke West, 19th floor, West Tower, Montreal, Quebec H3A 1B9, Canada

Danahé Paquin-Ricard
Department of Earth and Atmospheric Sciences. University of Quebec at Montreal.
Ouranos, 550 Sherbrooke West, 19th floor, West Tower, Montreal, Quebec H3A 1B9, Canada

Corresponding Author address:
Colin Jones
Department of Earth and Atmospheric Sciences
University of Quebec at Montreal
Ouranos, 550 Sherbrooke West, 19th floor, West Tower
Montreal, Quebec H3A 1B9, Canada
Tel: (514) 282-6464 (ext.293)
Fax: (514) 282-7131
E-mail: jones.colin@uqam.ca

Abstract

Components of the surface radiation budget (SRB) (Incoming Shortwave Radiation, [ISR] and Downwelling Longwave Radiation, [DLR]) and cloud cover are assessed for 3 Regional Climate Models (RCM) forced by analysed boundary conditions, over North America. We present a comparison of the mean seasonal and diurnal cycles of surface radiation between the three RCMs, and surface observations. This aids in identifying in what type of sky situation simulated surface radiation budget errors arise. We present results for total-sky conditions as well as overcast and clear-sky conditions separately. Through the analysis of normalised frequency distributions we show the impact of varying cloud cover on the simulated and observed surface radiation budget, from which we derive observed and model estimates of surface cloud radiative forcing. Surface observations are from the NOAA SURFRAD network. For all models DLR all-sky biases are significantly influenced by cloud-free radiation, cloud emissivity and cloud cover errors. Cloud-free DLR exhibits a systematic negative bias during cold, dry conditions, probably due to a combination of omission of trace gas contributions to the DLR and a poor treatment of the water vapor continuum at low water vapor concentrations. Overall, models overestimate ISR all-sky in summer, which is linked with an underestimate of cloud cover. Cloud-free ISR is relatively well simulated by all RCMs. We show that cloud cover and cloud-free ISR biases can often compensate to result in an accurate total-sky ISR, emphasizing the need to evaluate the individual components making up the total simulated SRB.

Key words: surface radiation, solar and longwave radiation, regional climate model evaluation, surface observations.

1. Introduction.

Downwelling longwave and shortwave radiation at the surface are two key terms in the surface energy budget and therefore important parameters to accurately simulate in climate models. Systematic biases in the representation of the surface radiation budget (SRB) can lead to errors in a number of key near surface climate variables (e.g. soil moisture, snow cover and sea-ice amounts).

A number of researchers have previously evaluated the surface radiation budget in climate models. Wild et al. (1995) compared various Global Climate Models (GCMs) against surface measurements. All the analysed models tended to overestimate the Incoming Shortwave Radiation (ISR) values. One of the main reasons cited was that the clear-sky atmosphere in the models absorbed less solar radiation that observations suggested. With respect to Downwelling Longwave Radiation (DLR), all models underestimated the observations due both to errors in the simulated cloud fraction as well as due to an underestimate of DLR under cloud-free conditions. Garrat and Prata (1996) compared the simulated DLR in several GCMs against surface observations over a variety of continental regions. They found annual mean DLR errors of $\sim \pm 10 Wm^{-2}$ for the GCMs evaluated. The authors linked DLR errors with neglect of trace gases (e.g. N_2O, SO_2, $CFCs$), aerosols, biases in boundary-layer humidity, errors in near-surface temperature or erroneous cloud cover. Wild et al. (2001) compared DLR from different GCMs and ERA15 against surface observations for all-sky and cloud-free conditions. They concluded that similar biases in simulated DLR between ERA15 and the GCMs arose primarily due to common errors in the respective radiation schemes, rather than due to differences in the thermodynamic input to the radiation scheme. DLR biases identified in all-sky conditions were generally associated with errors in the clear-sky DLR and tended to be largest, in a relative sense, in the winter season. Wild et al. suggested a probable cause of this bias was a poor representation of the water vapor continuum during cold

and dry atmospheric conditions. Results from Iacono et al. (2000) suggest a more detailed treatment of the water vapor continuum under dry conditions can potentially ameliorate this error. Roads et al. (2003) analyzed a number of Regional Climate Models, concentrating on the simulated ISR over North America. While their conclusions were limited by the availability of observational data, errors in simulated cloud cover were strongly linked with biases in the simulated ISR in the models analyzed.

In this study, surface observations at a number of sites across North America are used to evaluate downwelling ISR and DLR in 3 RCMs run for the recent past (1999-2004) using analysed lateral boundary conditions. Configuring a RCM to run forced by analysed boundary conditions constrains the model simulated large-scale meteorology to follow the observed evolution relatively closely. Along with a relatively high model resolution ($\sim 0.5^{\circ}$), this allows for a comparison of the performance of key parameterisation schemes, such as radiation and cloud schemes, against high quality surface observations.

The RCMs will be directly compared with available ground-based measurements over the continental USA. We evaluate the surface radiation budget in a variety of climate conditions, for cloudy and clear-sky conditions separately and as function of season and time of day. In doing this we aim to isolate conditions and situations where the respective cloud and radiation schemes operate poorly and thereby identify aspects of the respective parameterisation scheme that require improvement in order to improve the simulated SRB.

In Part 2 of this work we use the surface point observations to evaluate the satellite derived surface radiation budget from the ISCCP dataset and the SRB for the North American Regional Reanalysis (NCEP) and ECMWF (ERA40) reanalysis products. This is done to determine which of these spatially and temporally complete SRB datasets is most accurate and therefore most suitable as a validation tool for the

RCM simulated SRB over the entire North America. We subsequently evaluate the seasonal and annual cycle of the RCM simulated SRB against the most representative surrogate observation data set.

2. Models and Observations.

The models used in this assessment are: The Canadian Regional Climate Model (CRCM, version 4.0) (Caya and Laprise, 1999), GEM-LAM, the regional version of the Global Environmental Multiscale Model (Côté et al, 1998) and third, RCA3, the regional model from the Rossby Centre (Jones et al. 2004).

In CRCM shortwave (SW) radiation is treated using a photon path method with scattering incorporated through the Delta-Edington technique (Fouquart and Bonnel, 1980) with 4 bands in the visible and near IR. Longwave (LW) radiation is treated with a broadband flux emissivity approach, with temperature and pressure dependant gaseous absorption included, following Morcrette (1991). The Aerosol input in CRCM uses a prescribed, zonal mean distribution with different concentrations applied over ocean and land regions. Aerosols are assumed to be homogeneously distributed within the boundary layer, with the scattering and absorption properties based on the work of Shettle and Fenn (1979). In RCA3 clear-sky SW radiation is reduced from the top of the atmosphere value by: parameterised broad-band ozone absorption, water vapor absorption and Rayleigh scattering by air molecules. Aerosol effects in RCA3 are incorporated simply by multiplying the water vapour absorption term and the Rayleigh scattering term each by separate constants, that aim to represent the effects of clear-sky aerosol scattering and absorption on the surface solar radiation flux. A discussion of the appropriate values for these constants can be found in Sarvijarvi (1990). In the runs reported here the constant amplifying clear-sky absorption, caak, is set equal to 1.3, while that amplifying the clear-sky

scattering of the solar flux, cask, is set to 1.35. Cloud scattering and absorption of SW radiation follow the parameterisation of Slingo (1982). LW radiation is treated with a broadband emissivity scheme, following the approach of Rogers (1977) and Stephens (1984). The RCA3 radiation scheme is further described in Savijarvi (1990) and Räisänen (2000). The GEM-LAM radiation code includes IR absorption and emission from all of the following trace gases: H_2O, CO_2, O_3, N_2O, CH_4, $CFC11$, $CFC12$, $CFC13$ and $CFC14$, CRCM and RCA3 treat just the first three. GEM-LAM radiation uses a correlated-k distribution method (CKD) for gaseous transmission with 9 frequency intervals for LW and 4 frequency intervals for SW radiation. Cloud infrared scattering is included as is cloud vertical overlap (Li and Barker, 2005). In GEM-LAM 2 formulations describing the total optical thickness of aerosols are applied, one appropriate for land and the other over the ocean (Toon and Pollack, 1976). These distributions include a latitudinal gradient. Aerosols are assumed only to affect the solar absorption properties of the clear-sky atmosphere.

The cloud schemes in all 3 models follow the basic approach of Sundqvist et al. (1989) with some differences between each model. Cloud fraction is diagnosed as an increasing function of grid box mean relative humidity, beyond a threshold humidity value.

The surface ground measurements are taken from the Surface Radiation Network (SURFRAD) coordinated by NASA. We used six observational sites representing a cross-section of various climate types over North America (see Figure 1.1). SURFRAD stations have adopted the standards for measurement accuracy set by the Baseline Surface Radiation Network (BSRN), which are an accuracy of $\pm 15 Wm^{-2}$ for broadband solar measurements and $\pm 10 Wm^{-2}$ for thermal infrared measurements.

To correct for the effect of orographic differences between model and observations we apply a constant correction of $2.8\,Wm^{-2}$ per $100\,m$ to the model DLR values where the two orographic heights differ, as detailed by Wild et al. (1995).

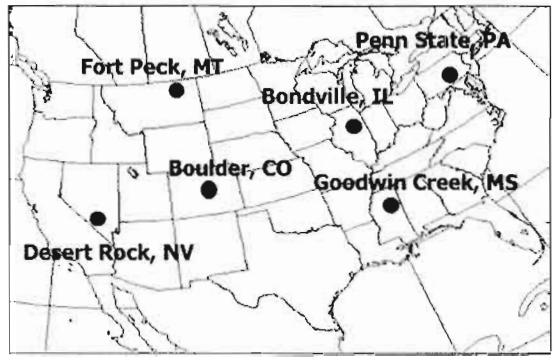

Figure 1.1: SURFRAD ground stations used in this study (Spatial map derived from: http://www.srrb.noaa.gov/surfrad/surfpage1.html).

3. Evaluating the simulated annual cycle of ISR and DLR at the 6 SURFRAD sites.

In this section we compare the simulated surface radiation from the 3 RCMs against surface observations. We extract 3-hourly average ISR and DLR from the 6 SURFRAD stations and from the 4 model grid boxes closest to each respective station. A comparison of RCM simulated SRB using the single grid box collocated with the SURFRAD stations versus an average of the 4 nearest grid boxes showed almost no difference (results not shown), hence all analysis in this paper uses a 4 grid box mean value for simulated SRB.

The analyzed period is determined by the common time period between the 3 RCM simulations and the availability of station observations, this results in a common analysis period of 2000-2004. We analyse the annual cycle of monthly mean all-sky radiation (including all-sky conditions irrespective of cloud fraction).

We further analyse frequency distributions of 3 hourly ISR and DLR from the 3 RCMs and surface observations, separately for winter (DJF) and summer (JJA). In later sections we will consider more closely the ISR and DLR in cloudy-sky and clear-sky conditions and include an evaluation of the surface cloud radiative forcing and the simulated diurnal cycle of the SRB.

Figure 1.2a shows the mean annual cycle of ISR averaged over the 6 sites, for the 3 RCMs and observations, while Figure 1.2c shows monthly mean biases in the simulated ISR. GEM-LAM and CRCM accurately represent ISR in winter, (~2 Wm^{-2} bias) while there is an overestimation of ISR in summer in these 2 models (~20-30 Wm^{-2}). In contrast, RCA3 is relatively accurate during summer but has the largest ISR biases in spring and winter (~10-20 Wm^{-2} overestimate). One probable cause of the summer season biases in ISR lies in an underestimate of cloud amounts in all 3 models. Figure 1.3 shows a time restricted, long-term mean diurnal cycle of cloud cover for all sites during the extended summer season (April-August). Cloud cover observations at the SURFRAD sites use an RGB cloud-detecting camera (http://www.srrb.noaa.gov/surfrad/tsipics.html), which operates only during daylight hours. Hence, for the summer season cloud cover analysis, we are constrained to using a common daylight period for the 6 sites, which is 15-00 UTC (approximately 9-18 in local time).

Two observational estimates are presented for observed cloud amounts (Figure 1.3). The first is directly from the RGB camera (in black). The second curve (in gray) utilizes the findings from a number of studies (e.g. Karlsson, 2003) that suggest surface based cloud cover observations are generally biased high in the summer season. This mainly results from surface observations and scanning cameras frequently observing the sides of vertically stacked cumulus clouds and attributing this cloud as an overhead cloud fraction. Satellite sensors typically view the projected

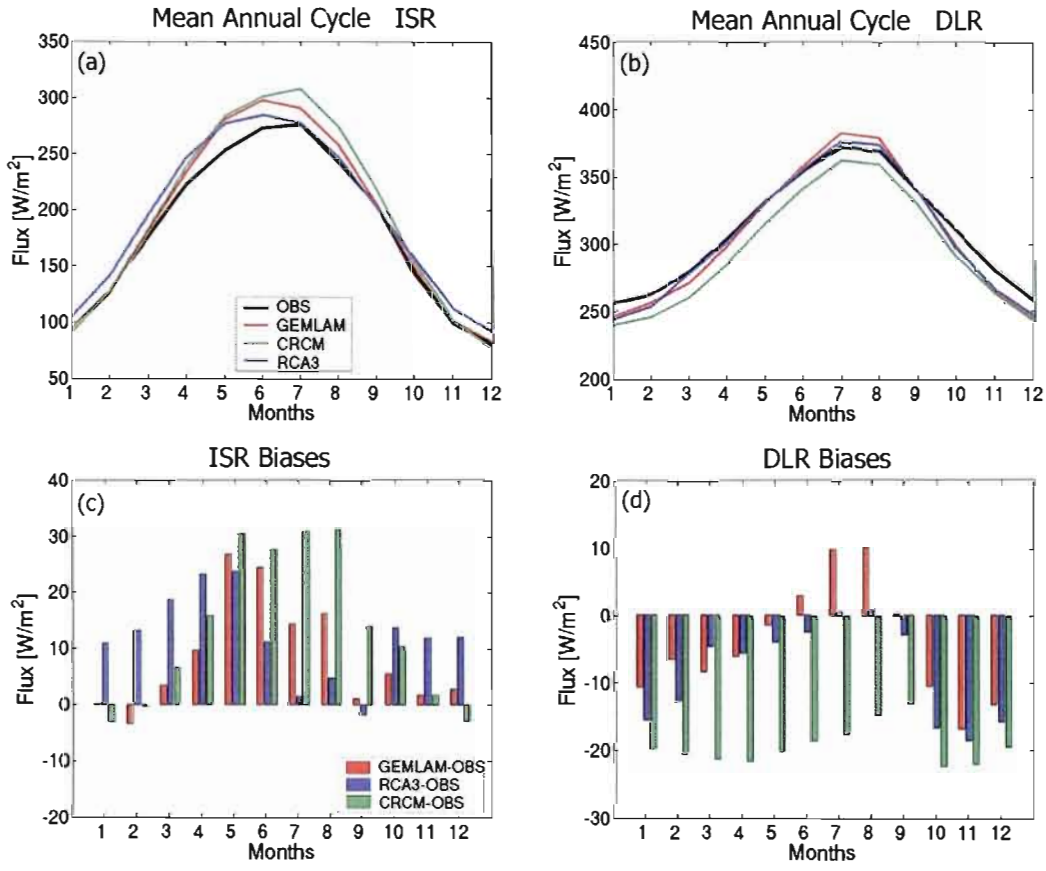

Figure 1.2: (a) Mean annual cycle of monthly mean ISR, (b) DLR, (c) monthly mean differences in ISR between each model and observations, (d) differences in DLR between each model and observations. All values are averaged across the entire diurnal cycle.

cloud top and therefore have a cloud cover more analogous to the overhead cloud fraction defined in numerical models. We have applied an approximate correction to the RGB cloud cover based on the findings of Karlsson et al. (2003), that suggest satellite cloud cover in the summer season over Scandinavia is systematically lower than surface based estimate by ~5-10%. Even with this correction it is clear that all 3 RCMs systematically underestimate cloud cover during this part of the summer season diurnal cycle, with CRCM being the worst offender. As a result they will

significantly overestimate all-sky ISR during this period of the day. Simulating the diurnal cycle of summer season convection and associated cloudiness is a problem common to many climate models (Lenderink et al. 2004, Yang and Slingo 2001). An inability to simulate sufficient convective activity in a given model will likely lead to an underestimate of cloud cover and overestimate of the surface solar radiation flux. This excess radiation will lead to a warm and dry bias developing at the surface, further compounding the initial convection-cloud error. In this manner, cloud-convection errors can be amplified by surface-atmosphere feedbacks, leading to a negative cloud bias accompanied by a mid-continent, surface warm/dry bias (Wild et al. 1996) A more detailed analysis of how the 3 models represent surface radiation as a function of cloud cover will be presented in Section 4.

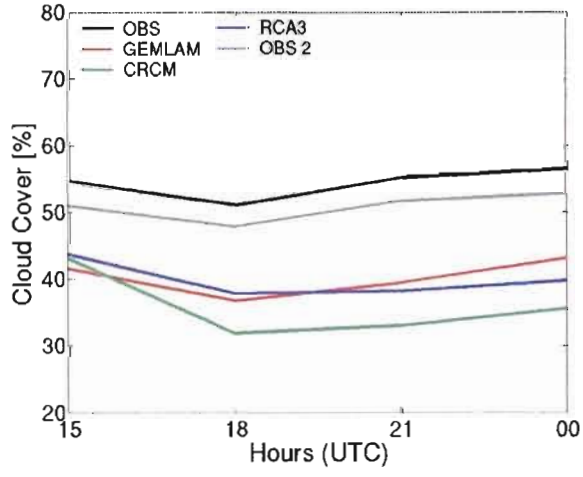

Figure 1.3: Long Term Mean Annual Cycle of Cloud Coverage. All Sites, Season April-August.

Figures 1.2b and 1.2d show the mean annual cycle of DLR for the 3 RCMs and surface observations, as well as presenting the mean annual cycle of DLR biases (RCM-OBS). GEM-LAM and RCA3 produce a relatively accurate representation of DLR, except in the winter season when there is an underestimate of ~10-20 Wm^{-2} in

both models. As with DLR winter errors in ERA15, this type of DLR error may be associated with problems in representing the water vapor continuum in cold, clear-sky conditions during winter (see Wild et al., 2001) or the neglect of trace gases in the calculation of DLR (Garrat and Prata, 1996). The trace gas contribution to total DLR will become relatively more important in cold, dry conditions as the total DLR becomes less dominated by water vapor emission. This issue will be returned to in Section 4 where we analyse in more detail the RCM simulated surface radiation in clear and cloudy conditions separately. GEM-LAM underestimates DLR in the winter by $\sim 10 Wm^{-2}$ with a slight overestimate in the summer season. The RCA3 winter negative bias is $\sim 15 Wm^{-2}$ with summer values being very accurate. CRCM gives a constant underestimate of DLR throughout the year of $\sim 20 Wm^{-2}$. We will subsequently indicate that this bias is consistent with a year round underestimate of cloud fraction and cloud liquid water path in this model.

As a further validation of the RCMs surface radiation we present a comparison of the 3 hourly surface flux values from the 3 RCMs and observations. Figure 1.4 presents normalized frequency distributions of surface ISR and DLR separately for summer (JJA) and winter (DJF) as derived from surface observations and the RCMs, both averaged over the 6 SURFRAD stations collocated with the RCM grid points. The normalized frequency distribution expresses the occurrence of a given 3 hourly ISR or DLR value as a fraction of the total number of 3 hourly occurrences in a given season. In making this analysis we wish to determine whether the RCMs not only simulate the monthly mean ISR and DLR but also the higher time frequency variability in the surface radiation budget, which makes up the seasonal mean values.

The period used in constructing the frequency distributions encompasses 5 years (2000-2004). The RCM data are 3 hourly average radiation fluxes, hence the observations have been averaged to the same time period. Values along the x-axes

indicate the band of ISR or DLR values for which a given frequency of occurrence has been calculated (e.g. a value of 350 in the ISR plot indicates a band of ISR between 300-350 Wm^{-2} while for DLR the value of 350 indicates a band of DLR between 330-350 Wm^{-2}. The band width for ISR is 50 Wm^{-2} for the entire range of values, while for DLR it is 20 Wm^{-2}). Nighttime is not included in the ISR analysis thus the first ISR band is 5-50 Wm^{-2}. Nighttime is included in the DLR distribution.

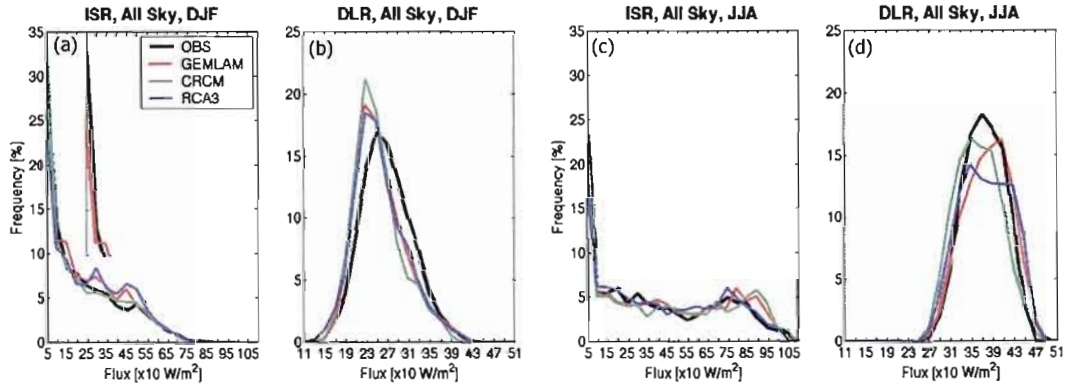

Figure 1.4: Distribution of 3 hourly fluxes from RCMs and observation, a) ISR winter season, b) DLR winter season, c) ISR summer season, d) DLR summer season. The inset on 1.4a shows in more detail GEM-LAM and observed values within the range 5-200.

The 3 RCMs represent winter and summer mean ISR and DLR with a reasonable degree of accuracy, nevertheless a few systematic biases can be seen in Figure 1.4. RCA3 overestimates DJF ISR (Figure 1.4a) in the range of 200-500 Wm^{-2} and slightly underestimates the occurrence of values less than 200 Wm^{-2}. This is consistent with its positive bias of DJF ISR in Figure 1.2a. We will show in Part 2 of this work that this error structure in the DJF ISR distributions is also seen in the ERA40 results (see Part 2, Section 3). This type of error structure is consistent with an overall underestimate of cloud amounts (see Figure 1.6). It is also consistent with simulated winter season clouds being not sufficiently reflective. RCA3 uses the same

functional form as ERA40 to partition cloud water into liquid and frozen fractions (The fraction of cloud water assumed as frozen increases from 0 to 1, as the second power of temperature in the range $0 \rightarrow -22^{\circ}C$). Recent observations (e.g. Shupe et al., 2006) suggest liquid droplets are present in clouds over the Arctic down to temperatures as low as $-39^{\circ}C$. As with ERA40 it is possible that RCA3 therefore has a systematic overestimate of the ice fraction in mixed phase clouds leading to an overestimate of the median effective radius and an underestimate of cloud reflectivity. This will be discussed more in Section 4 where cloud-free and cloudy-sky radiation along with cloud fraction are evaluated together. GEM-LAM also has a positive bias in the occurrence of ISR in the range of 250-500 Wm^{-2}, which is balanced by the underestimate of ISR low occurrences (< 200 Wm^{-2}, see the inset on Figure 1.4a). CRCM gives a very good representation of DJF ISR.

In the summer season (Figure 1.4c) GEM-LAM and CRCM overestimate the occurrence of very high (>800 Wm^{-2}) ISR values. These high values of ISR are likely associated with clear-sky conditions and the overestimate in this ISR range will result from an underestimate of cloud amounts in the middle of the day (as shown in Figure 1.3). RCA3 has a smaller positive bias in this range of ISR, even though it too has a similar underestimate of cloud fraction during early afternoon in summer (see Figure 1.3). This suggests that while RCA3 underestimates the fractional cloud amount during this period, the clouds simulated in this model are significantly more reflective than in GEM-LAM or CRCM, compensating for the underestimate of cloud amount in terms of total surface ISR. In Section 4 we will further show that the RCA3 *clear-sky* ISR is underestimated compared to the observed ISR in equivalent *clear-sky* conditions, implying the RCA3 clear-sky atmosphere is too opaque. This error will also act to ameliorate ISR errors, associated with an underestimate of cloud fraction, in terms of the total-sky ISR. These types of compensation indicate the importance of evaluating all terms controlling the surface radiation budget in a model in order to improve the physical realism of simulated cloud-radiation processes.

The winter DLR frequency distribution shows all models have a peak occurrence shifted towards lower values than observed. This shift leads to an underestimate in the mean DLR in winter (Figure 1.2b). In summer (Figure 1.4d) GEM-LAM and RCA3 follow the observed distribution quite well, while CRCM simulated DLR remains shifted towards lower values (Figure 1.2b). A discussion of the cause of these errors is deferred to Section 4 where we analyse the surface radiation frequency distributions separately for clear and cloudy conditions.

4. Understanding cloud-radiation errors in the 3 RCMs.

4.1 Evaluating simulated ISR and DLR under different cloud cover conditions.

In Figure 1.5 we present the daytime mean annual cycle of ISR and DLR under all-sky (Figures 1.5a and 1.5b) and cloud-free conditions (Figures 1.5c and 1.5d). All-sky condition refers to ISR and DLR values for all cloud cover conditions (0-100% cloud cover) while cloud-free ISR and DLR are those values when observations or models have cloud cover less then 10%. Conditions with less than 10% of cloud cover are taken as *cloud-free,* rather than using 0% as the threshold, which significantly reduces the number of cloud-free occurrences available for analysis. However, sensitivity tests on some SURFRAD sites done for 0% of cloud cover showed the same basic results.

Despite the shorter diurnal cycle used in this section, DLR and ISR all-sky model errors are similar to those seen when the entire diurnal cycle is used (Figures 1.2a and 1.2b). ISR errors are slightly amplified due to our concentration on daylight hours. We are therefore confident that cloud and clear-sky radiation errors found using this shortened diurnal cycle will be representative.

To better understand the underlying causes of the all-sky radiation errors we analyse cloud-free radiation fluxes separately. ISR in cloud-free conditions (Figure

1.5c is underestimated in the winter season by all models (a negative bias of ~15-20 Wm^{-2}). One possible reason for the winter ISR clear-sky biases could be that

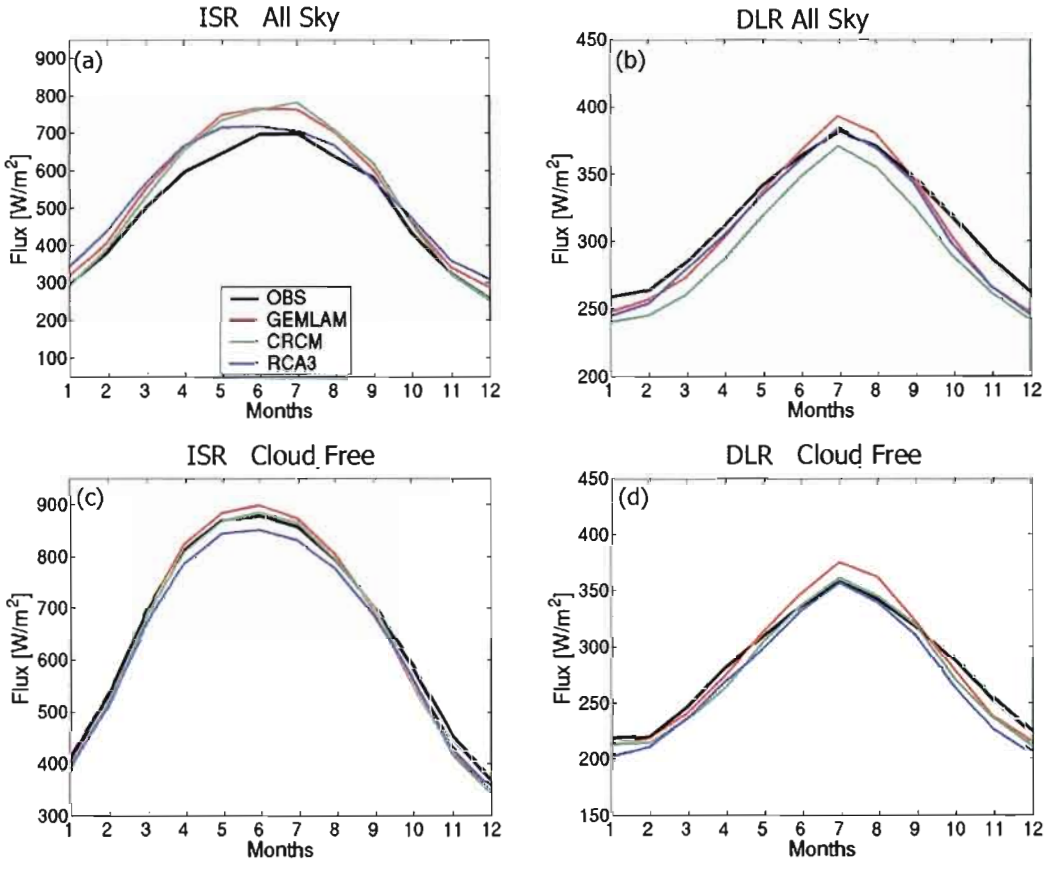

Figure 1.5: (a) Mean annual cycle of ISR, total-sky, (b) mean annual cycle of DLR, total-sky, (c) mean annual cycle of ISR, clear-sky, (d) mean annual cycle of DLR, clear-sky. Daytime, period 15-21UTC.

models underestimate the occurrences of cloud cover at high integrated water values compared to observations: hence the *simulated clear-sky* systematically samples higher integrated water vapor values and therefore experiences an atmosphere more opaque to solar radiation, resulting in an *apparent* negative bias in modeled clear-sky ISR. This negative clear-sky bias is in the opposite sense to the winter season ISR

biases in all-sky conditions (positive biases of ~10-50 Wm^{-2}) and strongly suggests the ISR all-sky biases in winter are dominated by an underprediction of cloud amount and or cloud reflectivity. In summer GEM-LAM and CRCM show only small biases in cloud-free ISR (5-15 Wm^{-2}), far better than in all-sky conditions. RCA3 underestimates clear-sky ISR during the summer season by 20-25 Wm^{-2}.

In Figure 1.6 we present a comparison of cloud cover for the 3 RCMs against observations from the SURFRAD stations. The annual cycle is constructed for the same daytime period as used in Figure 1.5. Even considering potential errors in the cloud observations all models underestimate cloud cover especially for the JJA season. In Figure 1.5c we showed that RCA3 underestimated ISR in summer season clear-sky conditions. This negative bias in cloud-free ISR will partially offset an underprediction of cloud cover in RCA3 (too frequent occurrence of cloud-free conditions) leading to a relatively accurate all-sky ISR due to 2 compensating errors (i.e. too frequent occurrence of clear-sky conditions which are excessively opaque to solar radiation). GEM-LAM and CRCM have relatively accurate cloud-free ISR. Due to the underestimate of cloud cover, they both significantly overestimate ISR for JJA all-sky conditions. Put in another way, the surface solar radiation flux in GEM-LAM and CRCM is (correctly) more sensitive to cloud errors than in RCA3.

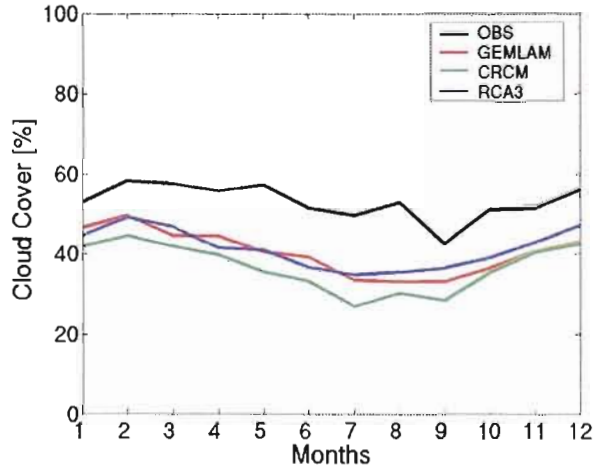

Figure 1.6: Mean annual cycle of cloud cover. Daytime period 15-21 UTC.

In order to investigate this problem further we made a sensitivity experiment with the RCA3 model, reducing the 2 constants (caak and cask) used to amplify clear-sky solar absorption and scattering. In the original RCA3 runs these constants were set to 1.3 and 1.35 respectively. In the new run (RCA3aero) the constants were reduced to 1.2 and 1.25. Figure 1.7 shows the original monthly-mean ISR all-sky and clear-sky biases for June, July and August. A relatively accurate all-sky ISR (black bar in Figure 1.7a) comes about partially from a negative bias in the clear-sky ISR (Figure 1.7b) balancing an underestimate of cloud fraction. Reducing the aerosol absorption/scattering terms improves the clear-sky ISR flux in RCAaero. The reduced clear-sky opacity is now not available to balance the cloud underestimate in RCA3, and as with GEM-LAM and CRCM, a significant positive bias in all-sky ISR develops, coincident with an accurate clear-sky surface flux. Figure 1.7b shows the difference in the clear-sky ISR due to the changed aerosol treatment, with ISR values increasing by ~40-50 Wm^{-2}. Figure 1.7a shows the change in the all-sky ISR flux between RCA3 and RCA3aero. The all-sky flux increase is slightly amplified over the clear-sky increase, presumably due to the increased absorption of solar radiation

in the model atmosphere leading to a warming and relative drying and therefore reduced cloud cover.

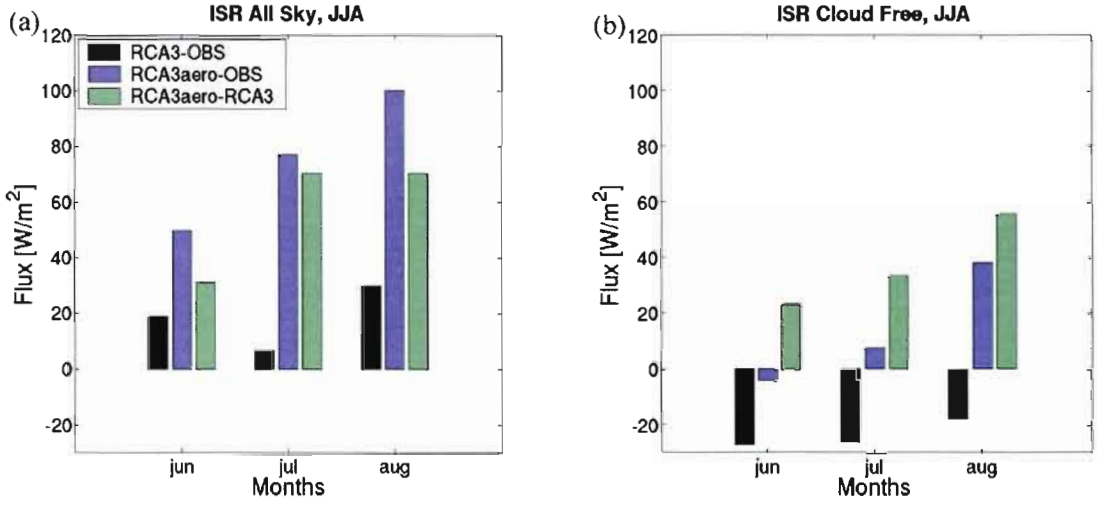

Figure 1.7: Comparison of JJA ISR biases for two RCA3 runs with the different aerosol treatment, a) all-sky, b) clear-sky. Daytime, period 15-21 UTC.

Cloud-free DLR errors in GEM-LAM and RCA3 look very similar to the all-sky DLR errors throughout the annual cycle, suggesting clear-sky DLR problems dominate the all-sky DLR in these two models. Cloud-free DLR errors in CRCM are comparable to the other two models across the annual cycle. This is not true for all-sky conditions where CRCM has a large year-round negative bias, suggesting the all-sky DLR error in CRCM is a result of both a clear-sky bias which is amplified by cloud-sky errors. It is worth noting that both GEM-LAM and RCA3 have a prognostic treatment of cloud water with a Sundquist type treatment of precipitation loss (Sundquist, 1989). Cloud water is consistently treated between the radiation and cloud microphysics. CRCM does not have prognostic cloud water, all supersaturation is assumed to be removed as precipitation in the microphysics and cloud water amounts in the radiation are diagnosed using the approach due to Betts and Harshvardan (1987). Errors in the DLR suggest this approach may be leading to a

systematic underestimate of cloud emissivity in CRCM. (We will return to this point later).

In order to expand the analysis untaken in this section, we present winter and summer season biases at individual SURFRAD sites for all-sky (Table 1.1) and cloud-free (Table 1.2) conditions. This is done to ascertain that the spatially mean results presented so far do not hide large error compensation in either of the SRB components. For JJA ISR in cloud-free conditions, GEM-LAM and RCA3 confirm the spatially mean results presented in Figure 1.5c, while some cancellation of opposite signed biases is seen in CRCM. We emphasize that the ISR results presented in Table 1.1 are averages across the approximate 6-hour period when solar flux is maximum. Hence the ISR biases are significantly larger than if they were averaged across the diurnal cycle, as frequently done. The DJF ISR cloud-free negative biases presented in Table 1.2 also confirm the general underestimate within all models seen in the spatial mean results. In JJA the only DLR term showing some spatial cancellation is the CRCM flux. Otherwise the majority of the conclusions drawn from the spatial mean results are valid when the 6 sites are considered separately.

		GEM-LAM		CRCM		RCA3	
All-sky		ISR	DLR	ISR	DLR	ISR	DLR
Bondville, IL	DJF	28.3	-6.4	13.5	-16.3	61.2	-15.2
Boulder, CO	DJF	36.4	-15.8	7.3	-22.4	62.5	-9.0
Desert Rock, NV	DJF	12.6	-13.1	-47.7	-13.2	28.1	-12.0
Fort Peck, MS	DJF	-1.8	-4.4	-23.2	-23.0	35.4	-8.0
Goodwin Creek, MT	DJF	50.5	-9.5	38.2	-15.6	89.0	-19.5
Penn State, PA	DJF	31.0	-12.7	22.3	-21.3	44.0	-12.4
Bondville, IL	JJA	81.1	15.6	104.4	1.5	10.5	6.8
Boulder, CO	JJA	55.0	6.9	54.4	-21.8	68.2	-5.8
Desert Rock, NV	JJA	1.0	2.0	-1.7	-30.3	1.1	-14.3
Fort Peck, MS	JJA	56.0	16.2	46.6	-15.3	62.2	0.6
Goodwin Creek, MT	JJA	110.4	8.5	153.5	-6.7	-30.6	6.9
Penn State, PA	JJA	110.4	-0.9	110.1	-8.9	-20.9	4.8

Table 1.1: Winter and summer season DLR and ISR biases for 3 RCMs on 6 individual SURFRAD stations for all-sky condition.

		GEM-LAM		CRCM		RCA3	
Cloud-free		ISR	DLR	ISR	DLR	ISR	DLR
Bondville, IL	DJF	-19.6	5.0	-16.5	3.6	-38.5	-9.0
Boulder, CO	DJF	-6.8	-8.7	-28.6	-8.2	1.6	-11.8
Desert Rock, NV	DJF	0.1	-13.1	-34.8	-12.5	-3.2	-16.1
Fort Peck, MS	DJF	-19.4	-0.7	-26.8	-4.8	-2.8	-19.8
Goodwin Creek, MT	DJF	-7.1	-7.1	-2.9	-11.8	-20.6	-10.6
Penn State, PA	DJF	-40.6	-0.8	-14.5	-2.6	-47.9	-13.2
Bondville, IL	JJA	2.9	34.5	8.4	31.5	-50.6	15.7
Boulder, CO	JJA	36.0	7.9	-6.2	-15.5	8.0	-18.8
Desert Rock, NV	JJA	16.1	-4.5	-15.0	-28.7	-10.9	-21.1
Fort Peck, MS	JJA	31.9	6.5	12.3	-14.0	0.5	-14.0
Goodwin Creek, MT	JJA	21.2	32.3	32.3	24.1	-30.3	10.4
Penn State, PA	JJA	-10.3	22.8	8.0	24.4	-61.9	17.0

Table 1.2: Winter and summer season DLR and ISR biases for 3 RCMs on 6 individual SURFRAD stations for cloud-free condition.

4.2 Evaluating surface cloud radiative forcing.

To summarize the cloud contribution to the total SRB we construct mean annual cycles of surface Cloud Radiative Forcing (CRF) for ISR and DLR (Figure 1.8). The definition of surface CRF used here is the difference in surface incoming radiation between all-sky and cloud-free conditions. Due to limitations in cloud observations, the CRF is constructed for the daytime period common to all SURFRAD sites, namely 15-21 UTC (9-15 approximate local time). ISR CRF errors will therefore be exaggerated relative to DLR CRF errors, compared to a full integration across the diurnal cycle. Two observational estimates of the ISR CRF are presented in Figure 1.8 (gray bars).

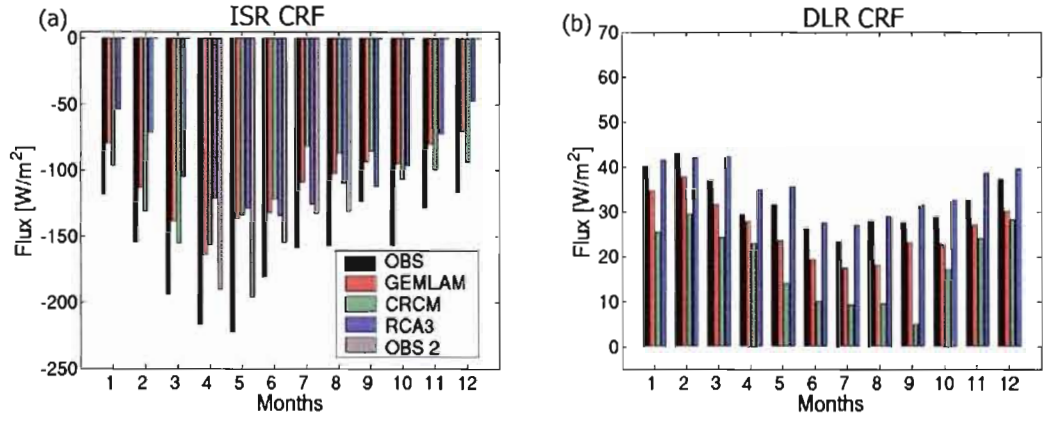

Figure 1.8: Mean annual cycle of cloud radiative forcing: a) ISR CRF, b) DLR CRF. Daytime period 15-21 UTC.

The second observational estimate of CRF attempts to account for the aforementioned overestimate of summer season clouds (~5-10%) by the RGB camera. Here we try to indicate the likely change in CRF if observed cloud amounts were reduced by 5-10% in the summer season. An estimate of the change of ISR for a given fractional change in cloud cover can be obtained by applying a linear best fit approximation to the figure representing observed surface ISR plotted as a function of observed cloud cover. As an example, Figure 1.9a and Figure 1.9b present observed ISR plotted against observed cloud fraction for the months April and July respectively for the Bondville station. To assess the sensitivity of the ISR-cloud fraction relationship, we separately plot 4 independent times of day. (Green corresponds to 12 LST, red to 9 LST, blue to 18 LST, and black to 15 LST). A linear best fit to these curves gives an estimate of the change in ISR for a percent change in cloud cover $\left(\frac{\partial ISR}{\partial cloud}\right)$. This technique was used for all SURFRAD sites for the period April to August and a mean $\frac{\partial ISR}{\partial cloud} \sim 3Wm^{-2}\%^{-1}$ was derived. This change in ISR was then translated into an implied ISR assuming 5-10% increase in observed cloud

amount and a second estimate of observed ISR CRF was derived. The sensitivity of DLR to this 5-10% change was an order of magnitude smaller than the ISR sensitivity and was therefore not included. The second estimate of observed CRF should be viewed simply as an uncertainty range for CRF due to uncertainties in the observed cloud fraction.

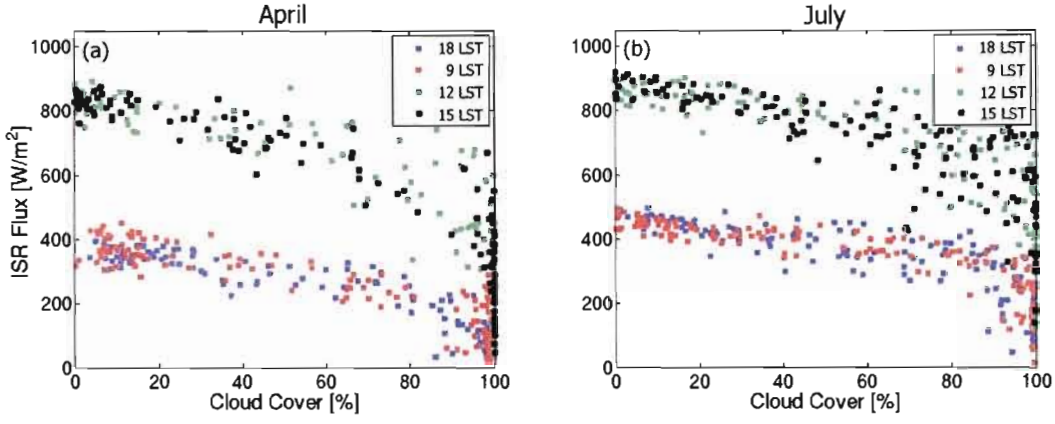

Figure 1.9: ISR occurrences through analysed diurnal cycle against different cloud cover for Bondville a) for the month of April, b) for the month of July.

The ISR CRF in Figure 1.8a shows all models underestimate ISR cloud radiative forcing compared to observations, especially for spring and summer, commensurate with the largest biases in all-sky ISR. For GEM-LAM and CRCM errors are mainly due to cloudy-sky errors (e.g. an underestimate of cloud fraction and possible underestimate of LWP). These errors are also present in RCA3 (e.g. cloud fraction underestimate and possible underestimate of CRCM LWP presented in Figure 1.10 and GEM-LAM LWP, personal communication from Danahé Paquin-Ricard) but are partially balanced by the clear-sky atmosphere being too opaque to ISR.

DLR CRF (Figure 1.8b) is underestimated by GEM-LAM and CRCM throughout the year. Again this is partially a result of the systematic underestimate of

cloud cover. RCA3 has an accurate simulation of DLR CRF even though it too underestimates cloud fraction. This underestimate must be partially compensated by RCA3 simulated cloud emissivity being too high.

Summer ISR CRF errors are smallest in GEM-LAM and RCA3 commensurate with smaller cloud errors in these two models compared to CRCM. In the winter season RCA3 has the largest negative bias in ISR CRF while having a very accurate estimate of DLR CRF. GEM-LAM and RCA3 have similar cloud amounts during the winter season, suggesting a problem in RCA3 specific to the treatment of winter (ice and mixed phase) clouds in the solar portion of the radiation scheme.

CRCM has the poorest DLR CRF, with an underestimate of $15\,Wm^{-2}$ throughout the year (Figure 1.8b). The primary reason for this underestimate is the relatively large cloud cover bias in CRCM and also a probable underestimate of cloud water path. To further explain CRCMs underestimate of DLR CRF (Figure 1.8b) we present a normalized frequency distribution of vertically integrated LWP used in the radiation scheme of the CRCM model and observed by the microwave radiometer at the ARM Southern Great Plains site (Figure 1.10). This site is the only location over the continental US providing LWP observations, using a microwave radiometer that measures LWP for non-precipitating periods only. In Figure 1.10, the black and green bars represent LWP for non-precipitating events only, for both observations and model respectively, while the blue bar represents model LWP, including all occurrences of precipitation. The values along the x-axes indicate the band of LWP quantity for which a given frequency of distribution has been calculated (e.g. value of 15 gm^{-2} indicates a band of LWP between 0-15 gm^{-2}). For both seasons CRCM has a very clear underestimate of LWP, confirming a general underestimate in cloud emissivity, which along with the cloud fraction underestimate contributes to the year round deficit in DLR in this model. The first band in Figure 1.10 (0-15 gm^{-2}) includes the LWP values of $0\,gm^{-2}$, which is the equivalent of clear-sky events, indicating an

overestimate of clear-sky events in CRCM. Even including model LWP when precipitation is occurring (blue bar in Figure 1.10) still results in a relatively large underestimate of LWP in CRCM simulated clouds.

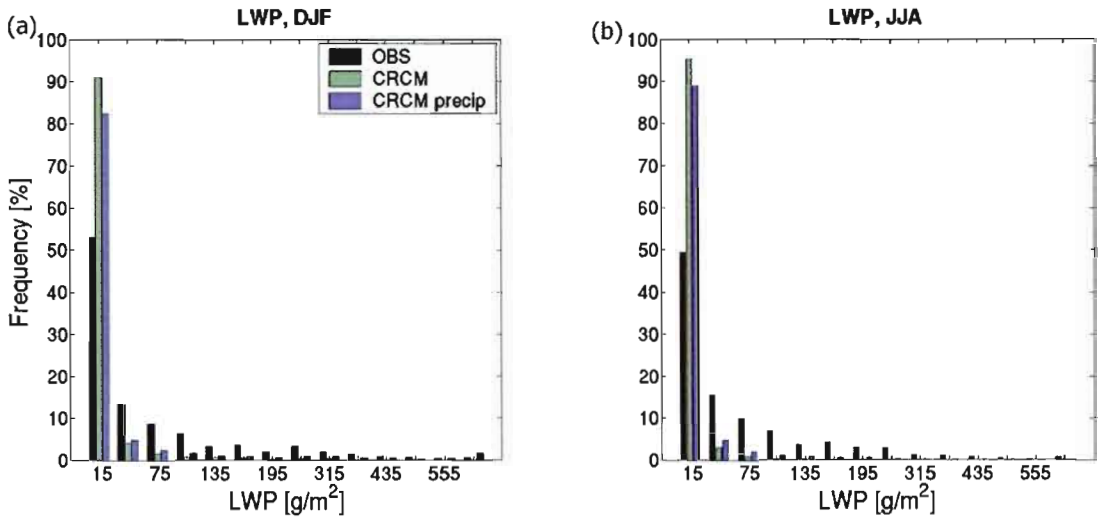

Figure 1.10: Distribution of LWP for CRCM against observations at Southern Great Plains site, a) winter season, b) summer season.

Inclusion of possible observational uncertainties in summer season cloud amounts (gray bar in Figure 1.6) and their effect of the observed ISR CRF reduce slightly the implied ISR biases in the models, nevertheless the basics conclusions remain unchanged.

4.3 Hourly histograms of ISR and DLR as a function of cloud cover.

In this section we present normalised frequency distributions of ISR and DLR where the distributions are constructed and normalised separately for all-sky, clear-sky (cloud cover <10%) and overcast (cloud cover > 90%) conditions. Frequency distributions are constructed for the daytime period 15-21 UTC (9-15h local time for

most sites) due to the observed cloud constraints, for the winter (Figure 1.11) and summer (Figure 1.12) seasons. The winter distribution of all-sky DLR (Figure 1.11d) shows that all models are systematically biased towards low values. For RCA3 and GEM-LAM this appears to be primarily due to a negative bias in the DJF DLR clear-sky frequency distribution (Figure 1.11e), DJF DLR for cloudy conditions (Figure 1.11f) being well simulated by these 2 models. CRCM has the same DJF DLR clear-sky error (Figure 1.11e) but also has a negative bias in DJF DLR during overcast conditions (Figure 1.11f). This error is when both model and observations have >90% cloud cover and is therefore not due to an underestimate of cloud fraction. This error in cloudy-sky DLR we feel is a direct consequence of the underestimate of LWP and cloud emissivity shown in Figure 1.10. The error in cloudy-sky DLR combines with the general underestimate of cloud cover in CRCM to produce the large DLR CRF negative bias seen in Figure 1.8b.

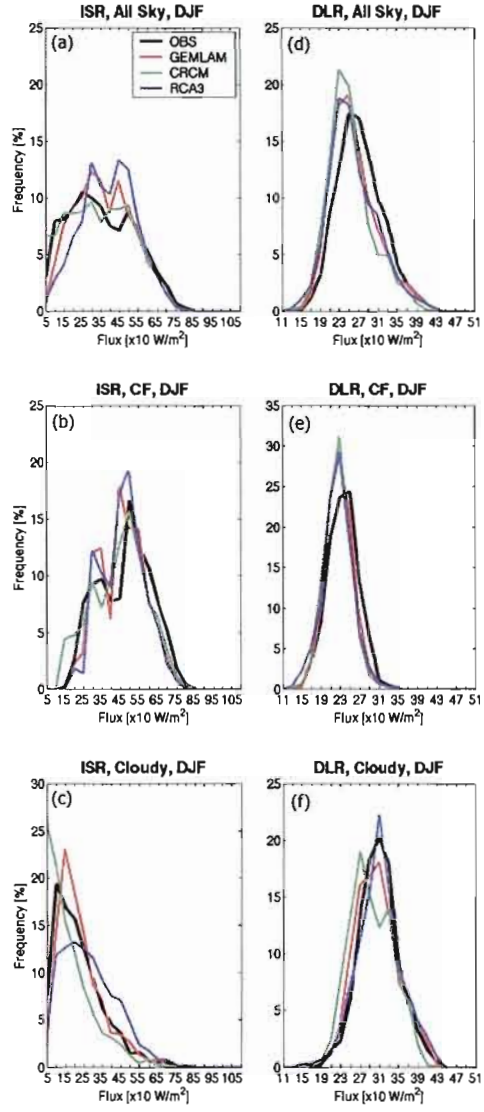

Figure 1.11: Distribution of winter season ISR and DLR 3 hourly fluxes from RCMs and observations. Analyzed day period 15-21 UTC: a) ISR all-sky, b) ISR cloud-free, c) ISR cloudy, d) DLR all-sky, e) DLR cloud-free, f) DLR cloudy. Cloud-free conditions are defined when the respective model and observations have cloud cover less than 10% for a given 3 hour period, overcast conditions are for cloud cover bigger than 90% for a 3 hour period.

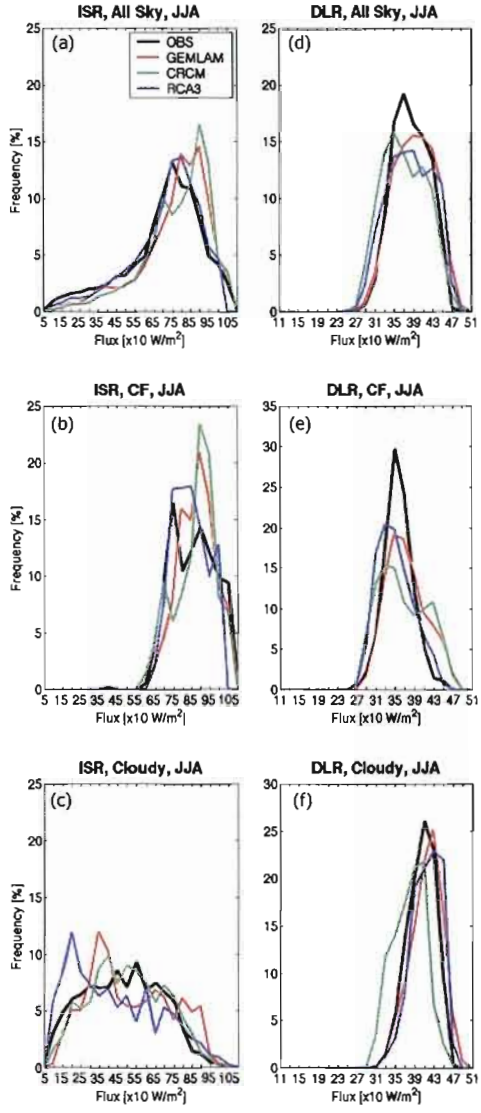

Figure 1.12: Distribution of summer season ISR and DLR 3 hourly fluxes from RCMs and observations. Analyzed day period 15-21 UTC: a) ISR all-sky, b) ISR cloud-free, c) ISR cloudy, d) DLR all-sky, e) DLR cloud-free, f) DLR cloudy. Cloud-free conditions are defined when the respective model and observations have cloud cover less than 10% for a given 3 hour period, overcast conditions are for cloud cover bigger than 90% for a 3 hour period.

GEM-LAM and CRCM represent the distribution of all-sky DJF ISR fairly well (Figure 1.11a). Clear-sky DJF ISR (Figure 1.11b) is quite accurate in both models while GEM shows the best results in cloudy conditions (Figure 1.11c). The DJF ISR in CRCM under cloudy conditions is biased low (i.e. not enough ISR getting to the surface in CRCM when the sky is completely covered by cloud). This error in cloudy-sky ISR (clouds too reflective) is contrary to the underestimate of DJF DLR in CRCM and suggests an inconsistent treatment of cloud water between the solar and longwave portions of the CRCM radiation scheme.

To better understand the surface radiation errors in Figure 1.11 we plot normalized frequency distributions of cloud fraction for DJF (Figure 1.13a) and JJA (Figure 1.13b) respectively. The gray ssurface on both figures represents an envelope between averaging periods of 3 and 6 hours for the surface point observations. Cloud cover in models represents an aerial fractional coverage over the entire model grid box, while the observations represent a vertical integral of cloud amount over a given point location. To adjust the observed cloud cover from a point value to be more representative of an aerial mean, we apply a time averaging of 3 and 6 hours. Figure 1.13 suggests the degree of time averaging in this range does not greatly change the histogram of observed cloud fraction occurrence. CRCM clearly overestimates the occurrence of clear-sky conditions in DJF and underestimates the occurrence of overcast skies (cloud fraction > 90%). The negative bias in cloudy-sky ISR in DJF (clouds too reflective) in CRCM (Figure 1.11c) is therefore balanced in the all-sky by a large overestimate of the occurrence of clear-sky conditions. (Note that ISR clear-sky (Figure 1.11b) values are always larger than the ISR cloudy values). RCA3 DJF ISR all-sky (Figure 1.11a) has a bias of too few ISR values in the range $< 200\,Wm^{-2}$ and too many occurrences in the range 200-600 Wm^{-2}. The clear-sky DJF ISR (Figure 1.11b) is quite accurate for this model, while cloudy DJF ISR underestimates low flux values and overestimates high values (Figure 1.11c), suggesting problems in the all-sky DJF ISR come from radiation in cloudy conditions. This error shows up as a

positive bias in the winter season ISR in this model in Figure 1.5a. In DJF simulated clouds in RCA3 appear to have a systematic negative bias in cloud reflectivity which may be related to a fractional distribution of total cloud water biased towards excessive ice fraction as discussed in Section 3.

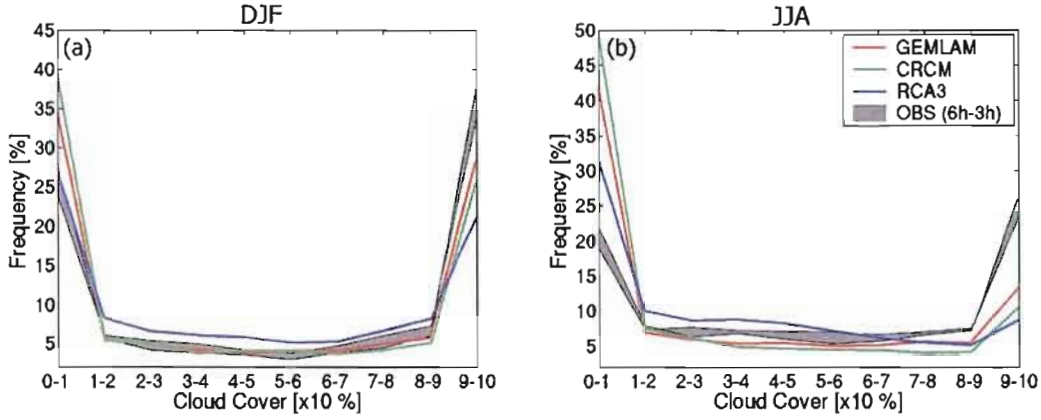

Figure 1.13: Distribution of cloud cover raw data from RCMs and observation. Analyzed daytime period 15-21 UTC, a) winter season, b) summer season.

All models have a slightly wider distribution of total-sky (Figure 1.12d) and clear-sky (Figure 1.12e) JJA DLR, which suggests greater variability in simulated boundary layer temperature and water vapor amounts than observed. A larger diurnal range of near surface temperatures is consistent with a general underestimate of cloud amounts. Excess daytime solar radiation leads to a warm bias by day and too little cloud at night allows excess infra-red cooling and a nighttime cold bias in the models.

With respect to clear-sky JJA DLR, due to the general underestimate of clouds in the 3 RCMs, it is conceivable that a fraction of the disagreement in the DLR frequency distributions stems from the RCMs classifying a range of atmospheric humidity states as clear-sky that are never clear-sky in the observations. This will particularly lead to the positive bias in the JJA DLR clear-sky distributions, with the

model clear-sky contributions being biased to higher emissivity values (higher integrated water vapor amounts) than observed.

CRCM has a bias towards too low values of JJA DLR in all-sky conditions. This seems strongly linked to an underestimate of cloudy-sky JJA DLR (Figure 1.12f) and is again consistent with an underestimate of cloud water and cloud emissivity in the CRCM radiation scheme. The cloudy-sky negative DLR bias in CRCM is partially balanced by a positive bias in clear-sky DLR in JJA for the reasons mentioned earlier. GEM-LAM also shows this bias in clear-sky JJA DLR (Figure 1.12e).

RCA3 gives a remarkably good JJA ISR total-sky (Figure 1.12a) distribution while, for the higher flux values, GEM-LAM and CRCM overestimate the occurrence of these ISR values. RCA3 has a bias towards to many occurrences of very low ISR ($< 200 Wm^{-2}$) in JJA cloudy conditions (Figure 1.12c). This is consistent with the findings of Karlsson et al. (2006) that RCA3 summer season clouds consistently are optically too thick (i.e. contain excessive amounts of liquid water).

GEM-LAM has too many occurrences of very high JJA ISR during overcast conditions (ISR $> 800 Wm^{-2}$) (Figure 1.12c). This amount of ISR during cloudy conditions is likely only to occur for optically thin cirrus clouds, suggesting in the summer season GEM-LAM too frequently (incorrectly) simulates clouds of low optical thickness. CRCM JJA ISR biases seem mainly related to clear-sky errors (e.g. the clear-sky is too transmissive). This will amplify the CRCM tendency to underestimate JJA cloud occurrence and lead to the poor JJA ISR in the seasonal mean (Figure 1.5a). All models tend to overestimate the occurrence of very small cloud fraction (0-10%) and to underestimate large cloud cover occurrences (90-100%) for both seasons (Figures 1.12a and 1.12b). This has a big influence on ISR all-sky (Figure 1.5a), especially for summer season, with all models exhibiting a positive bias in JJA ISR.

5. Evaluating the diurnal cycle of SRB in the 3 RCMs.

An accurate simulation of the diurnal cycle of surface radiation is very important requirement for climate modeling. Many of the systematic errors seen in the simulated seasonal mean SRBs may well result from persistent errors within the diurnal cycle. This is particularly the case with respect to the diurnal cycle of clouds and their interaction with solar radiation. In this section we evaluate the diurnal cycle in the 3 RCMs against surface observations for different conditions of cloud cover. Because cloud observations at the measurement sites are available only during daylight, we choose to analyse the period April-August (the hours 15-0 UTC, approximately 9-18 LST) in order to maximize the analysed period of the day. In Figure 1.14 we plot the mean diurnal cycle of DLR and ISR for cloud-free (cloud cover < 10%) and all-sky conditions.

For all conditions, we can split the diurnal cycle into a morning period (15 UTC, corresponding roughly to the local time 7-10am depending on the exact site location), afternoon (18-21 UTC, roughly 10-16 LST) and evening (00 UTC, roughly 16-19 LST). In the morning, GEM-LAM and RCA3 both have large positive biases in ISR. In the afternoon, the average overestimate for GEM-LAM remains high $\sim 70\, Wm^{-2}$ while for RCA3 it reduces to $\sim 35\, Wm^{-2}$. In the evening both models are remarkably accurate with small errors. In contrast, CRCM ISR is most accurate in the morning ($\sim 5\, Wm^{-2}$ error) while in afternoon and evening periods a positive bias in ISR of a $70\, Wm^{-2}$ develops.

Cloud-free ISR errors (Figure 1.14b) are smaller than the total-sky error in GEM-LAM and CRCM, indicating an amplification of the cloud-free error due to an underestimate of cloud amounts. RCA3 also shows smaller morning clear-sky ISR bias ($\sim 30\, Wm^{-2}$) compared to all-sky conditions, but for the afternoon and evening there is an increasing underestimate of ISR (e.g. the clear-sky atmosphere in RCA3 is too opaque to ISR partially balancing the underestimate of cloud fraction in the

model, leading to a relatively accurate all-sky ISR). Again highlighting the need to consider all components controlling the total simulated SRB in a model.

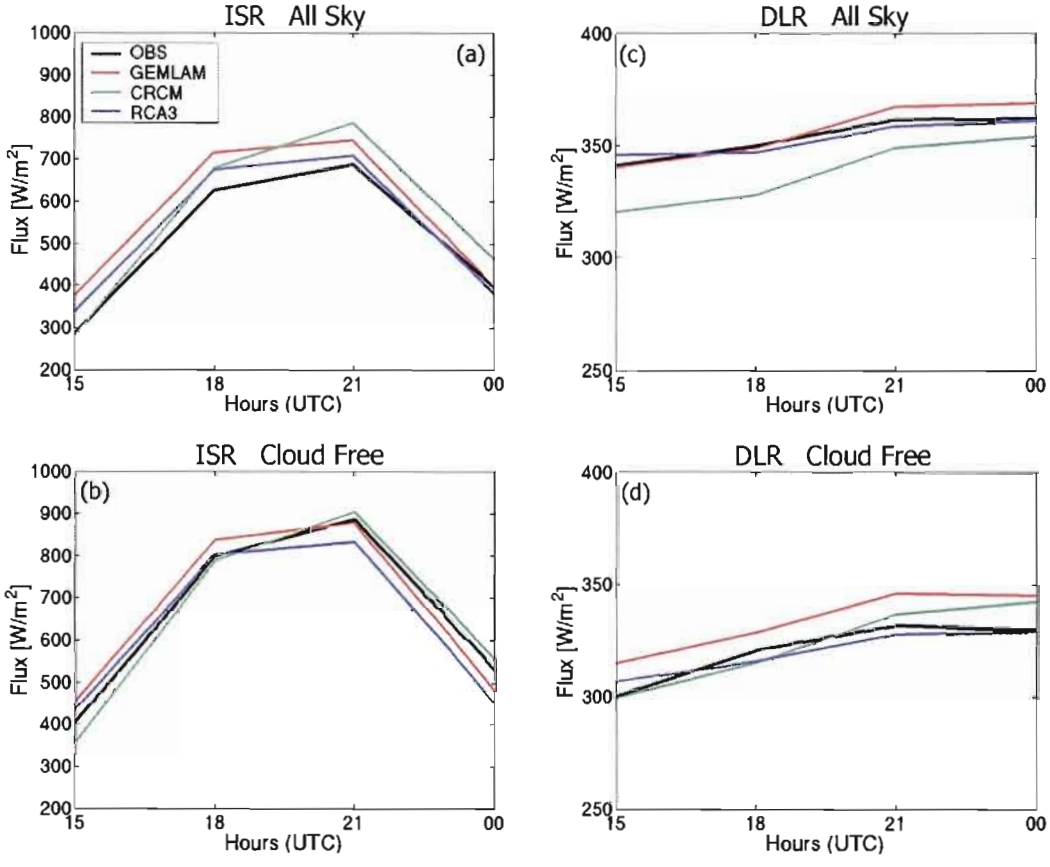

Figure 1.14: Mean diurnal cycle of :(a) ISR all-sky, (b) ISR cloud-free, (c) DLR all-sky (d) DLR cloud-free. Season April-August.

DLR exhibits a much weaker diurnal cycle than ISR, all-sky DLR (Figure 1.14c) is very well simulated by GEM-LAM and RCA3, with biases of less than $10\,Wm^{-2}$ for both models through the diurnal cycle. CRCM has a continuous negative bias in all-sky DLR ranging from 10-25 Wm^{-2} with the largest bias in the morning and afternoon. In the evening the CRCM all-sky DLR bias decreases due to a positive bias in clear-sky DLR. This is consistent with the CRCM lower atmosphere being too

warm probably due to the accumulated effects of the large positive bias in ISR in this model through the diurnal cycle (Figure 1.14a). As a result DLR values from clear-sky emission become increasingly large as the positive temperature error increases through the day. In cloud-free conditions GEM-LAM overestimates DLR, consistent with an atmosphere that is too warm. The underestimated cloud amounts (overall underestimate of total-sky emissivity) along with a too warm atmosphere (leading to excess clear-sky DLR emission) combine to produce an accurate estimate of all-sky DLR in GEM-LAM. RCA3 has a relatively accurate representation of the diurnal cycle of cloud-free DLR. Like GEM-LAM, RCA3 has a negative bias in simulated cloud amounts. The accurate all-sky DLR in RCA3 suggests that in the context of total-sky DLR, the underestimate of cloud fraction in RCA3 is balanced by clouds, when present, having systematically too high emissivity.

An improvement in the simulated diurnal cycle of cloud amounts and cloud liquid water path, in the summer season, therefore remains a crucial prerequisite for an improved simulation of both the diurnal cycle of ISR and summer seasonal mean ISR over North America.

To extend the evaluation of the diurnal cycle of simulated cloud-radiation interaction we evaluate the sensitivity of ISR to increasing cloud fraction for 3 different solar zenith angles (SZA) representing 3 solar heights in the diurnal cycle. Figure 1.15a shows the ISR distribution for the daytime period with maximal solar elevation SZA ($20-40°$), while Figures 1.15b and 1.15c represent $40-60°$ and $60-90°$ solar elevation. The analysed period in Figure 1.15 is April-August.

For a given cloud cover, RCA3 underestimates ISR for all 3 SZA. The biggest biases can be seen when the sun is highest in the sky (Figure 1.15a). The underestimate for 0% cloud cover is in accord with Figure 1.14b where RCA3 also has a negative bias (period 18-21 UTC) in cloud-free ISR. It is noteworthy that the trend of ISR with increasing cloud fraction in the RCA3 model runs parallel to the

observations across the entire cloud fraction range (0-100%). This suggests that the primary ISR cloud-radiation problem in this model is due to a clear-sky atmosphere that is to opaque too ISR. This error can prejudice ISR in cloudy conditions due to an underestimate of solar radiation incident at the top of frequent boundary layer clouds. In Figure 1.15 we also show the ISR-cloud fraction relationship derived from the RCA3aero integration, where the clear-sky absorption and scattering due to aerosols was reduced in the model (see Section 4.1). With reduced aerosol absorption and scattering the relationship between ISR and cloud cover is clearly improved in RCAaero for all SZAs and cloud fraction regimes.

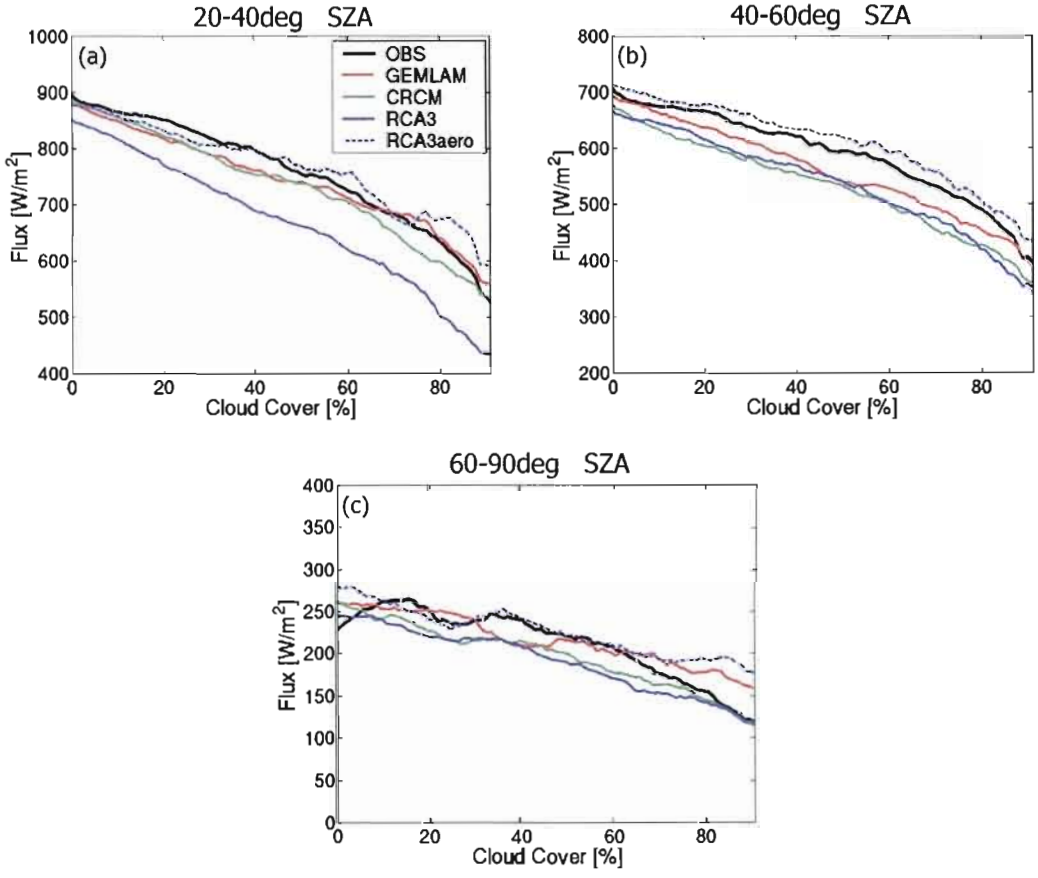

Figure 1.15: ISR plotted as a function of increasing cloud fraction for: (a) 20-40deg SZA, (b) 40-60deg SZA, (c) 60-90deg SZA. A mean ISR value has been calculated for each 1% step in cloud fraction for each site and then averaged across the 6 sites.

This procedure was performed separately for the 3 respective SZAs. A 10% running mean was then applied to each SZA curve to smooth the resulting curves presented in the figure.

CRCM and GEM-LAM show quite accurate ISR-cloud fraction relationship for the highest sun elevation (Figure 1.15a). Again, for 0% of cloud cover this is in accord with Figure 1.14b (18-21 UTC). For the lower SZAs, agreement with the observations decreases for both models, while the trend of ISR with increasing cloud fraction is relatively well captured.

6. Summary and conclusions.

The simulated SRB from 3 RCMs has been evaluated against surface observations from 6 SURFRAD sites distributed over the continental USA. Comparison of the mean annual cycles of ISR and DLR showed that GEM-LAM and CRCM accurately represented ISR in winter but overestimated in summer season. RCA3, on the contrary, gave a good ISR result in summer but overestimated in spring and winter. All models underestimated observed cloud cover. The mean annual cycle of DLR was well simulated by GEM-LAM and RCA3 with an underestimate in winter season while CRCM systematically underestimated DLR throughout the year. To better understand these biases we compared the mean annual cycles of DLR and ISR under cloud-free and all-sky conditions. Cloud-free comparisons showed that GEM-LAM and CRCM give fairly good ISR results, even for the summer season, suggesting that erroneous cloud cover is the principal reason for all-sky ISR biases in these 2 models. RCA3 had an underestimate of summer ISR for cloud-free conditions, which balanced a cloud underestimate and led to a relatively accurate all-sky ISR in this model. We subsequently showed that a large part of the clear-sky flux

errors in RCA3 could be attributed to an excess absorption and scattering by aerosol in the clear-sky portion of the radiation code.

DLR biases in cloud-free conditions for GEM-LAM and RCA3 were rather similar to the all-sky biases suggesting DLR biases in these models are mainly due to cloud-free errors. CRCM DLR was underestimated year round with this error being due both to a cloud fraction underestimate and a negative bias in cloud emissivity.

Cloud radiative forcing (CRF) was evaluated for the 3 RCMs against surface observations. All models underestimated ISR CRF primarily due to a lack of clouds. DLR CRF was underestimated in GEM-LAM and CRCM partially due to the cloud cover underestimate while the RCA3 DLR CRF was accurate due to a positive bias in cloud emissivity balancing the underestimate of cloud fraction.

Evaluation of normalised frequency distributions from the 3 RCMs and observations was split into winter and (DJF) and summer (JJA) seasons for different cloud cover conditions (cloud-free, all-sky and overcast). DJF ISR for cloud-free conditions was well represented by all models suggesting that DJF all-sky biases mainly come from ISR in cloudy conditions and cloud fraction underestimates. DLR for the DJF season in clear-sky conditions was biased low for all models consistent with earlier studies (e.g. Wild et al., 2001). For overcast skies the DLR frequency distribution improved for GEM-LAM and RCA3 while CRCM remained biased low, suggesting all-sky DLR biases in GEM-LAM and RCA3 come mainly from cloud-free DLR, while for CRCM both cloud-free errors and overcast biases contribute to the all-sky underestimate. Similar conclusions were found for DLR JJA. Improving the simulated LWP in CRCM appears an important requirement in order to achieve an accurate DLR balance at the surface.

JJA ISR under all-sky conditions was accurately simulated by RCA3 while GEM-LAM and CRCM exhibited positive biases mainly due to an underestimate of

cloudy-sky occurrence. A similar error in RCA3 cloud fraction was partially offset in the all-sky by the simulated clouds being too reflective and the RCA3 clear-sky ISR fluxes being too small. In cloudy conditions, the frequency of large ISR values during JJA was overestimated by GEM-LAM, suggesting an overestimate of low optical thickness (upper-tropospheric cirrus) clouds in summer in this model.

Comparison of the mean diurnal cycle of ISR showed that all models had smaller biases under cloud-free conditions indicating cloud cover as the primary cause of all-sky errors. The diurnal cycle of DLR for RCA3 model was well simulated for both cloud cover conditions. CRCM had a continuous DLR all-sky bias, which decreased in the evening, suggesting the CRCM lower atmosphere is too warm due to excess ISR values at the surface throughout the day. GEM-LAMs accurate representation of DLR all-sky as also a result of underestimated cloud cover along with its atmosphere being too warm, leading to overestimate of clear-sky DLR.

This work highlights the importance of analyzing the individual components of the total-sky surface radiation flux in climate models. In doing this we can better identify the actual cloud or radiation processes in a given model that are the root cause of errors in the total-sky SRB. To make progress in simulating cloud-radiation feedbacks it is important that the underlying physical processes controlling the surface radiative budget are well simulated. This is particularly true with respect to error compensation within the various components of the SRB.

Acknowledgements:

This work was funded by the grant provided by Canadian Foundation for Climate and Atmospheric Sciences grant number 61209 which funded Canadian Regional Climate Modeling and Diagnostics network.

2. AN EVALUATION OF THE SURFACE RADIATIVE BUDGET OVER NORTH AMERICA FOR A SUITE OF REGIONAL CLIMATE MODELS AND REANALYSIS DATA, PART: 2 COMPARISON OVER ENTIRE DOMAIN

This chapter will be present as second of two-part Article in a suitable format. The article will be submitted to the evaluation committee in the following months. List of figures from this chapter can be found in the opening part, while references are given at the end of this thesis.

An Evaluation of the Surface Radiation Budget Over North America for a Suite of Regional Climate Models and Reanalysis Data, Part 2: Comparison Over Entire Domain

Marko Markovic
Department of Earth and Atmospheric Sciences. University of Quebec at Montreal.
Ouranos, 550 Sherbrooke West, 19th floor, West Tower, Montreal, Quebec H3A 1B9, Canada

Colin Jones
Department of Earth and Atmospheric Sciences. University of Quebec at Montreal

Katja Winger
Department of Earth and Atmospheric Sciences. University of Quebec at Montreal.
Ouranos, 550 Sherbrooke West, 19th floor, West Tower, Montreal, Quebec H3A 1B9, Canada

Dominique Paquin
Consortium Ouranos
Ouranos, 550 Sherbrooke West, 19th floor, West Tower, Montreal, Quebec H3A 1B9, Canada

Corresponding Author address:
Colin Jones
Department of Earth and Atmospheric Sciences
University of Quebec at Montreal
Ouranos, 550 Sherbrooke West, 19th floor, West Tower
Montreal, Quebec H3A 1B9, Canada
Tel: (514) 282-6464 (ext.293)
Fax: (514) 282-7131
E-mail: jones.colin@uqam.ca

Abstract

While surface based radiation observations offer accuracy at high temporal resolution, they do not allow a full evaluation of model simulated Surface Radiation Budget [SRB] over a wide geographical area such as North America. In this paper we evaluate 3 different gridded SRB data sets against US SURFRAD SRB observations to determine the best surrogate observational data set. The gridded data sets used are: ERA40 - the global reanalysis of ECMWF, NARR - regional reanalysis of NCEP and the SRB derived from the ISCCP satellite project. After comparison against surface observations, the ERA40 SRB appears to be the most representative of the gridded data. We subsequently use the ERA40 data to evaluate the simulated SRB in 3 RCMs over continental North America. Spatial comparison of Incoming Shortwave Radiation, Downwelling Longwave Radiation and cloud cover reveal model errors consistent with those found in Markovic et al. (2007a), where comparison was made at a limited number of surface observation sites. With respect to surface solar radiation fluxes, simulated cloud cover biases are seen to be crucial, while for surface longwave fluxes both cloud fraction and incloud water content are important to simulate correctly. Error compensation frequently occurs between various components controlling the simulated total-sky SRB (e.g. cloud cover, cloudy-sky radiation, clear-sky radiation). This error compensation makes improvement in the total SRB difficult to achieve by improving one component of the model SRB in isolation and emphasises the importance of evaluating all components controlling the SRB in a given climate model.

Key words: surface radiation budget, surface observations, reanalysis, regional climate model evaluation

1. Introduction.

The goal of this two-part paper is to evaluate the components of the surface radiation budget (SRB) in 3 Regional Climate Models (RCMs). In Markovic et al., 2007a (from this point on referred as M07) we evaluated simulated Incoming Shortwave Radiation (ISR), Downwelling Longwave Radiation (DLR) and cloud cover against 6 SURFRAD ground based observations at different locations across North America, aiming to isolate specific parametric problems in the RCMs. The models used in this study were: The Canadian Regional Climate Model (CRCM, version 4.0) (Caya and Laprise, 1999), GEM-LAM, the regional version of the Global Environmental Model (Côté et al, 1997) and third, RCA3, the regional model from the Rossby Centre (Jones et al. 2004). Details of each respective model and the experimental configuration are available in M07.

The assessment of simulated DLR revealed common problems across the models in the winter season that appeared mainly to be associated with clear-sky DLR. This was also seen in Wild et al. (2001) and was thought to be related to either a poor treatment of water vapour emission during cold and dry atmospheric conditions, or the omission of trace gas contributions to clear-sky DLR. Our assessment indicated that in dry conditions, GEM-LAM, which includes the contribution of trace gases beyond H_2O, CO_2 and O_3, provided the best DLR clear-sky fluxes. It appears necessary that for an accurate DLR, trace gas contributions are included in the longwave portion of a radiation code. CRCM DLR errors were further compounded by systematic underestimate of cloud cover and a negative bias in cloud liquid water path (LWP), which led to a systematic negative DLR bias in overcast conditions. ISR errors were dominated by an underprediction of cloud fraction, which was amplified through the diurnal cycle in summer. Clear-sky ISR was more accurately calculated than all-sky ISR by GEM-LAM and CRCM. The total-sky ISR in RCA3 was found to be accurate due to a cancellation of errors; an underestimate of

cloud fraction was partially balanced with respect to all-sky ISR by a clear-sky atmosphere that was too opaque to solar radiation.

In this paper we wish to extend the assessment of the RCM simulated SRB beyond the individual station observations to encompass the entire North American continent. To do this we must first identify a suitably accurate, spatially discrete, gridded SRB dataset for model evaluation. To do this we use the 6 US-SURFRAD stations as a means to evaluate the quality of various available gridded SRB products. Once identified, this gridded data set will be used to evaluate the seasonal cycle of SRB in the 3 RCMs across North America.

2. Description of available surrogate SRB datasets.

We evaluate the SRB from 2 sets of reanalysis against ground observations, these are: ERA40 (Uppala et al., 2005) from the European Centre for Medium Range Weather Forecast (ECMWF) with a resolution of ~100 km and the NARR (Mesinger et al., 2004); North American Regional Reanalysis from the National Centre for Environmental Prediction (NCEP). These 2 datasets are chosen due to their wide use in the evaluation of climate model simulations for present climate conditions. In the case of NARR, this reanalysis was specifically generated for North America, at a resolution (32km) similar to that used by most Regional Climate Models. Hence it potentially provides a suitable, high-resolution quasi-observation for use in RCM evaluation. As with reanalyses, satellite-based measurements can also provide estimates of surface radiation over the entire North America. The SRB derived from the International Satellite Cloud Climatology Project (ISCCP) (Zhang et al., 2004; Rossow and Schiffer, 1991) provides a continuous, long-term record of satellite derived SRB available with a resolution of 2.5°. ISCCP SRB and cloud data are extensively used in model evaluation. We view it as important to evaluate the quality

of the ISCCP SRB against station observations before employing it for a wider RCM evaluation.

The data set showing the best agreement with surface observations at discrete points across North America will subsequently be used in Section 4 to evaluate the RCM SRBs across continental North America. As seen in M07, SRB components are strongly influenced by cloud cover, seasonal particularities (e.g. winter season mixed phase cloud types) and the diurnal cycle. Some climate regimes, more strongly influenced by these aspects, can favour particular models to give better results than others. Therefore in our analysis we aim to evaluate the RCM simulated SRB across a wide spectrum of sampled climate regimes. It is important to reiterate that the 3 RCMs were forced by analysed lateral boundary conditions, hence the large scale atmospheric evaluation is partially constrained to follow the observed evolution.

3. Determining the best gridded data set for model evaluation: Comparison to surface observations at the monthly mean timescale.

In order to evaluate the surrogate SRB datasets it is important we utilize as long a common time period as possible between the SURFRAD observations and the 3 gridded datasets. Table 2.1 presents the time series where observations, reanalysis and satellite data are all available at each respective SURFRAD station. The lower limit of the time series is determined from the period when the observations started at each site, while the upper limit (year 2001) is determined by the limit of the ERA40 reanalysis with respect to a complete annual cycle.

For the majority of stations at least 5 years of data are available for comparison, which we believe, allows robust conclusions to be drawn regarding the accuracy of the surrogate SRB products. For all three gridded data sets, time series of

ISR and DLR were extracted for each of the grid points closest to the observational sites.

Site	Lat.	Lon.	Period
Bondville, IL	40.06	-88.37	1996-2001
Boulder, CO	40.13	-105.24	1996-2001
Desert Rock, NV	36.63	-116.02	1999-2001
Fort Peck, MS	48.31	-105.10	1997-2001
Goodwin Creek, MT	34.25	-89.87	1996-2001
Penn State, PA	40.72	-77.93	1999-2001

Table 2.1: Observation time period used to compare with reanalysis and ISCCP.

In Figure 2.1 we present the mean annual cycle of monthly mean ISR and DLR, averaged across all 6-measurement sites. Figure 2.1a shows the observed (black) mean annual cycle of ISR compared to the same value from ISCCP (green), ERA40 (red) and NARR (blue). Figure 2.1c shows the mean annual cycle of ISR differences between each data set and the surface observations averaged across the 6 sites. The NARR reanalysis overestimates ISR throughout the annual cycle. NARR overestimates ISR by ~30 Wm^{-2} in winter (a ~30% positive bias) and by ~50 Wm^{-2} in the summer (~20% bias). These errors are considerably larger than the uncertainty of surface observations and seem primarily due to a significant underestimate of cloud fraction in NARR which reaches as large as a 25% underestimate in the summer season (not shown).

In winter, the average ISR error in ERA40 is ~9 Wm^{-2} and in summer ~7 Wm^{-2}. The quoted observational uncertainty for individual ISR observations at the SURFRAD site (http://www.srrb.noaa.gov/surfrad/surfpage4.html) is ~±10. ERA40 simulated monthly mean ISR therefore appear very accurate for these locations over North America. This good agreement is in line with an earlier study that documents very good agreement between the ISR from ERA15 and 700 observation sites across

the globe (Wild et al., 1998). ISCCP ISR in winter also agrees well with surface observations, while in summer an overestimate of ~7 Wm^{-2} is present. The ISCCP ISR errors are therefore also close to the range of observational uncertainty.

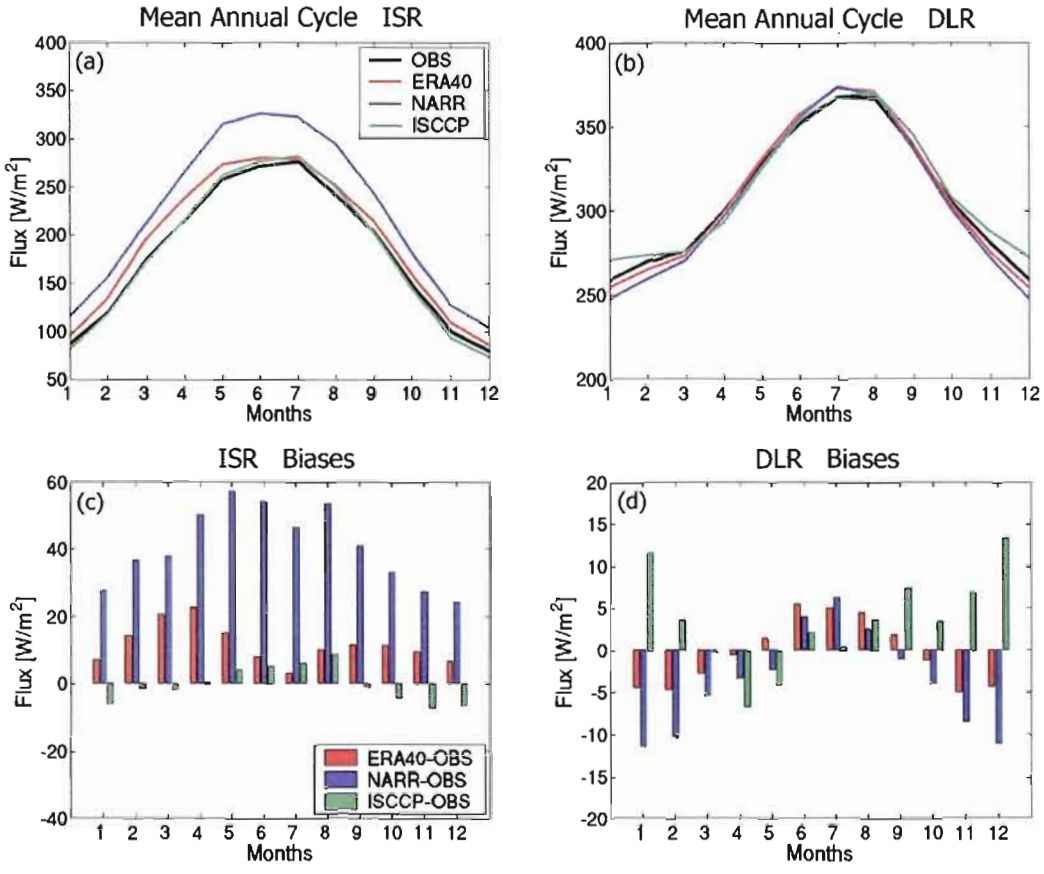

Figure 2.1: (a) Mean annual cycle of ISR, (b) mean annual cycle of DLR radiation, (c) differences in ISR between reanalysis, ISCCP products and station observations, (d) differences in DLR between reanalysis, ISCCP products and station observations.

Figures 2.1b and 2.1d present a similar comparison for DLR. With mean DJF and JJA biases less then 5 Wm^{-2} ERA40 is the closest to the surface observations, while larger winter season biases are found in NARR (~10 Wm^{-2} underestimate) and in ISCCP (~10 Wm^{-2} overestimate) To derive surface radiation components ISCCP uses observed shortwave and longwave TOA fluxes, estimated thermodynamic

atmospheric structure (e.g. temperature, water vapor, etc.) and satellite derived clouds. From these input parameters, surface radiation is estimated using a detailed radiative transfer model. The DLR winter errors are likely associated with the known difficulties in detecting clouds during the winter season, when the frequent presence of atmospheric inversions over a highly reflective snow surface makes satellite detection of clouds extremely difficult (Key and Barry, 1989; Schweiger and Key, 1992). Errors in the detection of winter season optically thin clouds will have a larger impact on the ISCCP DLR values than ISR values.

Winter biases found in all the gridded data sets, while small, are consistent with problems identified by earlier studies (e.g. Wild et al. 2001) specific to the simulation of clear-sky DLR during cold, dry conditions. Introduction of the Rapid Radiative Transfer Model (RRTM, Mlawer et al., 1997), with an advanced treatment of the water vapour continuum, into the ECMWF model used to generate the ERA40 reanalysis (as well as ECHAM5) reduced the negative biases in DLR from cold cloud-free atmospheres, compared to earlier versions ERA15 and ECHAM4 (see Wild and Roeckner, 2006).

Figure 2.1 suggests ERA40 is the most accurate gridded data set available for DLR while both ERA40 and ISCCP have very accurate ISR budgets, with biases generally less than $\pm 10 Wm^{-2}$ when averaged over the 6 SURFRAD sites. This level of accuracy suggests either the ERA40 or the ISCCP SRB can be used to evaluate model simulated ISR and DLR at the monthly timescale. Before we chose a surrogate for observations over the whole domain of interest, we first verify that the ERA40 and ISCCP surface radiation values are accurate at each individual station also. We wish to check that geographically discrete errors have not cancelled out in the averaging process across the 6 stations. In the next section we also evaluate the higher time frequency distributions of ISR and DLR in the surrogate observations, using

normalized frequency of occurrence plots of the raw 6-hourly fluxes. Surrogate DLR and ISR frequency distributions are compared to the equivalent station observations.

In Table 2.2 we present the differences between each surrogate data set and surface observations for each site separately. Results are presented as the seasonal mean differences (e.g. ERA40-OBS., NARR-OBS. and ISCCP-OBS.) for ISR and DLR. The site of Fort Peck has a small negative bias for ERA40 ISR in winter of about $-4\,Wm^{-2}$, otherwise the ISR differences across all sites are similar. Equally, for ERA40 DLR there appears little spatial error cancellation with maximum negative bias in the winter of $\sim 10\,Wm^{-2}$. NARR overestimates ISR across all stations in both analysed seasons, indicating a systematic error. The winter season ISR values in ISCCP do appear to exhibit spatial cancellation in the sign of the bias across the 6 SURFRAD sites. This spatial cancellation, while of smaller magnitude, is also evident in both ISCCP ISR and DLR estimates for the JJA season. In particular, the site of Desert Rock in Nevada consistently balances positive (ISR) and negative (DLR) errors at the 5 other stations, contributing to an accurate spatial mean value.

		ERA40		NARR		ISCCP	
Site	seas.	ISR	DLR	ISR	DLR	ISR	DLR
Bondville, IL	DJF	16.1	-6.6	34.9	-11.7	-2.3	8.2
Boulder, CO	DJF	13.1	-11.2	28.6	-17.2	14.6	0.6
Desert Rock, NV	DJF	1.5	-0.4	21.3	-10.4	-5.4	19.8
Fort Peck, MS	DJF	-3.9	1.9	21.7	-9.3	-13.9	27.7
Goodwin Creek, MT	DJF	19.9	-9.1	41.9	-8.6	4.2	5.0
Penn State, PA	DJF	7.5	-1.3	27.2	-7.9	2.8	-3.4
Bondville, IL	JJA	4.8	10.1	49.3	6.3	-1.2	0.7
Boulder, CO	JJA	11.0	2.6	88.9	-9.9	24.1	-11.1
Desert Rock, NV	JJA	10.6	1.3	33.9	4.2	-11.4	37.0
Fort Peck, MS	JJA	3.9	6.3	50.6	11.2	8.9	-5.8
Goodwin Creek, MT	JJA	3.5	5.7	27.7	13.4	13.5	-2.6
Penn State, PA	JJA	9.9	2.2	59.8	-1.3	7.1	-7.3

Table 2.2: Winter and summer season DLR and ISR biases for ERA40, NARR and ISCCP against surface observations on 6 individual SURFRAD stations for all-sky conditions.

4. Evaluating the higher time frequency SRB variability in surrogate data sets.

As in Section 3 of M07, we evaluate the 6-hourly SRB values for ERA 40, NARR and ISCCP raw (6 hourly) surface fluxes against observational data in terms of normalized frequency distributions of a given ISR and DLR value. Figure 2.2 presents the normalised frequency distribution of ISR and DLR separately for winter (DJF) and summer (JJA) averaged across all 6-observation sites in the SURFRAD Network. The top row of the figure 2.2 (Figure 2.2^{TR}) presents a comparison between ERA40 and observations, the middle row (Figure 2.2^{MR}) and lower row (Figure 2.2^{LR}) between NARR, ISCCP and observations respectively. The periods used here are the same as in Table 2.1. The ERA40 data is available as six hourly averages, we therefore averaged the NARR, ISCCP and observations to this time frequency also, with the entire diurnal cycle included. The values along the x-axes in Figure 2.2 indicate the band of ISR or DLR values for which a given frequency of occurrence has been calculated (e.g. a value of 350 in the ISR plot indicates a band of ISR between 300-350 Wm^{-2} while for DLR the value of 350 indicates a band of DLR between 330-350 Wm^{-2}). Nighttime is not included for the ISR analysis thus the first ISR band is 5-50 Wm^{-2}.

In winter ERA40 (Figure 2.2^{TR}) tends to underestimate the frequency of occurrence of very low ISR with a slight shift in the normalized distribution towards high values. We are unable to determine the actual cause of this error but suggest it may be associated with an underestimate of cloud reflectivity of optically thick winter clouds in ERA40. We mentioned in M07 that the RCA3 model had a similar shift in frequency distribution for DJF ISR. Both, the ECMWF and RCA3 models use the same temperature dependent fraction to partition cloud water into liquid and ice, with the fraction of cloud water assumed solid increasing as the second power of local air temperature in the range $0°C$ (zero ice fraction) to $-22°C$ (100% ice fraction). Recent observations in the Arctic (e.g. Intrieri and Shupe, 2004; Shupe et al., 2006)

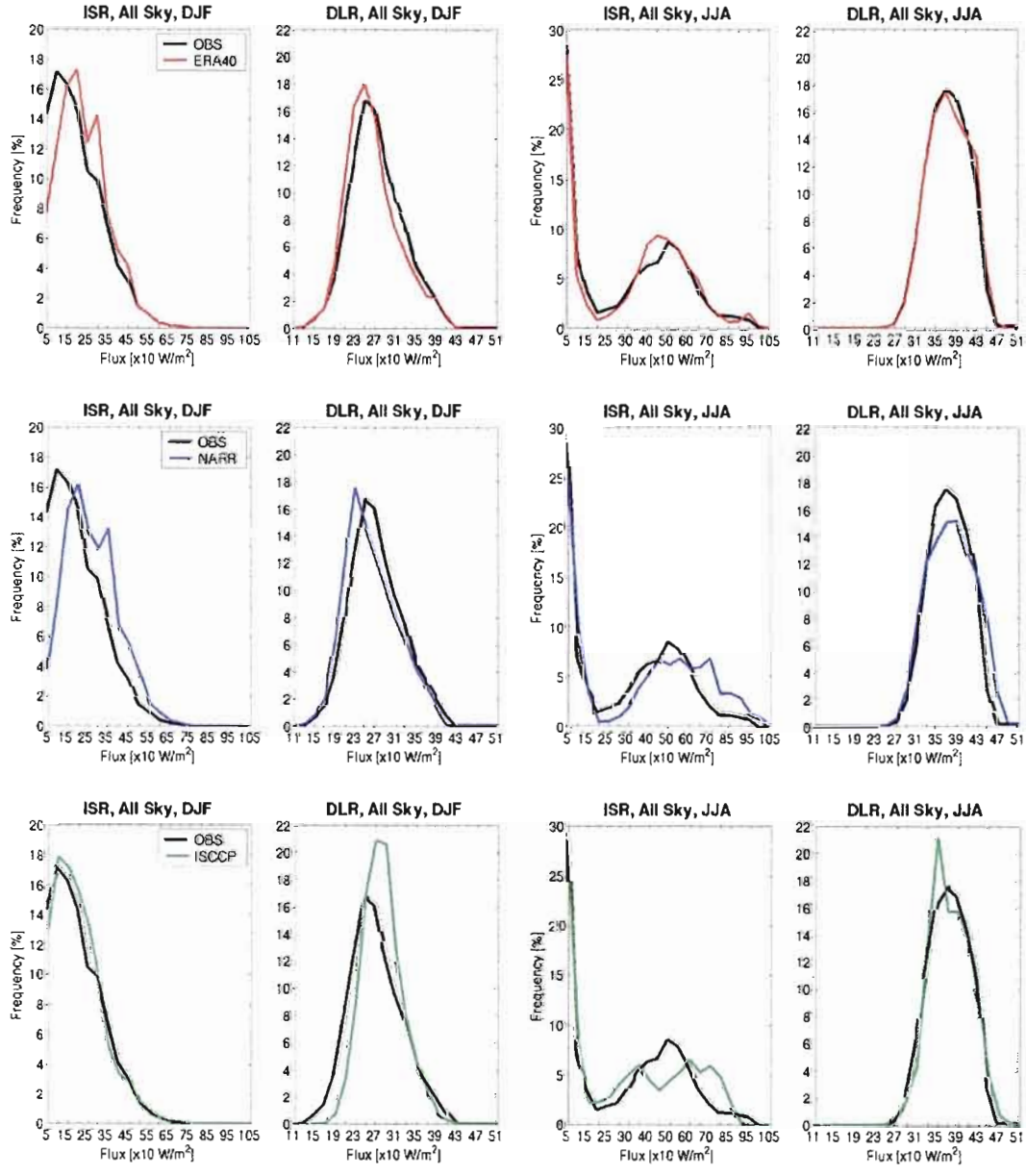

Figure 2.2: Normalised frequency distribution comparison of seasonal ISR and DLR 6 hourly fluxes from: top row – ERA40 and observation, middle row – NARR and observation, lower row – ISCCP and observation.

suggest liquid droplets are present in mixed phase clouds at temperatures as low as $-39^{o}C$, suggesting a possible underestimate of the liquid fraction in ERA40 mixed phase clouds. Such an underestimate will lead to a systematic overestimate of cloud effective radius and an underestimate of cloud albedo.

For DJF DLR (Figure 2.2^{TR}), the peak occurrence in ERA40 is shifted slightly towards lower values. It is noteworthy that the positive ISR and negative DLR frequency distribution shifts compensate each other in term of the simulated total surface radiation budget in ERA40 and that the positive ISR shift and negative DLR shift are both consistent with clouds that are optically too thin during the winter. The ERA40 DJF DLR shift also looks like the RCM shift (see M07, Figure 1.4), which seemed to be mainly due to clear-sky DLR errors. It is probable that ERA40 has a similar clear-sky DLR bias. To assess the clear-sky and cloudy-sky radiation fluxes from ERA40 requires observed cloud information, which are available during daylight hours only. In DJF the 6 hourly frequency of ERA40 surface fluxes along with the limited daylight period makes is impossible to determine if the ERA40 DLR all-sky bias in DJF arises from clear-sky DLR errors. We decided to use the months of February and March as a surrogate for DJF as during these months we were able to construct observed clear-sky and cloudy-sky DLR fluxes. During daylight hours, the all-sky ERA40 DLR fluxes *did not* show a negative bias in the DLR normalised frequency distribution, while the all-sky DLR for the entire diurnal cycle did show a shift consistent with that seen in (Figure 2.2^{TR}) for DJF. We are left to conclude that the winter season negative bias in ERA40 DLR must arise during nighttime conditions. Unfortunately we are unable to discriminate further the cause of this error due to the lack of nighttime cloud observations. For the summer season, both ISR and DLR frequency distributions are very accurate indicating the ERA40 SRB is a good representation of observed values.

As in ERA40, NARR underestimates the occurrence of low ISR values in the winter (Figure 2.2^{MR}) with this underestimate being somewhat larger. DJF ISR in NARR exhibits a systematic shift towards too high flux values, consistent with a cloud fraction underestimate. The winter season DLR values in NARR show a shift towards too low values of a similar magnitude to that seen in the 3 RCMs in M07. Summer ISR values in NARR continue to show a systematic shift towards too high flux values while the summer DLR also has a tendency for too high values, perhaps linked to a near surface warm bias developing in the NARR forecast-assimilation system.

Winter season ISR in ISCCP (Figure 2.2^{LR}) closely follow the observational curve. JJA ISR, on the other hand, has an important underestimate in the 350-600 Wm^{-2} band and overestimate in the 600-900 Wm^{-2} band, which combine to give a very accurate result in the form of mean seasonal fluxes. DJF DLR presented in Figure 2.2^{LR} reveals that ISCCP fails to reproduce DLR values below 190 Wm^{-2}, which we believe indicates a problem in defining clear-sky situations in extremely dry, cold and, therefore, stable conditions in the ISCCP data. The erroneous presence of a cloud in the ISCCP radiation calculations for these conditions will produce such a positive shift seen in the ISCCP DLR values.

This assessment further supports the results of the spatial mean, annual cycle analysis, whereby the ERA40 SRB was identified as the most accurate surrogate observation when both DLR and ISR are considered across all seasons. In the next section we will use the ERA40 SRB to evaluate the 3 RCM simulated SRBs across the North American continent.

5. Evaluating the SRB seasonal cycle in 3 RCMs over continental North America: Comparison to ERA40.

5.1 Seasonal mean distribution over North America.

In this section we use the ERA40 downwelling solar and longwave radiation fields to evaluate simulated surface radiation in the 3 RCMs, over the entire North America. In doing this we recognize that inaccuracies may still exist in the ERA40 data in regions where we have been unable to evaluate them (e.g. Northern Canada). Nevertheless, the accuracy of the ERA40 fields where it was feasible to evaluate them gives us some confidence that any large differences we identify between the ERA40 surface radiation and simulated values will indicate a genuine model deficiency. In this section we will compare seasonal mean SRB and associated cloud cover. We will also evaluate the mean annual cycle of simulated cloud cover and surface radiation over a number of spatially averaged regions that encompass the range of climate conditions encountered over North America. The period analysed in this section encompasses 4 years (1999-2002).

In Figure 2.3 we present a comparison of the absolute DJF seasonal mean ISR, DLR and cloud cover values for ERA40 (first column) and the seasonal mean biases (RCM-ERA40) for DJF ISR, DLR and cloud cover for GEM-LAM (second column), CRCM (third column) and RCA3 (fourth column). All 3 models have small biases in the far north where ISR fluxes are relatively small in DJF. In the mid-latitude region RCA3 has a larger positive bias in ISR of order 10-20 Wm^{-2}. This error is consistent with the underestimate of ISR cloud-radiative forcing identified against station observations (see Figure 1.7a, M07) and appeared to be primarily due to an underestimate of winter season cloud albedo. GEM-LAM in particular, has an accurate ISR field across the entire continent in DJF.

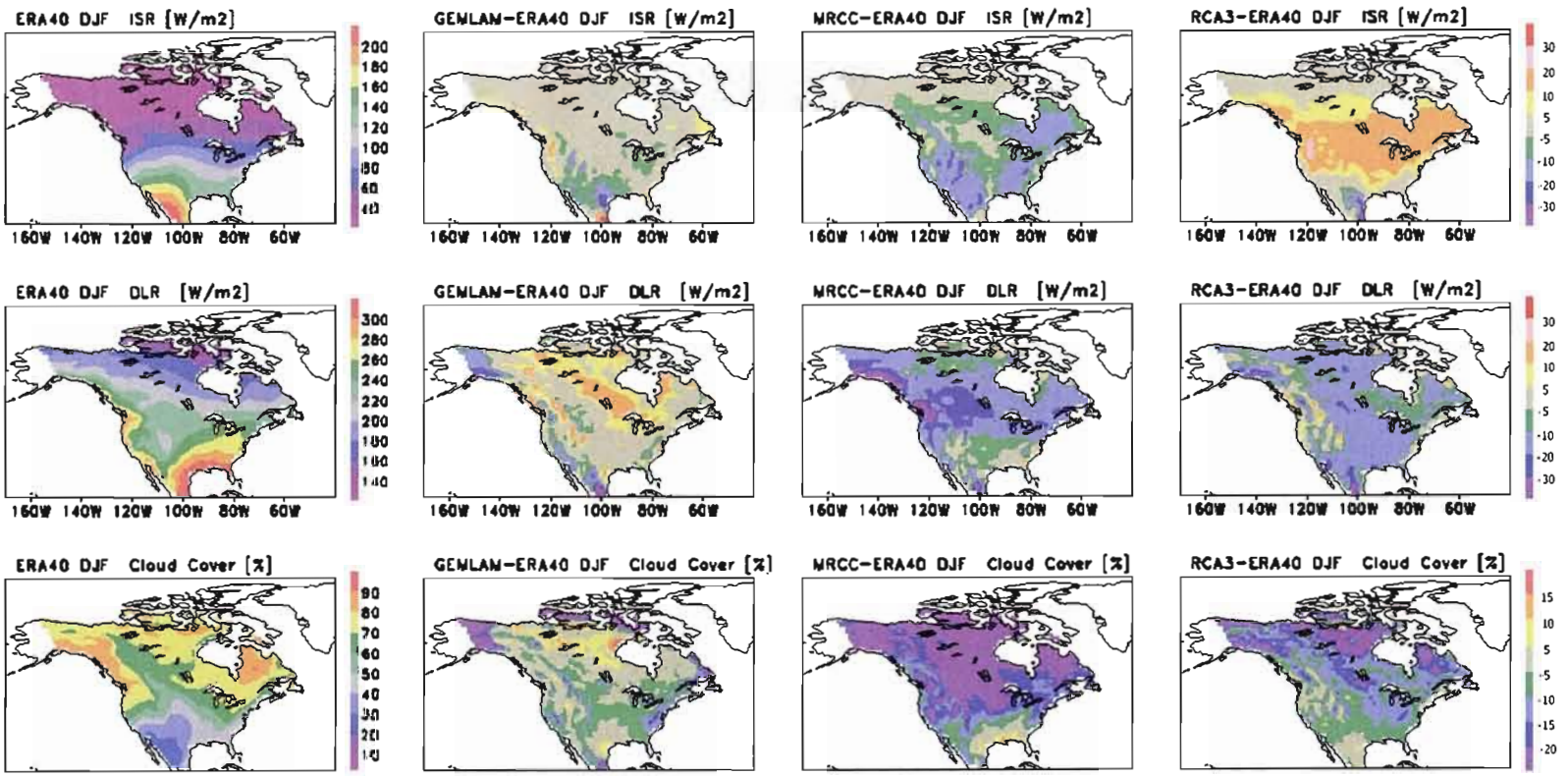

Figure 2.3: Comparison of ISR, DLR and cloud cover between 3RCMs and ERA40 for the season of DJF. Gray color represents biases from –5 to +5 Wm-2.

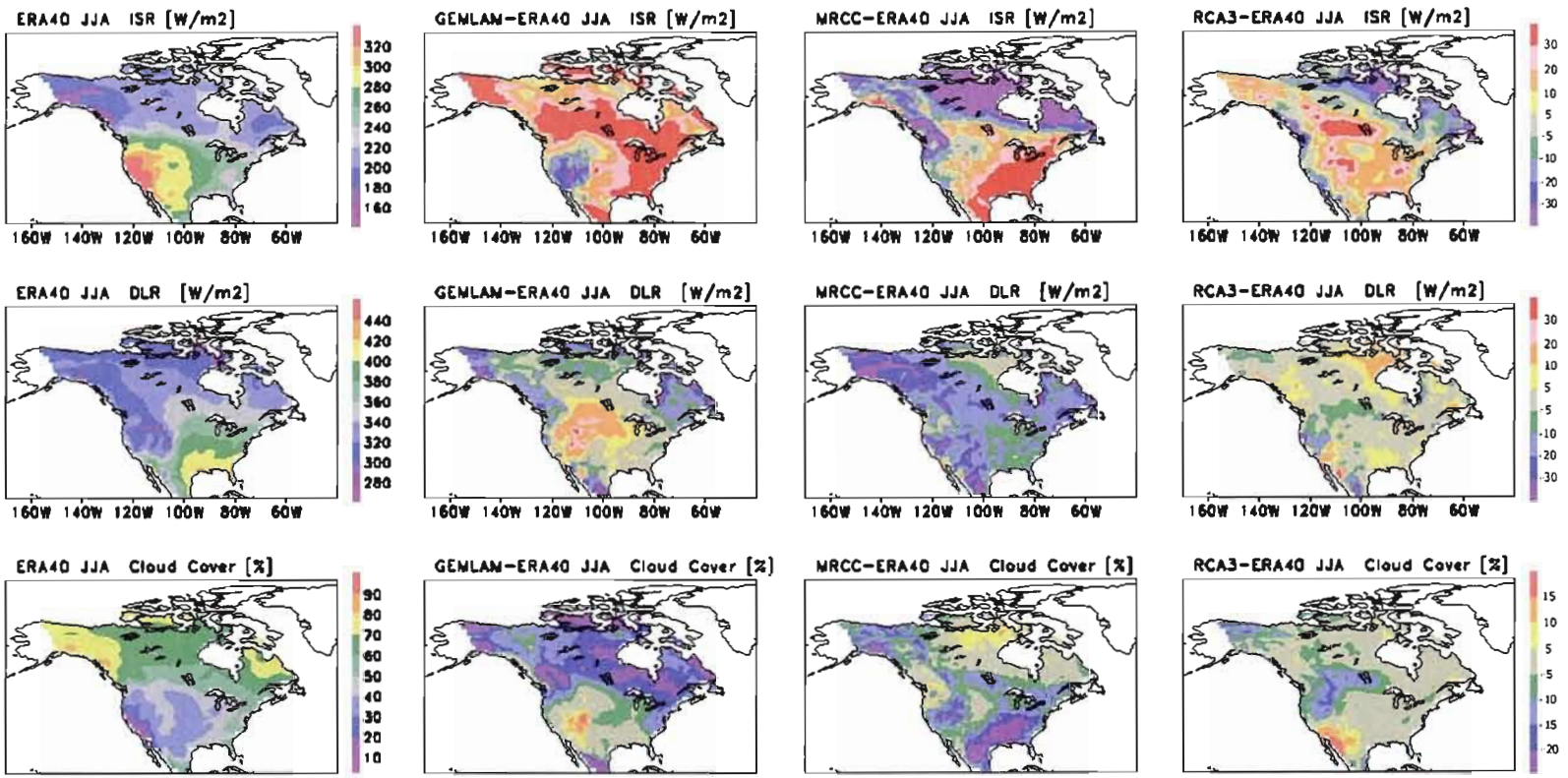

Figure 2.4: Comparison of ISR, DLR and cloud cover between 3RCMs and ERA40 for the season of JJA.
Gray color represents biases from –5 to +5 Wm-2.

DLR during DJF in GEM-LAM shows a similar distribution to ERA40 (Figure 2.3), with biases generally in the range $\pm 10 Wm^{-2}$, while RCA3 and CRCM both have a tendency to underestimate the winter DLR flux. This underestimate is largest in CRCM with errors of 10-30 Wm^{-2}. It was shown in Section 4 of M07, that the majority of the DJF DLR errors in GEM-LAM and RCA3 were associated with negative DLR biases in clear-sky conditions. CRCM also had a negative bias in DJF DLR in clear-sky conditions, but this was further compounded by an underestimate of DLR for overcast skies. The bottom row in Figure 2.3 shows the mean DJF ERA40 cloud cover and the errors in simulated total cloud cover (RCM-ERA40). We recognize that biases may exist in the ERA40 cloud cover, hence simulated errors in the RCM cloud amounts should be treated with caution. There is some consistency between errors in cloud cover and those in surface radiation as should be expected from model generated cloud and radiation fields. In particular CRCM has a large negative bias in cloud cover which appears to be a significant factor in the underestimate of DLR (This is consistent with the analysis of this model against station data in M07, Section 4). RCA3 also has a tendency to underestimate cloud amounts although with smaller biases than CRCM, consistent with the smaller negative bias in DLR in this model. Finally GEM-LAM overestimates cloud amounts in Northern Canada, consistent with the positive bias in DJF DLR in this region.

Figure 2.4 presents the same comparison as Figure 2.3 but for the JJA season. Absolute ISR errors in the summer season will clearly be larger than in DJF due to the larger incoming flux at the top of the atmosphere. GEM-LAM has a large positive bias in ISR ($> +30 Wm^{-2}$) over much of North America, which, in general, is spatially coherent with a negative bias (0 to -20 Wm^{-2}) in DLR. Both of these errors appear consistent with an underestimate of JJA cloud cover. CRCM underestimates ISR JJA (Figure 2.3) in the north of the continent (-20-30 Wm^{-2}) while it has a large overestimate in the southern parts of the domain ($\sim +30 Wm^{-2}$). Both errors are again coherent with cloud cover biases in CRCM. As in M07 Section 4, RCA has the

smallest ISR JJA biases. There is also some spatial coherency in the simulated errors in this model, with the positive ISR biases collocated with negative DLR biases and negative cloud cover errors (and vice versa for opposite signed errors). In Section 4 of M07 we showed that RCA3 ISR errors in JJA for all-sky conditions were less sensitive to underestimated cloud cover than the other 2 models due to error compensation. Specifically RCA3 ISR in clear-sky conditions was systematically underestimated and clouds that were present were systematically too reflective. As a result an underestimate of cloud cover in RCA3 is partially offset by these two biases in terms of the total ISR, making the RCA3 total ISR budget less sensitive to cloud errors. JJA DLR is quite accurate in both GEM-LAM and RCA3 with biases generally in the range $\pm 10 Wm^{-2}$. As in DJF, CRCM has a larger negative bias in DLR (~ -10 to $-30 Wm^{-2}$). Summer season cloud cover errors in CRCM do not appear greater than those in RCA3 or GEM-LAM suggesting an amplification of the cloud cover bias in CRCM, in terms of DLR, due to an underestimate of cloud emissivity as suggested in M07, Section 4 (see Figure 1.6).

5.2 Spatial averaged SRB components.

To obtain a more complete evaluation of the annual cycle of SRB, in this section, we compare the 4-year mean annual cycle of ISR, DLR and cloud cover spatially averaged over 3 distinct regions of North America. The aim of this analysis is to identify systematic errors in portions of the annual cycle encompassing the full range of climate conditions over North America. The analysis covers three regions. Region 1 is a cold, continental climate, the second region, in the southwest, is an arid climate, while the third region over the Atlantic seaboard is a typical moist, mid-latitude region. The 3 regions are presented in Figure 2.5.

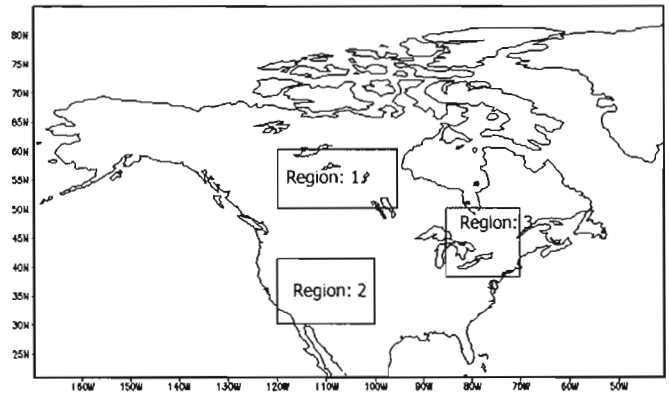

Figure 2.5: Three analysed climate type regions.

In Figure 2.6 we present comparisons of the mean annual cycle of ISR (Figure 2.6a), DLR (Figure 2.6b) and cloud-cover (Figure 2.6c) as spatial averages for region 1. GEM-LAM has an accurate representation of the annual cycle of ISR outside the extended summer season (May-August). In Section 4 of M07 we have shown that GEM-LAM generally has an accurate representation of clear-sky radiation, suggesting the main contribution to total-sky ISR errors is related to cloud cover. This is supported in Figure 2.6c where GEM-LAM cloud cover has a maximum negative bias in the summer season (compared to ERA40 clouds). CRCM simulates the annual cycle of ISR extremely accurately over region 1. Also in M07 we showed that CRCM has an accurate clear-sky ISR, but overestimates JJA total-sky ISR due to a systematic underestimate of cloud cover. In region 1 the simulated cloud cover in CRCM is quite accurate in the summer, resulting in an accurate ISR for total-sky conditions in this region. It is noteworthy that CRCM simulated DLR is systematically underestimated by ~20 Wm^{-2} throughout the annual cycle, even though cloud fraction errors are small in the summer season further suggesting a systematic underestimate of cloud emissivity in the CRCM radiation scheme. Contrary to GEM-LAM, CRCM appears to underestimate cloud cover outside of the summer season. This error impacts in a consistent manner on the simulated DLR (a negative bias) but

has only a minimal impact on simulated ISR. In a similar sense the negative bias in DLR in the summer season is temporally collocated with a relatively accurate simulation of cloud cover while ISR values are accurate in this season. This configuration suggests an inconsistent treatment of cloud water between the solar and longwave portions of the radiation scheme in CRCM.

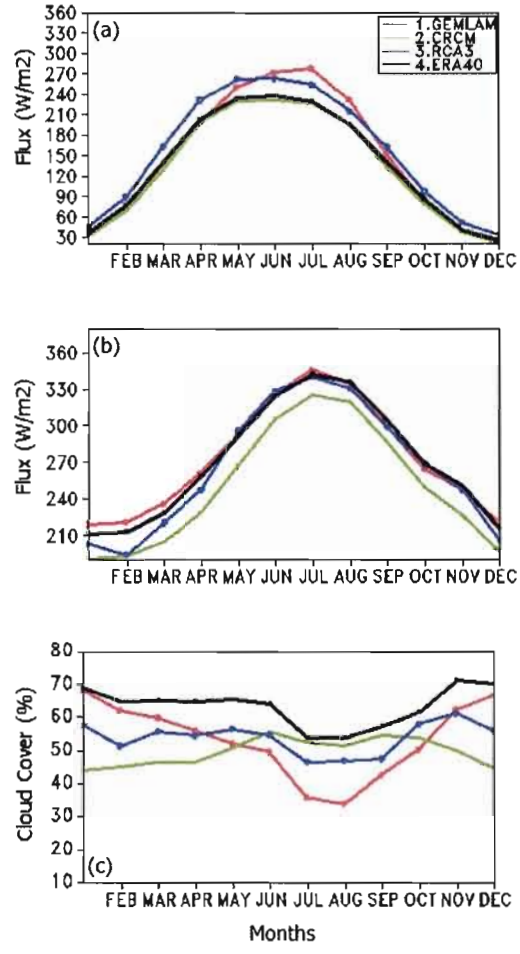

Figure 2.6: Region: 1 mean annual cycle of: a) ISR, b) DLR, c) cloud cover. ERA40 (black), GEM-LAM (red), CRCM (green), RCA3 (blue).

RCA3 overestimates ISR and underestimates DLR outside of the period May-October and these errors are again consistent with underestimated cloud-cover. In the summer, ISR remains overestimated while DLR is quite accurate (this basic summer season picture is also true for GEM-LAM). We suggest here that the underestimate of summer season clouds in those 2 models impacts directly on simulated total-sky ISR. For DLR the implied underestimate of cloudy-sky DLR is less important for the total-sky DLR because a large fraction of the surface DLR emanates from clear-sky emission below cloud base in a relatively moist and warm lower atmosphere (Niemela et al., 2001). Furthermore, the ISR positive bias will generally lead to a positive bias in near surface temperatures. Hence near surface clear-sky longwave emission may be positively biased and balance a negative bias contribution from an underestimated cloud fraction. As a result the differences between cloudy and clear DLR are relatively small in the summer season leading to a reduced sensitivity of total-sky DLR to cloud errors.

Over the warm and arid region 2, ISR is very well simulated by all models throughout the year (Figure 2.7a). DJF biases are about ~-5 to ~+15 Wm^{-2} while JJA are ~10-15 Wm^{-2}. The more accurate ISR results in region 2 are partly explained by smaller cloud amounts in this region and smaller cloud errors (see Figure 2.7c). Also one might expect that in a dry atmosphere, as over the southwest USA, that clouds when present, are dominated by relatively optically thin clouds. The misrepresentation of optically thin clouds will have a smaller impact on solar radiative fluxes than cloud bias associated with optically thicker clouds. In region 2 DLR is mostly influenced by clear-sky radiation (Figure 2.7b). RCA3 and CRCM both have negative biases in DLR during winter of ~10 Wm^{-2}, GEM-LAM also has a tendency for a similar bias in the early winter. This is consistent with the negative clear-sky bias seen in the frequency distributions for DLR in M07 (see Figure 1.11e). This error seems associated with an underestimate of DLR in dry atmospheric conditions. In these situations more of the IR emission/absorption lines are not filled

by water vapor, hence other trace gases play a larger role in the total atmospheric emission of longwave radiation. It is likely that deficiencies in fully representing these gases in the RCM radiation schemes becomes more evident in very dry situations.

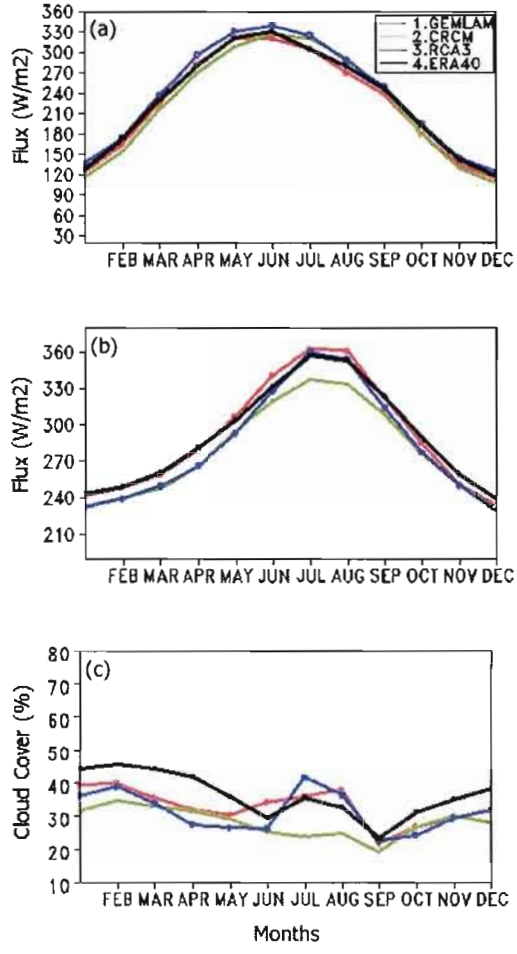

Figure 2.7: Region: 2 mean annual cycle of: a) ISR, b) DLR, c) cloud cover. ERA40 (black), GEM-LAM (red), CRCM (green), RCA3 (blue).

GEM-LAM has the most accurate representation of DLR over this region compared to ERA40. The radiation scheme in GEM-LAM, due to Li and Barker

(2005), is the most modern of all 3 of the RCMs. Based on the correlated-k approach, the scheme uses 9 bands to represent the longwave portion of the electromagnetic sprectrum and includes absorption and emission of 9 trace gases including H_2O, CO_2, O_3, N_2O, CH_4, $CFC11$, $CFC12$, $CFC13$ and $CFC14$. The RCA3 and CRCM radiation schemes only explicitly consider the first 3 gases in the calculation of clear-sky DLR. We believe this level of sophistication, while computationally expensive, is necessary for an accurate treatment of clear-sky longwave radiation. The closest observational point to region 2, that was evaluated in M07 Section 3, is Desert Rock. The individual comparison between the respective RCMs and station observations at Desert Rock (not shown) leads to very similar conclusions to those derived here with respect to ERA40. We therefore have confidence these identified errors indicate real model shortcomings and emphasize the importance of including trace gases in radiation schemes.

In region 3 DJF ISR is well simulated by GEM-LAM and CRCM (~3-10 Wm^{-2} negative bias) while both substantially overestimate ISR in JJA (~30-45 Wm^{-2}) (Figure 2.8a), the latter problem appears directly associated with an underestimate of cloud amounts in the 2 models (see Figure 2.8c). RCA3 overestimates DJF ISR (bias of ~+12 Wm^{-2}) while the summer season is very accurate. The accurate ISR results between April to September in RCA3 are concurrent with very small cloud cover biases (Figure 2.8c) while the winter ISR overestimate is associated with a negative cloud bias. DLR is again very well simulated by GEM-LAM with year round biases of 5-10 Wm^{-2} (Figure 2.8b). RCA3 underestimates DLR in winter (~10 Wm^{-2} bias) while for JJA it is very accurate (~5 Wm^{-2} bias). CRCM again shows a systematic underestimate of DLR of order ~10-20 Wm^{-2} throughout the year. As discussed earlier, while a portion of the CRCM DLR bias appears directly related to underestimated cloud amounts we have also shown that cloud water amounts and cloud emissivity are systematically underestimated in this model also contributing to an underestimate of DLR. The nearest SURFRAD

station associated with region 3 is Penn State. Comparison between the individual RCMs and surface observations at Penn State lead to similar conclusions as sees in Figure 2.8 with respect to ERA40 values (not shown).

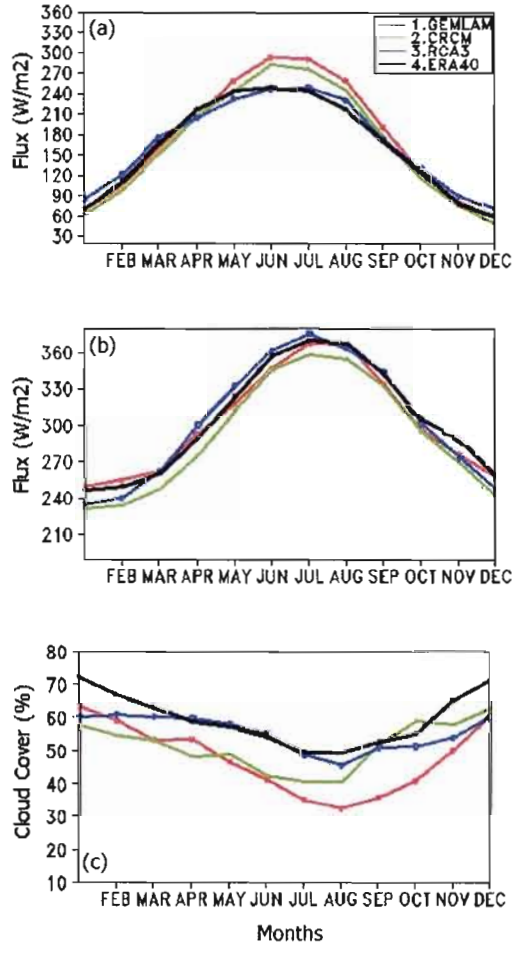

Figure 2.8: Region: 3 mean annual cycle of: a) ISR, b) DLR, c) cloud cover. ERA40 (black), GEM-LAM (red), CRCM (green), RCA3 (blue).

6. Summary and conclusions.

To determine which gridded data set was the most accurate surrogate for surface SRB observations, we evaluated ERA40, NARR and ISCCP SRB values.

Mean annual cycles of downwelling longwave radiation and incoming shortwave radiation from these 3 data sets were compared to surface observations averaged over the 6 SURFRAD stations. ERA40 was shown to represent the surface observations most accurately when both components of the surface radiation budget were considered. Winter season DLR ERA40 values were biased slightly towards low values, consistent with earlier findings of Wild et al. (2001). Comparison of ISR and DLR normalised frequency distributions between ERA40 and surface observations showed that ERA40 accurately described the variance of surface flux values with a slight shift in winter time DLR towards low values and a compensating shift in the DJF ISR distribution.

Seasonal means of the 2 components of the surface radiation budget as simulated by 3 RCMs were compared to ERA40 over the entire continental North America. DJF ISR was well represented by GEM-LAM and CRCM, while RCA3 showed larger DJF ISR biases. RCA3 and CRCM underestimated DJF DLR, while GEM-LAM had more representative results, partly as a result of the inclusion of trace gases in the longwave radiation scheme in the latter model. For the summer season, all models underestimated cloud cover hence they overestimated ISR. As seen in M07 this ISR overestimate is not as pronounced for the RCA3 model due to compensation of the negative cloud cover bias by a clear-sky atmosphere that is too opaque to solar radiation and clouds, when present, being optically too thick. CRCM simulated DLR in summer remained biased low by ~20 Wm^{-2} due to an underestimate of cloud cover compounded by a systematic underestimate of cloud emissivity, while GEM-LAM and RCA3 had fairly accurate estimates of JJA DLR. In general, the SRB biases identified in M07 were confirmed when a more spatially complete evaluation was made against ERA40 data.

Over the continental cold region 1, the RCM simulated ISR showed strong dependence on cloud cover. For the JJA season, GEM-LAM and RCA3

underestimated ISR while CRCM was in accord with observations due to an accurate annual cycle of cloud cover. DLR was very well represented by GEM-LAM and RCA3 with already explained winter biases in the latter. CRCM systematically underestimated DLR, due to a poor representation of cloud emissivity. In the warm and arid region 2, cloud cover was relatively well simulated by all 3 RCMs, as a result all RCMs had accurate values of ISR. For the dry region, both CRCM and RCA3 underestimated DLR, while GEM-LAM had more accurate values, likely due to the inclusion of trace gas contributions to DLR. In the mid-latitude, moist region 3 simulated ISR was sensitive primarily to cloud errors with GEM-LAM and CRCM both overestimating JJA ISR. RCA3 gave a better representation of cloud amounts and hence had a more accurate ISR budget. DLR was well simulated by GEM-LAM and RCA3 in this region, while CRCM gave a systematic underestimate across all 3 climatic regimes.

This study emphasizes biases in simulated cloud cover as the fundamental error compromising the quality of simulated SRB in Regional Climate Models. This is particularly true for the ISR budget in the summer season. Error compensation between individual components influencing the surface radiation budget (e.g. cloud cover, cloudy-sky and clear-sky radiation fluxes) along with compensation between the 2 SRB components (ISR and DLR), in terms of total SRB, emphasize the need for careful evaluation of all terms influencing the individual components of the simulated SRB. It is crucial that accurate observations are used in this evaluation and the assessment be made both for seasonal and diurnal timescales separately. Only through this type of detailed evaluation can key errors in cloud-radiation interaction be identified, allowing physically based improvements to be developed that faithfully represent the underlying physics controlling the surface radiation budget.

Acknowledgements:

This work was funded by the grant provided by Canadian Foundation for Climate and Atmospheric Sciences, grant number 61209 which funded Canadian Regional Climate Modeling and Diagnostics network. The authors wish to thank to Mr. Patrice Constanza from the GEC3 centre and to Dr Zav Kothavala from the centre ESCER/UQAM for providing the Reanalysis data in a suitable format.

3. AN EVALUATION OF ERA40 RADIATION BUDGET OVER DIFFERENT CLOUD COVER CONDITIONS.

In Chapter 2, we saw that ERA40 was the most representative surrogate gridded data set representing both the ISR and DLR. Analysing frequency distributions confirmed that ERA40 ISR and DLR variability was simulated accurately with only a slight bias in winter season DLR and ISR. In this chapter we evaluate the ERA40 SRB as a function of different cloud cover and try to understand probable causes in ERA40 DJF frequency distribution biases.

To investigate further the cause of the ERA40 DJF biases in ISR and DLR, we present normalized frequency distributions of surface ISR and DLR separately for different sky conditions (all-sky, cloud-free and cloudy) averaged for the months February-March (FM). Cloud-free conditions include all radiative flux values when the cloud cover is less than 10%, cloudy conditions are when observed or simulated cloud fraction is >90%, while all-sky represents situations irrespective of cloud conditions. The FM season is used as a surrogate for DJF due to the presence of observed cloud amounts only during daylight hours and for the 6 hourly frequency of ERA40 data made it impossible to find sufficient cloud observations in the DJF season for robust conclusions to be drawn with respect to cloud and clear-sky SRB values. We therefore choose to use February and March as surrogate winter months where sufficient cloud data is available.

The ERA40 and surface observations analyzed cover just 2 years (2000-2001) and the analyzed day period is 18-0 UTC (one quarter of diurnal cycle, approximately 12-18 LST). The data limitations in this chapter are due to a combination of the SURFRAD cloud observations only being available during daylight and the temporal frequency (6 hourly only) and duration of the ERA40 dataset. The only common

overlap period for each data set is therefore the 18-0 UTC section of the ERA40 diurnal cycle and the years 2000 and 2001.

We take a mean across all the sites listed in Part 2 Table 2.1 except Penn State due to the lack of cloud information. The main reason for this analysis is to try to determine if the DJF bias in all-sky ISR and DLR arises systematically under completely cloudy or cloud-free conditions. This we achieve by constructing normalized histograms of ISR and DLR selected separately for cloudy and clear-sky conditions in both data sets.

Results are presented in Figure 3.1 for FM months for all-sky, cloudy and cloud-free conditions. DLR all-sky (Figure 3.1d) is very well simulated by ERA40 and exhibits to only a very slight overestimate in cloud-free (Figure 3.1e) and underestimate in cloudy conditions (Figure 3.1f), leading to a very accurate histogram of DLR under all-sky conditions. This all-sky DLR for daytime FM periods therefore differs from the DJF DLR values, calculated for the entire diurnal cycle, presented in Part 2 Figure 2.4b which showed a systematic negative bias in DLR occurrence. Constructing the all-sky DLR for the FM months using the entire diurnal cycle (Figure 3.2) period reproduces the ERA40 DLR errors, seen for DJF (i.e. a shift towards too low DLR values).

We therefore conclude that errors in the winter season DLR in ERA40 are mainly resulting from errors in the nighttime representation of DLR and factors contributing to the DLR (e.g. near surface temperature and humidity, cloud cover). Nighttime conditions contribute significantly to the mean diurnal cycle DLR values in DJF, hence this error contribution is seen in the monthly mean values. Due to the lack of cloud observations at night, we are unable to discriminate further as to the cause of this nighttime DLR bias in ERA40 but conjecture a link with the representation of near surface temperature and moisture during statically stable conditions in the nocturnal winter boundary layer.

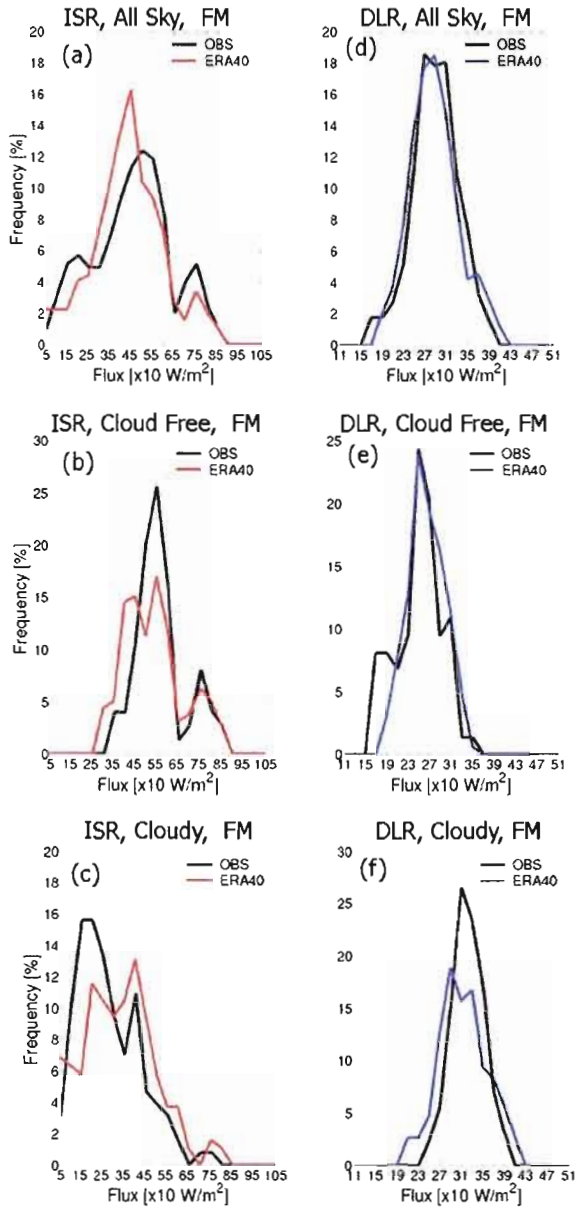

Figure 3.1: Distribution of ISR and DLR 6 hourly data from ERA40 and observations, February-March season. Analyzed day period 18-0 UTC: a) ISR all-sky, b) ISR cloud-free, c) ISR cloudy, d) DLR all-sky, e) DLR cloud-free, f) DLR cloudy.

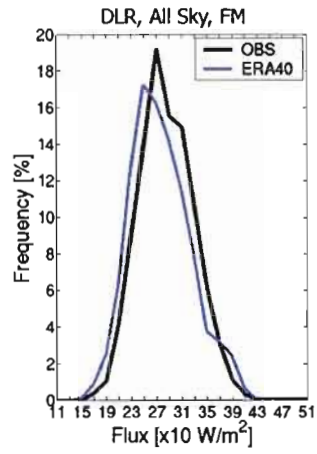

Figure 3.2: Distribution of DLR raw data from ERA40 and observation, February-March. Entire diurnal cycle included.

The lower end of ISR values, in the all-sky histograms (50-250Wm^{-2}), is underestimated by ERA40. This appears to mainly arise from an underestimate in cloudy conditions (Figure 3.1c). This is either due to problems in representing ISR absorption and reflection at low solar elevation angles or due to an underestimate of very reflective clouds in ERA40. The general shift towards higher ISR values in the ERA40 cloudy histograms suggested ERA40 winter season clouds are generally not sufficiently reflective. One possible cause of this is the fractional partitioning of cloud water solid and liquid components in the ECMWF cloud parameterisation. According to the ECMWF-IFS (Integrated Forecast System) documentation (http://www.ecmwf.int/research, Accessed April 23, 2007) the fraction of cloud water considered to be frozen increases from 0 at $0°C$ to 1 at $-22°C$, with the fraction increasing with the second power of decreasing temperature in this range. Observations in the Arctic (e.g. Shupe and Matrosof, 2001; Shupe et al., 2006) indicate the liquid phase is present in observed clouds even at cloud temperatures as low as $-39°C$. An underestimate of the liquid fraction of a mixed phase cloud and commensurate overestimate of the solid fraction will cause an overestimate of the

median effective radius of cloud water in the ECMWF radiation scheme and therefore an underestimate of cloud reflectivity, consistent with the results in Figure 3.1c. The slight shift towards a low bias in DLR in FM cloudy conditions in ERA40 (Figure 3.1f shows ERA40 overestimates the fractional occurrence of DLR under cloudy conditions in the range ~190-260 Wm^{-2} while underestimating the range ~270-350 Wm^{-2}) is also consistent with overestimate of ice fraction in the ECMWF radiation scheme and a slight underestimate of cloud emissivity.

We now compare the mean seasonal cycle of ERA40 ISR and DLR against observations for cloud-free and all-sky conditions (Figure 3.3). Due to the limited availability of direct cloud observations during daytime only, restrictions in the annual cycle (February-August) and in the diurnal cycle (18-0 UTC) must be applied. The analyzed period covers only 2 years (2000-2001) and the station of Penn State is excluded for the reasons mentioned earlier. ISR, all-sky (Figure 3.3a) is overestimated by ERA40 from the month of March to June, while for the summer season (JJA) and for month of February the accordance is very good. For clear-sky conditions (Figure 3.3b), ERA40 underestimates observations overall in February and in JJA. Figure 3.4 represents the comparison of cloud cover, ERA40 against observations, with the restrictions in annual and diurnal cycle as for Figure 3.3.

We find that ERA40 overestimates cloud cover in February but gradually underestimates it from March to August. In FM season, underestimation of ISR frequency of distribution for cloud-free conditions (Figure 3.1a) is balanced by an overestimate in cloudy conditions (Figure 3.1c) resulting in a relatively accurate all-sky radiation flux (Figure 3.3a). From March to June, an overall underestimate of cloud cover in ERA40 and fairly good representation of ISR in cloud-free conditions leads to an overestimate of ISR in all-sky conditions. Cloud-free ISR errors (Figure 3.3b) we speculate may be related to errors in the diurnal cycle of clouds in ERA40 causing a clear-sky sampling bias in ERA40.

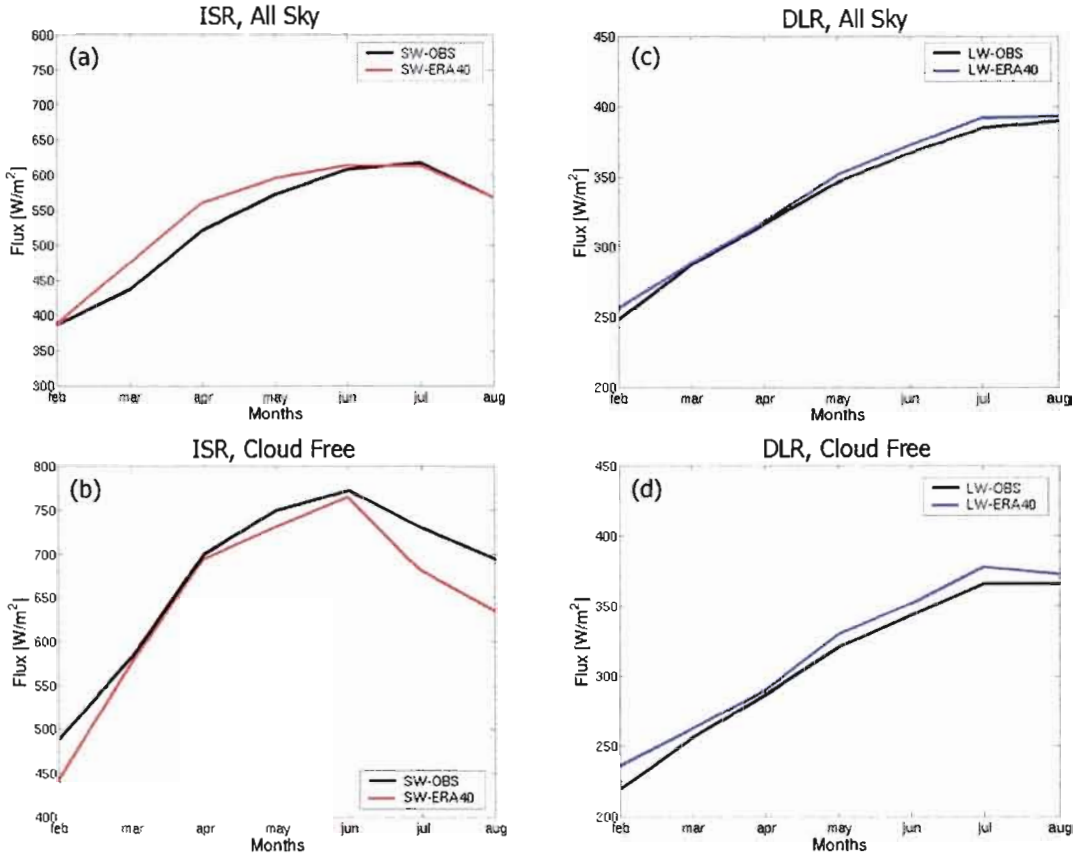

Figure 3.3: Mean seasonal cycle of: a) ISR, all-sky, b) ISR, cloud-free, c) DLR all-sky, d) DLR, cloud-free. Annual cycle is calculated for period 18-0 UTC.

For observed cloud amounts during the summer season we have analysed the fractional occurrence of clear-sky conditions as a function of time of day within the 6-hour window analysed here (roughly 12-18 LST). This analysis indicates that clear-sky conditions occur more frequently in observations for the 3-hour period centered at local noon than the period 15-18 LST. This reflects the well-known tendency for cloud cover to increase through the diurnal cycle in the summer season over North America. Phasing of this preference for clear-sky conditions around local noon with maximum in the TOA incoming solar radiation will maximize clear-sky surface ISR values in the observations for the period 12-18 LST. We are unable to perform a

similar 3-hourly analysis of cloud cover and therefore cloud-free conditions in the ERA40 data set. Nevertheless a number of studies highlight the tendency for models to simulate cloud cover increases too early with the afternoon-evening section of the diurnal cycle over summer season continental region (e.g. Guichard et al., 2004; which included an analysis of the ECMWF convection scheme due to Tiedtke, 1989). We therefore speculate that cloud-free conditions in ERA40 may be biased in a relative sense, towards the latter half of the 6-hour daytime period analysed here. The diurnal cycle of TOA ISR accompanied with a shift in the fractional occurrence of clear-sky in ERA40 would then naturally lead to an excess of surface ISR in ERA40 even in common clear-sky condition at the 6-hourly accumulation time scale.

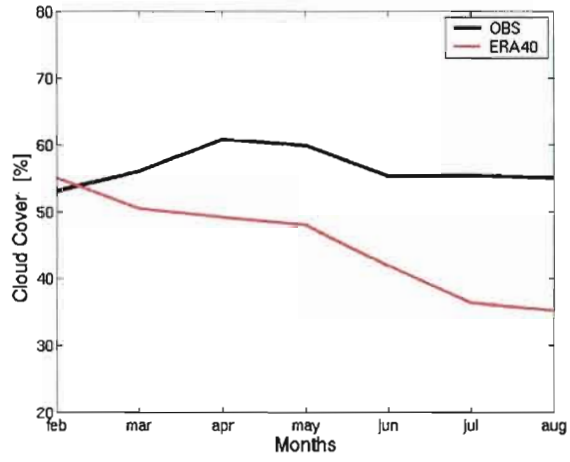

Figure 3.4: Mean seasonal cycle of cloud cover for ERA40 and observations. Annual cycle is calculated for period 18-0 UTC.

DLR all-sky (Figure 3.3c) is well represented in ERA40 with a small overestimate in February and in JJA. The DLR overestimate in February (when analysed period is 6h daytime) and underestimate of DLR for FM (Figure 3.2, period when entire diurnal cycle included) suggest erroneous representation of DLR during the night. Our earlier suggestion that ERA40 underestimates the effective radius of

winter season clouds is consistent with a systematic underestimate of cloudy-sky DLR balancing a slight overestimate of DLR in cloud-free conditions. The overall underestimate of cloud amount in ERA40 will further balance the cloud-free overestimate of DLR in the context of all-sky DLR in ERA40. In cloud-free conditions ERA40 DLR has slightly bigger biases than for all-sky. Underestimate of cloud amounts in ERA40 combined with the cloud-free results of DLR will alleviate biases in the all-sky conditions. The underestimate of cloud cover in ERA40 balances clear-sky ISR and DLR errors in different directions, acting to reduce a negative bias in cloud-free ISR (i.e. cloud-free ISR is underestimated in JJA while the occurrence of clouds is also underestimated so their combination would lead to an accurate all-sky ISR).

Figures 3.5a and 3.5b show the comparisons of ERA40 and observational ISR CRF and DLR CRF respectively. Both CRFs are underestimated by ERA40. The effect of cloud cover is bigger for ISR hence the underestimate of CRF for this component of SRB is greater. It is interesting that ISR CRF underestimation, by ERA40, is alike for the entire annual cycle given on Figure 3.5 (except for June). Net CRF (Figure 3.5c) represents the addition of ISR and DLR CRFs and it is dominated by ISR CRF due to the analyzed time period (day time) hence the underestimation of Net CRF by ERA40.

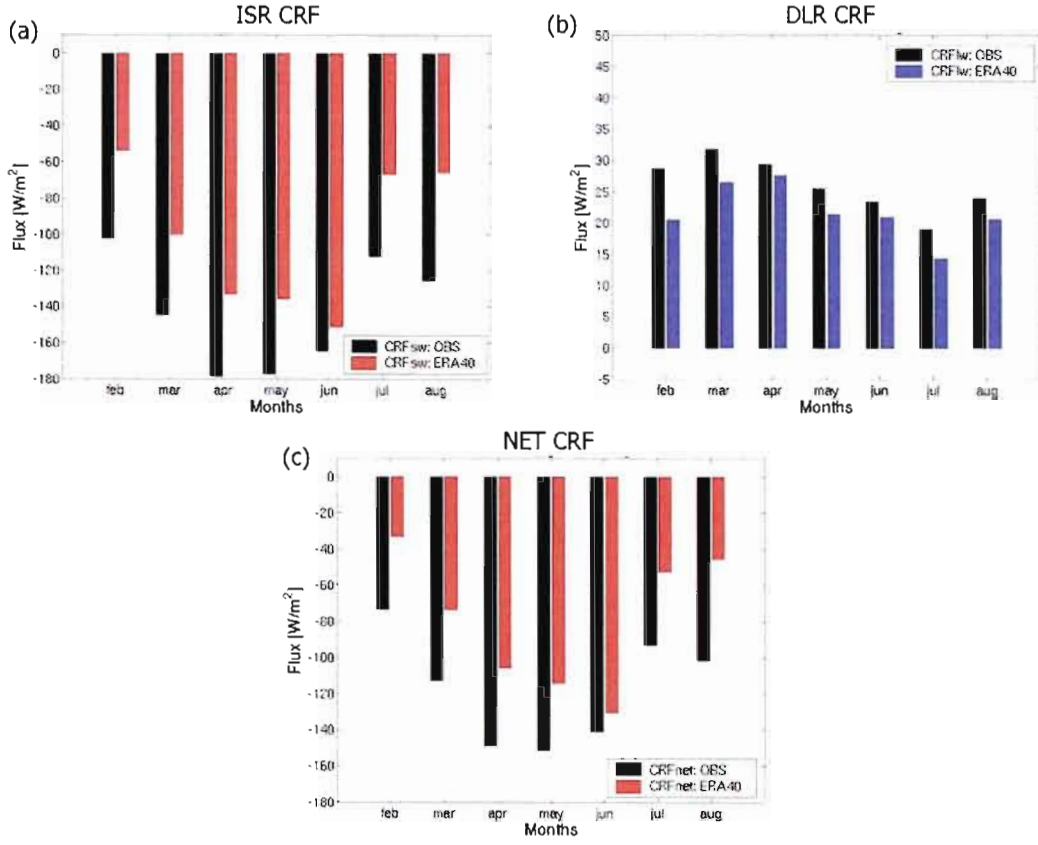

Figure 3.5: Mean seasonal cycle of Cloud Radiative Forcing (CRF) for ERA40 and observations: a) ISR CRF, b) DLR CRF, c) Net CRF. All for period 18-0 UTC.

CONCLUSION

An accurate representation of the individual components of surface radiation budget (SRB) is an important requirement of climate models. These components are directly related to and forced by other prognostic variables in climate models, such as temperature, water vapor, hydrological cycle constituents etc. In this work, we have evaluated the incoming surface shortwave radiation (ISR), downwelling longwave radiation at the surface (DLR) and cloud cover in three climate models: 1. the Canadian Regional Climate Model (CRCM), 2. the Global Environment Multiscale model (GEM) and 3. the Rossby Centre regional Atmospheric climate model (RCA3). Each of these models has different radiation and cloud schemes and are widely used in a number of different regional climate change assessment studies. A primary reason for testing these models is to compare the results of these schemes under different conditions. Each model showed differing levels of accuracy in different climate conditions or sky cover (e.g. cloud-free, cloudy). The models also exhibited sensitivity in their simulated SRB to time of year and day. Isolating periods when the respective simulated SRB is more or less accurate will aid in identifying aspects of the parameterized physics requiring improvement in a given model.

The aim of this study is to compare the components of SRB of 3 RCMs over the domain of North America and it is done in three stages. First, we evaluated SRB components from the 3 RCMs against direct surface observations intending to identify conditions where they operate poorly. Second, due to lack of a complete SRB observation data set covering the entire North America we evaluated the SRB in the ERA40 reanalysis, NARR reanalysis and ISCCP products against surface observations. The reanalysis and ISCCP products represent spatially and temporally complete surrogates for SRB observations, the most accurate of these products can be used to evaluate the RCM simulated SRB across North America. In the final stage, a

comparison of the 3 RCMs against the best surrogate set is done for the entire domain of North America aiming to test how the 3 RCMs operate in different climate conditions.

Compared to surface observations, DLR from all RCMs showed the biggest biases in the winter season. This error was dominated by a negative clear-sky DLR bias. GEM-LAM had the smaller bias of the 3 RCMs in cold, dry clear-sky conditions, which appeared to be due to a more complete inclusion of trace gasses (e.g. CH_4, $CFC11$, $CFC12$, $CFC113$ and $CFC114$) in the calculation of DLR. The other 2 RCMs did not include these gases considering only H_2O, $CO_2$and O_3 in DLR calculations.

The emissivity of clouds proved to be very important factor in DLR all-sky simulation. It was shown that the origin of DLR biases in GEM-LAM and RCA3 were mainly in clear-sky radiation, while for CRCM it was a combination of both. Cloud cover errors dominated ISR biases, especially in the summer season in GEM-LAM and CRCM, while RCA3 ISR results were influenced both by cloud cover errors and a clear-sky atmosphere, which was too opaque to solar radiation.

Compared with surface observations, ERA40 proved to be the best surrogate observational data set for representing ISR, DLR and cloud cover. The ERA40 SRB components when averaged over the 6 SURFRAD station exhibited seasonal mean biases of $\sim$10-15 Wm^{-2} with little spatial cancellation of error between the various sites. All models were compared over the entire North America against the best gridded surrogate set (ERA40). The results found over the entire domain were consistent with the respective model errors found when the RCMs were compared to the 6 SURFRAD stations. ISR showed to be very dependent on simulated cloud cover. GEM-LAM and CRCM underestimated ISR again for the summer season, while RCA3 showed moderate biases due to the cancellation effect already shown in this model for the summer season. DLR winter season biases were seen in all RCMs

and CRCM showed year round DLR biases related to a systematic underestimate of cloud emissivity and cloud cover. Comparison over 3 different climate regions showed great ISR dependency on simulated cloud cover. Overall GEM-LAM had the most accurate representation of DLR when evaluated across all climate regimes.

In an attempt to better understand the ERA40 DLR winter season biases, we analysed ERA40 normalised frequency distributions for different sky conditions for this season. Due to cloud cover observations on SURFRAD measurement sites being available only during the daytime, DLR frequency distributions for varying cloud cover could only be constructed for the daytime period (18-00 UTC). For this shorter period, ERA40 DLR was simulated accurately suggesting DLR winter season biases in ERA40 were mainly due to errors in the representation of nocturnal DLR (potentially arising from a systematic nightime warm bias).

We further compared mean annual cycles of ISR and DLR for ERA40 against surface observations. For the analysed daytime period, ERA40 generally underestimated cloud-free ISR but combined with an underestimate of cloud cover gave a fairly good result in all-sky conditions. ERA40 DLR in all-sky conditions was represented quite accurately although this result was influenced by underestimate of DLR in cloudy condition and by overestimate of DLR in cloud-free condition. Due to underestimate of ISR in cloud-free condition, ERA40 underestimated ISR CRF. Likewise, ERA40 DLR cloud-free positive biases are responsible for an underestimate of ERA40 DLR CRF. ERA 40 Net CRF represents an addition of underestimated ISR and DLR cloud radiative forcings, hence is also underestimated.

One of the largest uncertainties in the analysis presented in this study relates to the accuracy of the observed cloud cover. The RGB (Red-Green-Blue) camera, which is used for cloud observation, cannot distinguish cloud height or thickness and cannot tell anything about cloud overlapping. The camera just gives rough percentage of total cloud cover irrespective of cloud height, optical thickness or constituent size,

all of which strongly influence ISR and DLR. To better evaluate the full components influencing the SRB a logical next step in this work would be to evaluate the components of the simulated and observed SRB classified by different cloud heights, LWP values and implied optical thickness. In doing this, one could further isolate key weaknesses in a given RCM that causes errors in the simulated SRB. Observations to support this type of analysis are available at only a few sites around the globe (e.g. the ARM SGP site in southern USA and the ARM North Slope in Alaska).

Another possible evaluation of model simulated SRB can be seen in testing radiation schemes in stand alone mode. In this mode, radiation packages use input from ground observations and atmospheric soundings rather than from model-calculated parameters. With this approach, we can be more confident that any errors in the simulated SRB come directly from the radiation schemes and are not due to errors in the representation of the basic thermodynamic variables.

Considering the improvements of errors that we have found in this study, DLR in clear-sky condition can be improved by better describing the water vapor continuum (e.g. including more water vapor bands) and by including extra trace gases (as was seen for GEM-LAM results). Errors seen in all-sky comparisons can also be improved. Cloud fraction remains the key variables to improve in all models. Liquid water path, which can influence cloud reflectivity and emissivity can be improved with an improved treatment of precipitation processes and a better representation of both liquid and solid (ice) microphysical processes.

ANNEX A
AN EVALUATION OF DIURNAL CYCLE OF CLOUD RADIATIVE FORCING

In this appendix we use the results from Chapter 1 expanding our analysis to the diurnal cycle of cloud radiative forcing. Previously, we saw the role of monthly mean based CRF, nevertheless it is diurnal cycle of CRF who generates possible monthly CRF biases and thus this analysis is needed. The impact of simulated cloud cover on surface radiation can also be seen through the diurnal CRF analysis.

Figure 1.3 from Chapter 1 Section 3 shows the diurnal cycle of cloud-cover averaged over the 6 observation sites, results are presented for the common time period when cloud observations were available 15-00 UTC (approximately 9-18 LST).

The underestimate of cloud cover through the diurnal cycle helps explain the positive bias in ISR in all 3 models (see Chapter 1, Fig. 1.12a). The increasing underestimate of cloud cover in CRCM through the diurnal cycle also helps explain the increasing size of the all-sky ISR positive bias in this model. Similarly the negative bias in all-sky DLR (see Chapter 1, Fig. 1.12c) is consistent with the underestimate of cloud cover in CRCM (Fig. 1.3, Chapter 1). The cloud underestimate in RCA3 is balanced in the ISR by an overly opaque clear-sky, while for DLR the accurate all-sky results suggest the clouds that are present have too high emissivity. Finally GEM-LAM all-sky DLR is well simulated because the underestimate of cloudy-sky DLR is partially compensated by excess of clear-sky DLR (see Chapter 1, Section 4).

The dependence of ISR and DLR on an accurate simulation of cloud cover can be appreciated by considering the diurnal cycle of cloud radiative forcing. As in

Chapter 1, Section 4 we construct ISR CRF (Fig. A1a), DLR CRF (Fig. A1b) and Net CRF (Fig. A1c). Two values of observed CRF are presented. The first (in black) shows the CRF implied by using the observed cloud fractions directly from RGB camera. The origin of second observational ISR CRF and Net CRF (in gray) is introduced in Chapter 1, Section 4 and comes from a 5% change (decrease) in observed cloud amount and this leads to a $\sim 15 Wm^{-2}$ change in surface CRF. Comparing this cloud cover change effect on ISR with DLR excess due to doubling CO_2 concentration ($\sim 4 Wm^{-2}$) we emphasize the importance of accurate cloud cover simulation.

ISR CRF is underestimated by all models, which can be explained by two reasons. First, erroneous cloud cover (Fig. 1.3, Chapter 1) (e.g. not enough clouds to block ISR radiation) and second, a poor simulation of cloud reflectivity (i.e. distribution of water droplets, effective radius, presence of ice instead of water phase). DLR CRF (Fig. A1b) is very well simulated by RCA3. This, once again, confirms good cloud effect on DLR for this model. Other models underestimate DLR CRF, especially CRCM, and the effect is clearly seen on Figure 1.12c, Chapter 1. Underestimate of DLR CRF is probably related to wrong LWP or IWP simulated in GEM-LAM and CRCM (see Fig. 1.9, Chapter 1). SW diurnal CRF is much greater than the DLR CRF, hence Net CRF is underestimated by all RCMs. For RCA3, this underestimate is equal to the one of ISR CRF. Even with the second estimate of ISR CRF (gray bar) all models tend to underestimate it though with smaller biases. Same result is found for Net CRF.

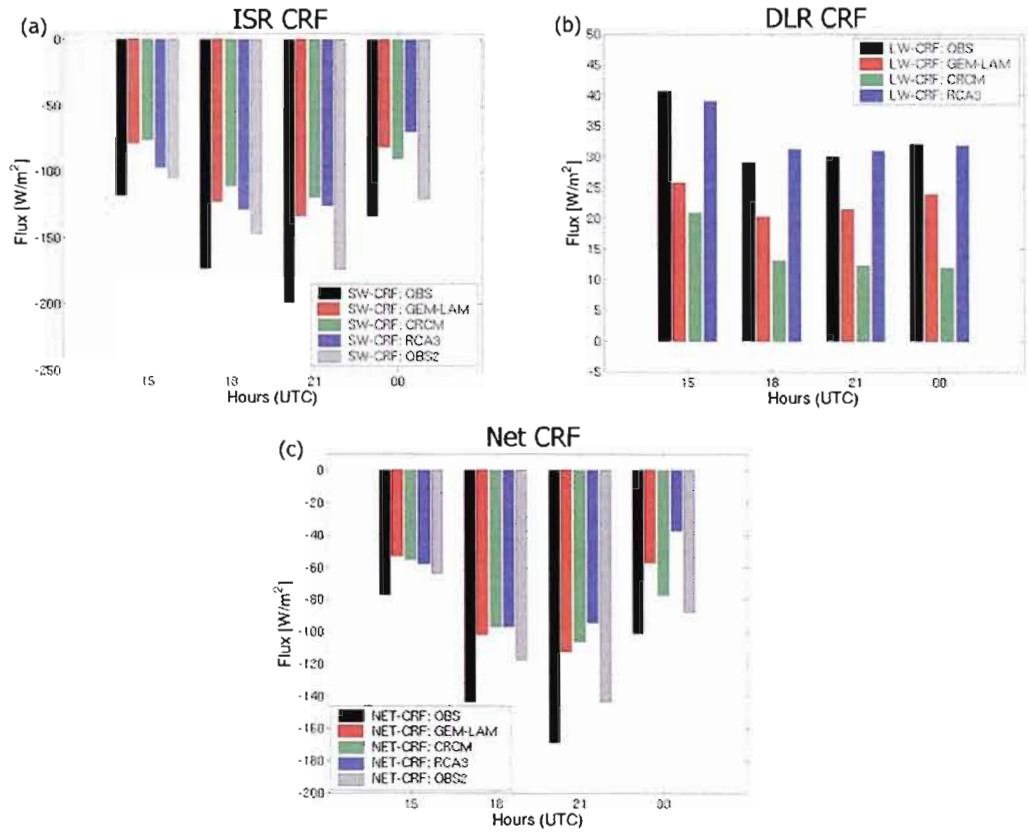

Figure A1: Mean diurnal cycle of cloud radiative forcing:(a) SW CRF, (b) LW CRF, (c) Net CRF.

REFERENCES

Albrecht, B.A., 1989: Aerosols, cloud microphysics, and fractional cloudiness, *Science*, **245**, 1227-1230.

Barkstrom, B. R., 1984: The Earth Radiation Budget Experiment (ERBE), *Bull Am. Meteorol. Soc.*, **65**, 1170-1185.

Betts and Harshvardan, 1987: Thermodynamic Constraint on the Cloud Liquid Water Feedback in climate Models. *J. Geophys. Res.*, **92**, 8483-8485.

Caya and Laprise, 1999: A Semi-Implicit Semi-Lagrangian Regional Climate Model: The Canadian RCM. *Monthly Weather Review*, **127**, 341-362.

Cess, R. D., M. H. Zhang, P. Minnis, L. Corsetti, E. G. Dutton, B. W. Forgan, D. P. Garber, W. L. Gates, J. J. Hack, E. F. Harrison, X. Jing, J. T. Kiehl, C. N. Long, J. J. Morcrette, G. L. Potter, V. Ramanathan, B. Subasilar, C. H. Whitlock, D. F. Young, and Y. Zhou. 1995. *Science*. **267**,496-499.

Côté, J., J.-G. Desmarais, S. Gravel, A. Méthot, A. Patoine, M. Roch et A. Staniforth, 1998: The operational CMC-MRB global environnemental multiscale (GEM) model. Part I: Design considerations and formulation. *Mon. Wea. Rev*, **126**, 1373-1395.

Fouqart, Y. and B. Bonel, 1980: Computation of Solar Heating of the Earth's Atmosphere : A New Parameterization. *Contributions to Atmospheric Physics*, **53**, No.1, 35-62.

Garrat and Prata, 1996: Downwelling Longwave Fluxes at Continental Surface – A Comparison of Observations with GCM Simulations and Implications for the Global Land-Surface Radiation Budget. *Journal of Climate*, **9**, 646-655.

Guichard, F., Petch, J. C., Redelsperger, J.-L., Bechtold, P., Chaboureau, J.-P., Cheinet, S., Grabowski, W. W., Grenier, H., Jones, C. J., Koehler, M., Piriou, J.-M., Tailleux R., and Tomasini, M., 2004:Modelling the diurnalcycle ofdeep precipitating convection over land with cloud-resolving models and single column models, *Quart. J. Roy. Meteor.*, in press.

Intrieri, J. M., M. G. Shuppe, 2004: Characteristics and Radiative Properties of Diamond Dust over the Western Arctic Ocean Region. *Journal of Climate*, **17**, 2953-2960.

Jones, C. G., U. Willén, A. Ullerstig, U. Hansson, 2004: The Rossby Centre Regional Atmospheric Climate Model Part I: Model Climatology and Performance for the Present Climate over Europe. *Ambio 33:4-5,* 199-210.

Karlsson, K. G., 2003: A 10 Year Cloud Climatology Over Scandinavia Derived From NOAA Advanced Very High Resolution Radiometer Imagery. *International Journal of Climatology,* **23**, 1023-1044

Karlsson, K. G., U. Willén, C. Jones, K. Wyser, 2006: Evaluation of Regional Cloud Climate Simulations Over Scandinavia using Ten-Year NOAA AVHRR Cloud Climatology. Submitted to *Journal of Geophysical Research*

Key, J., and R. G. Barry, 1989: Cloud Cover Analysis with Arctic AVHRR data. 1: Cloud Detection. *J. Geophys. Res.*, **94** (D15), 18 521-18 535.

Kiehl and Trenberth, 1997: Earth's Annual Global Mean energy Budget. *Bulletin of the American Meteorological Society*, **78**, 197-208.

Lenderink, G., A P Siebesma, S Cheinet, S Irons, C G Jones, P Marquet, F Mller, D Olmeda, J Calvo, E Sanchez, and P M M Soares, 2004 The diurnal cycle of shallow cumulus clouds over land: A single-column model intercomparison study *Q. J. R. Meteorol. Soc*, 130,3339–3364.

Li, J. and H. W. Barker, 2005: A Radiation Algoritm with Correlated-k Distribution. Part I: Local Thermal Equilibrium. *Journal of the Atmospheric Science*, **62**, 286-309.

Markovic, M., C. G. Jones, P. A. Vaillancourt, D. Paquin, D. Paquin-Ricard, 2007a: An Evaluation of the Surface Radiation Budget Over North America for a Suite of Regional Climate Models and Reanalysis Data, Part 1: Comparison to Surface Stations Observations. Submitted to the *Climate Dynamics.*

Mesinger, F., G. DiMego, E. Kalnay, P.Shafran, W. Ebisuzaki, D. Jovic, J. Woollen, K Mitchell, E. Rogers, M. Ek, Y. Fan, R. Grumbine, W. Higgins, H. Li, Y. Lin, G. Manikin, D. Parrish, and W. Shi, 2004: North American Regional Reanalysis. Submited to the *Bulletin of the American Meteorological Society.*

Mlawer, E. J., S. J. Taubman, P. D. Brown, M. J. Iacono, and S. A. Clough, 1997: Radiative transfer for inhomog-eneous atmospheres: RRTM, a validated correlated-kmodel for the longwave. *J. Geophys. Res.*, 102, 16,663-16,682.

Morcrette J. -J, 1991: Radiation and Cloud Radiative Properties in the European Centre for Medium Range Weather Forecast Forecasting System. *Journal of Geophysical Research.*, **96**, 9121-9132.

Niemelä, P. Räisänen , H. Savijärvi, 2001: Comparison of surface radiative flux parameterizations, Part I: Longwave radiation. *Journal of Atmospheric Research* vol **58** (2001) pp 1-18.

Peixoto and Oorth, 1992: Physics of Climate, AIP.

Räisänen, P., M. Rummukainen and J. Räisänen, 2000: Modification of the HIRLAM radiation scheme for use in the Rossby Centre regional Atmospheric Climate model. Report 49, Department of Meteorology, University of Helsinki, 71pp.

Ramanathan, V., R. D. Cess, E. F. Harisson, P. Minnis, B. R. Barkstrom, E. Ahmad, D. Hartmann, 1989: Cloud Radiative Forcing and Climate: Results from the Earth Radiation Budget Experiment. *Science*, **243**, 57-62 .

Rogers C. D., 1977: Radiative Processes in the Atmosphere. ECMWF Seminars, Reading, 5-66.

Rossow, W, B., and R. A. Schiffer, 1991: ISCCP cloud data products, *Bull. Am. Meteorol. Soc.*, **72**, 2-20

Savijarvi H., 1990: Fast Radiation Parameterisation Schemes for Mesoscale and Short-Range Forecast Models. *Journal of Applied Meteorology*, **29**, 437-447.

Schweiger, A. J., and Key J. R., 1992: Arctic Cloudiness: Comparisob of ISCCP-C2 and Nimbus-7 Satellite derived Cloud Products with a Surface-based Cloud Climatology. *Journal of Climate*: Vol. **5**, No. 12, pp. 1514–1527

Shettle E.P. and R.W. Fenn, Models for the aerosols of the lower atmosphere and effects of humidity variations on their optical properties, *Air Force Geophys. Laboratory, Environmental Papers* No. 676, 1979.

Shupe, M.D., T. Uttal, S.Y. Matrosov, A.S. Frisch, 2001: Cloud Water Contents and Hydrometeor Sizes During the FIRE-Arctic Clouds Experiment. *J. Geophys. Res.*, **106**, 15,015-15,028.

----------, S.Y. Matrosov, and T. Uttal, 2006: Arctic mixed-phase cloud properties derive from surface-based sensors at SHEBA. *J. Atmos. Sci.*, **63**, 697-711.

Slingo, A. and H.M. Schrecker, 1982. On the shortwave radiative properties of stratiform water clouds. *Q. J. R. Meteorol. Soc.*, **108,** 407-426

----------, 1990: Sensitivity of the earth's radiation budget to changes in low clouds. *Nature*, **343**, 49–51.

Stephens G. L., and P. G. Webster, 1980: Clouds and Climate: Sensitivity of Simple Systems. *Journal of the Atmospheric Sciences*, **38**, 235-247.

----------, 1984: Review of the Parameterisation of Radiation for Numerical Weather Prediction and Climate Models. *Mon. Wea. Rev.*, **112**, 826-867.

Sundquist, H., E. Berge, J. E. Kristjansson, 1989: Condensation and Cloud Parameterisation Studies with a Mesoscale Numerical Weather Prediction Model. *Mon. Wea. Rev.*,**117**, 1641-1657.

Tiedtke, M., 1989: A Comprehensive Mass Flux Scheme for Cumulus Parametrization in Large-Scale Models, *Mon. Weather Rev.*, **117**, 1779–1800.

----------, 1993: Inclusion of Ice Phase of Hydrometeors in Cloud Parameterisation for Mesoscale and Largescale Models. *Contr. Atmos. Phys.*,**66**, 137-147.

Twomey, S., 1974: Pollution and planetary albedo. *Atmos. Environ.*, **8**, 1251–1256.

Uppala, S. M.; Kallberg, P. W.; Simmons, A. J.; Andrae, U.; Bechtold, V. D.; Fiorino, M.; Gibson, J. K.; Haseler, J.; Hernandez, A.; Kelly, G. A.; Li, X.; Onogi, K.; Saarinen, S.; Sokka, N.; Allan, R. P.; Andersson, E.; Arpe, K.; Balmaseda, M. A.; Beljaars, A. C. M.; Van De Berg, L.; Bidlot, J.; Bormann, N.; Caires, S.; Chevallier, F.; Dethof, A.; Dragosavac, M.; Fisher, M.; Fuentes, M.; Hagemann, S.; Holm, E.; Hoskins, B. J.; Isaksen, L.; Janssen, P. A. E. M.; Jenne, R.; McNally, A. P.; Mahfouf, J. F.; Morcrette, J. J.; Rayner, N. A.; Saunders, R. W.; Simon, P.; Sterl, A.; Trenberth, K. E.; Untch, A.; Vasiljevic, D.; Viterbo, P.; Woollen, J., 2005: The ERA 40 re-analysis. *Q. J. R. Meteorol. Soc.* **131** 2961-3012.

Wallace and Hobbs, 1997: Atmospheric Science: An Introductory Survey, Academic Press.

Wild, M, A. Ohmura, H. Gilgen, and E. Roeckner, 1995: Validation of GCM simulated radiative fluxes using surface observations. *Journal of climate*, **8**, 1309-1324

----------, ----------, ----------, 2001: Evaluation of Downward Longvawe Radiation in General Circulation Models. *Journal of Climate*, **14**, 3227-3239.

----------, ----------, 2004: BSRN Longwave Downward Radiation Measurements Combined with GCMs Show Promise for Greenhouse Detection Studies. *GEWEX News*, **14**, No.4.

Yang, G.-Y. and Slingo, J., 2001: The dirunal cycle in the tropics. *Mon. Weather Rev.*, 129:784–801.

Zhang, Y-C., W.B. Rossow, A.A. Lacis, V. Oinas, and M.I. Mishchenko, 2004: Calculation of Radiative Fluxes From the Surface Top of the Atmosphere Based on the ISCCP and Other Global Data Sets: Refinements of the Radiative Transfer Model and the input Data. *J. Geophys. Res.* **190.**